Spring 5-5-2011

Protein-Nucleic Acid Interactions in Nuclease and Polymerases

abdur rob
Abdur Rob

PROTEIN - NUCLEIC ACID INTERACTIONS IN NUCLEASE AND POLYMERASES

by

ABDUR ROB

Under the Direction of Professor Zhen Huang

ABSTRACT

DNA polymerase binds to the double stranded DNA and extends the primer strand by adding deoxyribonucletide to the 3'-end. Several reactions in the polymerase active site have been reported by Kornberg in addition to the polymerization. We observed DNA polymerase I can act as a pyrophosphatase and hydrolyze deoxyribonucletide. In performing the pyrophosphatase activity, DNA polymerase I requires to interact with RNA. RNA in general, was found to activate the DNA polymerase I as pyrophosphatase. This hydrolysis causes depletion of dNTP and inhibits DNA polymeration synthesis *in vitro*. In this RNA-dependent catalysis, DNA polymerase I catalyzes only dNTP but not rNTP. We have also observed that many other DNA polymerases have this type of the RNA-dependent pyrophosphatase activity. Our experimental data suggest that the exonuclease active sites most likely play the critical role in this RNA-dependent dNTP hydrolysis, which might have a broader impact on biological systems.

On the basis of the crystal structure of a ternary complex of RNase H (*Bacillus halodurans*), DNA, and RNA, we have introduced the selenium modification at the 6-position of guanine (G) by replacing the oxygen (^{Se}G). The ^{Se}G has been incorporated into DNA (6 nt. - 6 nucleotides) by solid phase synthesis. The crystal structure and biochemical studies with the modified ^{Se}G-DNA indicate that the ^{Se}DNA can base-pair with the RNA substrate and serve as a template for the RNA hydrolysis. In the crystal structure, it has been observed that the selenium introduction causes shifting (or unwinding) of the G-C base pair by 0.3 Å. Furthermore, the Se-modification can significately enhance the phosphate backbone cleavage (over 1000 fold) of the RNA substrate, although the modifications are remotely located on the DNA bases. This enhancement in the catalytic step is probably attributed to the unwinding of the local duplex, which shifts scissile phosphate bond towards the enzyme active site. Our structural, kinetic and thermodynamic investigations suggest a novel mechanism of RNase H catalysis, which was revealed by the atom-specific selenium modification.

INDEX WORDS: DNA polymerase, Klenow fragment, Selenium-modified DNA, RNA, Phasing and crystallization, Template, Substrate, Scissile bond, K_m, K_{cat}, K_{app}, Electrophoresis, Mass spectrometry, Pyrophosphorylosis, X-ray diffraction, MIR, MAD, SAD, Anomalous scattering, RNase H, Base pair shifting.

PROTEIN - NUCLEIC ACID INTERACTIONS IN NUCLEASES AND POLYMERASES

by

ABDUR ROB

A Dissertation Submitted in Partial Fulfillment of the Requirements for the Degree of

Doctor of Philosophy

in the College of Arts and Science

Georgia State University

2011

PROTEIN - NUCLEIC ACID INTERACTIONS IN NUCLEASES AND POLYMERASES

by

ABDUR ROB

Committee Chair: Dr. Zhen Huang

Committee: Dr. Stuart Anthony Allison

Dr. Yujun George Zheng

Electronic Version Approved:

Office of Graduate Studies

College of Arts and Sciences

Georgia State University

May 2011

While most are dream about success,

winners wake up and work hard

to achieve it

To my son,

Tanjeem Rhyne

ACKNOWLEDGEMENTS

A dissertation only lists one author's name, but no one could receive a Ph.D., nor should want to receive it, without the help of many others. Acknowledging them here is not nearly enough, but it is a start. Earning a Ph.D. degree is a long journey, mixed with excitement and pain; nobody can overcome without sincere assistance from others.

Prof. Zhen Huang has been my advisor over the past five years and it would not be enough to say that he always appears to me as friend, philosopher, and guide. I am very much proud of and appreciate him, especially because he allowed me to work in two exciting projects. At the beginning, when I had very little idea about how to study a problem scientifically, he gave me ideas for projects that could build on the previous work and be tailored to my interests. As I gained experience, he gave me more and more freedom to explore the questions myself. He is always interested in my research and progresses and has suggestions for improvements. In particular, he has taught me the importance of verifying the significance of a result, no matter how exciting the first observation seems. I will always be thankful for the environment he has created for me to learn and to become a scientist.

I have also learned enormously from the other members of our group. Drs. Jia Sheng and Josef Salon helped me in synthesizing DNA and RNA oligonucleotides whenever I need them, which helped me to keep my research forward. Drs. Julianne Caton-Williams, Lina Lin and Sarah Spenser provided me much scientific information and encouragement in many ways. I am offering special thanks to Dr. Jianhua Gan for introducing X-ray crystallography, a new research area for me, which helped me to understand the science in details. I am also thankful for the

friendship and discussions with the other members of the lab during my time here, especially the Ph.D. graduate students, including Bo Zhang, Manindar Kaur, Sibo Jiang, Wen Zhang, Lilian Kamau, Huiyan Sun, and Xifang Liu. My time here has allowed me to meet many more people, more than I have space to mention, without whom the time I spent would not have been nearly as rewarding.

TABLE OF CONTENTS

LIST OF TABLES

LIST OF FIGURES

Chapter 2:

Chapter 3

LIST OF SCHEMES

Chapter 2

Chapter 3

Chapter 1

Protein-Nucleic Acid Interactions in Nulceases and Polymerases

Introduction

Interaction of protein and nucleic acid is the central of life, and this central dogma dictates life. The life is based on the intricate interplays among DNA, RNA, and protein. DNA is transcribed to RNA, which is translated to protein. Protein is never reverse-translated to RNA or DNA. Except for retroviruses, DNA is never created from RNA either. Furthermore, DNA is never directly translated to protein.

The replication and transcription of the genetic material found in DNA is catalyzed by protein enzymes, and the expression of genes by translating RNA into proteins is regulated by protein transcriptional factors. In addition, DNA can be modified by modifying enzymes through protein-DNA interactions. Protein-DNA, protein-RNA, DNA-RNA, or protein-protein interactions are responsible for gene expression. Gene expression is the process where information from a gene is used in synthesizing a functional genetic product. These products are often proteins, but in non-protein coding genes, such as rRNA or tRNA genes, the products functional RNAs. The process and reglulation of gene expression is used by all known lifies - eukaryotes (including multicellular organisms), prokaryotes (bacteria and archaea) and viruses - to generate the macromolecular machinery for life. There can be dire consequences for the cell if the interactions are lost. One example of the consequences of protein-DNA mis-interactions is cancer. While the protein (e.g., p53) carries out many functions, one very important function is to

alter the expression of genes in response to stress related to the tumor development (*1*). In many forms of cancer, there has been a mutation to the DNA binding region of p53 (*2, 3*). The result of many of these mutations is that p53 is no longer able to bind DNA strongly (*4*), which suppreses the cancer formation. Many other transcriptional factors can also play roles in cancer development. For example, the basic leucine zipper AP-1 is known to be involved in the spread of tumor cells to other organs (*5, 6*).

Recently identified microRNAs (miRNAs) have emerged as key post-transcriptional regulators of gene expression and involved in diverse physiological and pathological processes (*7-9*). MicroRNAs (miRNAs) are large and ubiquitous classes of non-coding RNAs that regulate post-transcriptional silencing of target mRNA. Over 700 miRNAs have been identified in the human genome. MicroRNA has binding recognition sequences in 57.8% of human mRNAs, with 72% containing of those mRNAs having multiple miRNA recognition sites (*10, 11*). The miRNA are 70-100 nt. transcripts (pre-miRNA) and contain a 6-8 nt. seed region at its 5'-end for mRNA binding. The pre-miRNA is first cleaved by DROSHA, a nuclear endoribonuclease III, and then binds to the double-stranded RNA-binding proteins, followed by a active exportion to the cytoplasm via a mechanism dependent on Exportin 5 and Ran GTPase. The pre-miRNA is further processed in a ribonucleoprotein (RNP) complex consisting of Argonaute proteins and Dicer (endoribonuclease III), which cleave the pre-miRNA into the mature 19-22 nucleotide miRNA. The miRNA-Argonaute complex then binds to target mRNAs and recruits additional unidentified proteins for regulating target mRNAs (*7, 12-14*). It has been reported that the central tumour suppressor, p53, enhances the post-transcriptional maturation of several miRNAs with

growth-suppressive function, including miR-16-1, miR-143 and miR-145, in response to DNA damage (*15, 16*).

Protein interactions occur through similar physical forces with DNA and RNA which include electrostatic interactions (salt bridges) (*17, 18*) dipolar interactions (hydrogen bonding, H-bonds) (*19, 20*) entropic effects (hydrophobic interactions) (*21, 22*) and dispersion forces (base stacking) (*23-25*). These forces contribute in varying degrees to proteins binding in a sequence-specific (tight) or non-sequence specific (loose) manner (*26*).

The secondary and tertiary structure formed by nucleic acid sequences (especially in RNA) provides an important additional mechanism by which proteins recognize and bind particular nucleic acid sequences. The DNA- or RNA-binding function of a protein is localized in discrete conserved domains within its tertiary structure. An individual protein can have multiple repeats of the same nucleic acid binding domain or can have several different domains found within its structure. The identity of the individual domains and their relative arrangement are functionally important within the protein. Several common DNA binding domains include zinc fingers (*27*) helix-turn-helix (*28*), helix-loop-helix (*29*), winged helix(*30*) (*31*) Ketan S Gajiwala and Stephen K Burley) and leucine zipper (*32*). RNA-binding specificity and function are constituted by zinc finger, KH (K homology) (*33*), S1 (serine rich domain) (*34-36*), PAZ (*37, 38*), PUF (Pumilio/FBF) (*39, 40*) and RRM (RNA recognition motif (*41, 42*) domains. Multiple nucleic acid binding domains with a single protein can increase specificity and affinity of the protein for certain target nucleic acid sequences, mediate a change in the topology of the target nucleic acid,

properly position other nucleic acid sequences for recognition or regulate the activity of enzymatic domains within the binding protein (*43*).

Protein-RNA interactions are required in every step of gene expression. Proteins interact with RNA in order to splice, protect, translate or degrade the message. The first interaction occurs just after transcriptional initiation, when the complement to the promoter sequence is cleaved out of the mRNA and the capping machinery incorporates a "GpppN" cap at the 5' end of the mRNA (*44, 45*). This results in recruitment of elongation factors that regulate the reset of mRNA transcription. Elongation is followed by 3'-end processing and splicing, resulting in a mature RNA transcript that is exported to the cytoplasm for translation. All of these processes require significant protein-RNA interactions and are highly regulated and complex. Many of the regulatory elements for this process reside in non-coding regions 3' and 5' untranslated regions (UTRs) of the mRNA (*46*). However, regulatory microRNAs (miRNAs) also occur in coding regions of introns, as well as exons, non-coding genes and repetitive elements. In recent years, increased emphasis has been placed on the importance of these non-coding RNA sequences and their roles in cellular regulation and disease states (*15, 47*). However, tools for the study of critical protein RNA interactions have been limited. If we can better understand how these proteins interact with nucleic acids, we may be better able to treat the cancers that result from incorrect protein-DNA and protein-RNA interactions.

Although there are plentiful methods have been developed in detecting protein-DNA or protein-RNA interactions, and numerous studies have been made in elucidating their functions, still there are many interactions and functions remain unravealed. In this dissertation we have been

reporting some novel properties and functions of two well studied proteins in two separate chapters. These proteins are RNase (H) and DNA polymerase I; both are extensively studied in three dimensional and mechanistic details. RNase H protein is an endonuclease that binds to RNA-DNA duplex and cleaved RNA non-specifically. DNA polymerase I is a *E.coli* DNA polymerase which add deoxyribonleotides at the 3'-primer end that consider as DNA repair enzyme. This enzyme was discovered and characterized by Arthur Kornberg in 1967 (*48, 49*). We have studied DNA polymerase I and we found that this DNA-dependent DNA polymerase can also interact with RNA; this interaction causes hydrolysis of DNA precursor, the dNTP, in a fairly higher rate. Our biochemical and kinetic analysis showed the DNA polymerases as a whole preserve this RNA interacting property that causes dNTP hydrolysis.

Selenium now emerges as a major area of research. It is found as an essential trace element for all living organisms. Selenium containing amino acid selenocysteine recognized as the 21st amino acid. It is incorporated into protein by ribosome mediated protein synthesis. There are at least 25 specific, genetically determined human selenoproteins have been identified, many of which have only recently been discovered. Besides physiological role of selenium, its anomalous scattering property is made possible to circumvent the phase problem in X-ray crystallography. Now selenium is routinely being introduced into protein via selenomethionine for solving crystal structure. Selenium is also using in nucleic acid for structure determination. Selenium has been introduced in a variety of position in nucleobases and in ribose moiety of DNA and RNA. The crystal structure of the selenium modified DNA and RNA provided new details about the interactions and mechanism. It has also found that the selenium introduction produce better resolution in X-ray crystal structure. The quality of crystal is better and it grows much faster than

without selenium. We investigated X-ray structure of RNase H (*Bacillus halodurans*) co-crystallized with with selenium modified DNA/RNA duplex. In selenium modified DNA, which serve as a template for RNase H (BH), seleno G (^{Se}G) located at two positions of the 6-nts DNA. It has been observed that the selenium modified DNA forms stable base pair with substrate RNA in the enzyme active site. It has also been observed that selenium atom on the DNA template causes shifting of base pair (d^{Se}G….rC) 0.3 Å. This shifting pushed the scissile phosphorous atom of the RNA substrate towards active site although it located remotely on the template DNA. We performed kinetic analysis for the RNase H (BH) with selenium modified DNA and RNA to observe the shifting effect. We found that this base pair shifting resulted in enhanced catalytic performance of RNase H (BH) over thousand folds compare to the native. The RNase H is a ubiquitous protein found in many organisms, from bacteria to human. The role of RNase H1 has been implicated in mitochondrial DNA replication in eukaryotes (*50*) , primer removal from Okazaki fragment in lagging strand DNA synthesis (*51, 52*) , and DNA repair (*53-55*).

Our observations suggest that RNase H activity can be enhanced by introducing selenium atom in DNA. This novel function can be addressed in unraveling mechanism of protein-DNA or protein RNA interactions; also this strategy could be helpful to design DNA or RNA that could enhance enzyme activity.

Chapter 2

RNA-dependent Pyrophosphatase Activity of DNA polymerase I

2.1 Abstract

Constitutively expressed *Escherichia coli* DNA polymerase I is a DNA-dependent DNA polymerase and belongs to group I of DNA polymerase. Removal of N-terminal 5′-3′ exonuclease domain of this tri-functional enzyme produces bi-functional Klenow fragment. Polymerase, located on the C-terminal, function includes incorporation of deoxyribonucleotide monophosphates (dNMPs) at 3′ primer end while 3′-5′ exonuclease activity excises misincorporated dNMP form the same site, if any. The function of 5'--->3' exonuclease domain is implicated in removing primer during Okazaki fragment synthesis. In order to carryout canonical functions, the DNA polymerase I requires minor groove specific binding to primer-template complex. Here, we report that, *in vitro*, in the presence of RNA, the DNA polymerase I functions as pyrophosphatase that degrade deoxyribonucleotide triphosphates (dNTPs) into their corresponding dNMPs and pyrophosphates. However, this catalysis is primer-template independent and requires RNA activation. The binding of RNA with DNA polymerase I is fairly strong, very close to binding with double stranded DNA duplex. In RNA dependent catalysis substrates are highly specific, dNTPs were being degraded while ribonucleotides (rNTPs) were not. All four dNTPs were found to be degraded by the DNA polymerase I unlike to most other dNTP pyrophosphatases and triphosphatases, such as MutT and dGTPase, respectively. It also found that the DNA polymerases in general activated by RNA and hydrolyze dNTP into

corresponding dNMP and pyrophosphate. From kinetic analysis it was observed that the DNA polymerases with 3'---->5' exonuclease active site were more efficient in RNA dependent dNTP hydrolysis. This suggested the involvement of 3'--->5' exonuclease active site in RNA dependent dNTP hydrolysis. The molecular mechanism of the RNA-dependent dNTP pyrophosphatase activity of the DNA polymerase I, however, remains to be elucidated. In summary, we found that the DNA polymerase I has a novel dNTP pyrophosphatase activity in the presence of RNA. Importantly, this phenomenon may be generally present *in vivo* and may help fine tuning dNTP pool level and participate in DNA replication regulation.

2.2 Introduction

Escherichia coli DNA polymerase I (pol I) belongs to 'family A' repair enzymes involved in proofreading (*56, 57*), nucleotide excision repair (*58*), primer removal (*59*), and Okazaki fragment synthesis (*60*). Pol I is a single chain tri-functional enzyme includes the N-terminal 5′-3′ exonuclease, 3′-5′ exonuclease (proofreading), and C-terminal polymerase functions. 5′-3′ exonuclease activity removes RNA primers from Okazaki fragments generated during the replicative DNA synthesis. The proteolytic removal of N-terminal 5′-3′ exonuclease domain produces bi-functional Klenow fragment that retains 3′-5′ exonuclease (proofreading) and polymerase active site of the parent molecule (*61*). The function of the 3′-5′ exonuclease active site is to remove misincorporated dNMPs from 3′ primer ends (proofreading function), and several dNMPs from the point of lesion in 3′-5′ direction during repair. The C-terminal polymerase activity is used to fill gaps resulted from the removal of Okazaki fragment and from removal of bases at DNA lesions (*62*).

DNA polymerase I is a DNA-dependent DNA polymerase as it requires binding to DNA for their activity. The binding of DNA polymerase I to dsDNA is very strong and it also could bind to ssDNA but weakly in this case (*63*). When it binds to ssDNA, the Pol I hydrolyzes phosphodiester bond and removes dNMP from 3′-5′ direction by its 3′-5′ exonucleolytic active site (*64-67*). Here, we report that, DNA polymerase I interacts with RNA and that interaction enables DNA polymerase I to hydrolyze dNTP into dNMP and inorganic pyrophosphate. This catalysis is RNA dependent and only dNTPs, not rNTPs, are recognized and hydrolyzed. The molecular mechanism of this RNA dependent dNTP pyrophosphatase activity of the Pol I, however, remains unclear. Since this is our *in vitro* study and it is unclear also whether this

phenomenon persists in the cellular level. If this observed dNTP degradation occurs in living system it could be significant for several reasons. Organism needs to maintain dNTP pools in a narrow range. The dNTPs do not have any known function other than serve as a DNA precursors require for genome replication and repair. The imbalanced dNTP pool size may initiate mutagenesis, stimulation of genetic recombination, chromosomal abnormalities, DNA break down, and cell death (*56, 68-71*). To prevent these genomic abnormalities, organisms have evolved multiple layers of control in dNTP biosynthesis. There are also several degradation mechanisms exists in living system in keeping the four dNTPs concentrations in a narrow range, just enough needed for genome replication and maintenance. The biosynthetic regulations occur at transcription (*72-75*), translation (*76, 77*), and post-translational (*78, 79*) levels. Beside these differential biosynthetic regulations, which are cell-cycle dependent (*76*) and compartmentalized (*80*) also, another level of control is extended by degradation of DNA precursor molecules. Pyrophsophohydrolase enzymes such as *E.coli* MutT, which prefers substrate in order of 8-OH-dGTP>8-OH-ATP but active on all canonical nucleoside triphosphates (*81, 82*), or its human counterpart hMTH1 that also has substrate preference in order of 2-OH-dATP >8-OH-dGTP or 8-OH-dATP (*83*) hydrolyze the oxidized purine nucleoside triphosphates into nucleoside monophosphates and thereby 'sanitize' them from dNTP precursor pools. *E.coli* has a unique enzyme, deoxyguanosine triphosphate triphosphohydrolase (dGTPase) which was first discovered by Kornberg *et al.* (1958) as a contaminant in partially purified *E.coli* DNA polymerase I preparations. This enzyme specifically degrades dGTP into deoxyguanosine and triphosphate or in some extent rGTP, with the Km 2-5 μM for dGTP and 150 μM for rGTP (*84-86*). It has also been reported that the dGTPase could binds and stimulated by RNA as well as ssDNA (*87*) and this enzyme in wild type *E.coli* could lead to 5-fold decrease in intracellular

dGTPs concentration (*88-90*). Although the physiological significance is ambiguous, it has been hypothesized that the interactions of dGTPase with nucleic acids may prevent bacteriophage gene T7 1.2 protein binding that would otherwise required for successful phage infection. There is another class of enzyme called (deoxy) nucleotidases present in prokaryote and mammal in different subcellular localization that cleaves (deoxy) mononucleotides into (deoxy) nucleosides and phosphates (*91-93*). In effect, the intricate regulations of dNTP biosynthesis and degradation rates determine the cell cycle dependent, balanced and asymmetric ((*94*) concentration of dNTP in the intracellular milieu.

The DNA polymerase I is the most extensively studied DNA polymerase in perspective of molecular, mechanistic, and structural details. In this article, this is the first time reporting of another novel pyrophosphatase function of the Pol I which is activated by RNA. Apparently, the RNA binding to the Pol I is different from the usual binding property of the Pol I because it is established that it binds to ssDNA, dsDNA, and primer-template complex. In primer-template complex binding occurs through the Arg668 residue of the Klenow fragment that makes critical hydrogen bond to the *N*3 of purines and O^2 of pyramidines of the minor groove of the 3′- primer terminus (*95*) as well as to the ring oxygen of the deoxyribose group of the incoming dNTP (*88*) which eventually insure the fidelity of dNTP incorporation (*96, 97*). Another unusual property we observed here is that, comparing to other nucleotide hydrolytic enzymes (discussed above), the Pol I degrades all the four dNTPs, but not when the substrates are rNTPs. Furthermore, we found that the RNA –dependent dNTP hydrolytic property is not limited only to Pol I, rather a number of DNA polymerases from different polymerase family interact in the same manner and hydrolyzes dNTP. The K_m and K_{cat} of the DNA polymerases have detrmined by Michaelis-

Menten method. Different DNA polymerases showed differential values of kinetic parameters. It has been noticed that the DNA polymerases with the three functional domains, 5′--->3′ exonuclease, 3′--->5′ exonuclease (proofreading), and polymerase, have the highst RNA-dependent dNTP hydrolytic activities. This analysis indicated that the exonuclease active site of the DNA polymerase may involve in RNA-dependent dNTP hydrolysis.

Based on our limited studies the physiological implications of the RNA-dependent dNTP hydrolysis property of the DNA polymerases is not immediately apparent. Nevertheless, among many dNTP pools control mechanisms, our observed phenomenon may exists in the living system which suggests an additional mechanism that may "fine-tune" the dNTP pools.

In this study, we have made a series of biochemical and kinetic studies *in vitro* and the experimental results allow us to propose that the DNA polymerase I can acts as RNA-dependent dNTP pyrophosphatase which hydrolyzes dNTP into corresponding dNMP and inorganic pyrophosphate. This RNA interacting functions of DNA polymerase I is novel and it is rationale to revisit the extensively studied DNA polymerase I.

2.3 Materials and Methods:

2.3.1 Synthesis and purification of oligonucleotides:

Oligonucleotides:

RNA24.1 5′-AUGUGGAUUGGCGAUAAAAAACAA-3′,

Template: DNA55.1: 5′-d(TGTACGTTTCGGCCTTTCGGCCTCATCA-

GGTTGCCTATAGTGAGTCGTATTA CGC)-3′,

DNA Primer 21.1: 5′-d (GCGTAATACGACTCACTATAG)-3′

The RNA 24.1 was purchased or synthesized chemically. Chemical synthesis was performed on a 1.0 or 10 μmol scale using an ABI392 DNA/RNA Synthesizer and the deprotection of RNA was done as described (*98*). Products were separated by 19 % polyacrylamide, 7 M urea in 1X TBE buffer (89 mM Tris, 89 mM boric acid and 2 mM EDTA) gel (40 X 35 cm X 0.8 mm). The gel was pre-run for 1 hr at 40-50 watts without cooling and electrophoresis was performed at 40-50 watts for 2 hours. After electrophoresis, the gel over a TLC plate was visualized under UV light and desired bands were cut, crushed in 1.5 ml eppendorf tube. Gel was placed in a rotator after addition of 3 volumes of RNase free water. The soaking was done overnight at room temperature. RNA 24.1 was recovered by ethanol precipitation and its concentration was measured by UV spectrophotometer. RNA 24.1 was also purchased from Dharmacon Research Inc. and 2′-protection groups were deprotected according to the manufacturer instructions. After synthesis, the DNA oligonucleotides were cleaved from solid support and fully deprotected by aqueous ammonia (concentrated) treatment for 14 h at 55 °C (*99*). Separation and purification were done by the methods described above.

2.3.2 Extraction of total RNA

Total RNA from *E.coli* and Yeast were extracted using RNA purification kit (purchased from Epicentre Biotechnologies). Briefly, 0.1 -0.5 µL of an overnight culture of *E.coli* (0.5-3 X 10^6 cells) were lysed with 300 uL 'Tissue and Cell lysis solution' containing Proteinase K incubating at 65ºC for 10 min. 150 µL of MPC protein precipitation reagent was added, centrifuged (10 minutes ≥10,000 X g) and supernatant was collected. Precipitation of RNA was performed by centrifugation with 70 % isopropanol at 4ºC for 10 minutes (≥10,000 X g). Contaminated DNA was removed by incubating RNA with 200 µL DNase I solution (5 µL of RNase-Free DNase I up to 200 l with 1X DNase Buffer) for 10 minutes at 37ºC. 200 µl of 2X 'T and C Lysis Solution' was added, vortex for 5 seconds, and 200 µl of MPC Protein Precipitation Reagent was added. Debris was removed by centrifugation for 10 minutes at ≥10,000 X g. Supernatant was collected and RNA was precipitated by centrifugation with 70 % isopropanol and RNA was washed (twice) with 70 % ethanol dissolved in water after air drying. Total RNA from Human Prostate Cancer cells and RNA ladder were purchased from Ambion Technologies (USA).

2.3.3 Synthesis of γ-^{32}P-dATP

γ-^{32}P-dATP was prepared by transphosphorylation of dADP from γ-^{32}P-ATP catalyzed by baker's yeast nucleoside diphosphate kinase (EC. 2.7.4.6; Ndk, Sigma Chemical Co, St, Louis, MO). A 20 µL reaction mixture containing 50 mM Tris-HCl buffer (pH 7.5), 5 mM MgCl2, 2.5 mM dADP, 1.25 µM γ-^{32}P-ATP (4 x 10^6 Ci /mol), 3.4 unit of Ndk was incubated at 37 ºC for 15 min. The reaction mixture was spotted on PEI-cellulose TLC plates (Aldrich) and developed in 0.6 M triethylammonium bicarbonate buffer (pH 8.0). Radioactive nucleotides were visualized

by autoradiography, and the cellulose in the area that contained γ-^{32}P-dATP was removed. γ-^{32}P-dATP was eluted from the cellulose with 1 ml of 0.6 M triethylammonium bicarbonate buffer (pH 8.0), and the mixture was centrifuged. The supernatants from three washes were combined and lyophilized, and 500 µl of 15 mM dATP was added to the lyophilized sample, yielding 15 mM γ-^{32}P-dATP.

2.3.4 Degradation reaction

Reactions (5 µl) contained 0.2 µl of DNA polymerase (144 nM), 0.5 µl buffer (10 mM Tris-HCl, 10 mM MgCl2, 50 mM NaCl, 1 mM dithiothreitol pH 7.9), 0.1 µl α -^{32}P-dCTP or α -^{32}P-dATP or α -^{32}P-rCTP or α -^{32}P-rATP, 2 µl RNA (200 ng/ µl) and 2.2 µl water were incubated in water bath for 1 hr at 37ºC. For control experiment equal volume of water was supplemented for RNA or DNA polymerases. Different DNA polymerases were purchased from New England Biolab.

2.3.5 Alkali hydrolysis

A total of 14 µl reaction was prepared for NaOH hydrolysis. 2 µl γ-^{32}P-ATP, 1.4 µl 100 mM NaOH (final 10 mM), and 10.6 µL water were mixed and heated at 90 °C and aliquots were collected at 0,1, 5, 10, 30, and 60 min.

2.3.6 Pyrophosphatase reaction

In a total 5 µl reaction that contains 2 µl of the reaction materials , 0,5 ml buffer (10 mM Tris-HCl, 10 mM MgCl2, 50 mM NaCl, 1 mM dithiothreitol, pH 7.9), 2.25 µl H2O, and 0.05 unit of inorganic pyrophosphatase (EC 3.6.1.1) were incubated at 37 °C for 15 min.

2.3.7 Polynucleotide kinase reaction

A total 10 µl reaction containing 1 µl of 1 µM (1 pmol) primer 21.1 mixed with 1 µl 10X PNK buffer, 4 µl γ-^{32}P-ATP, 1 µl polynucleotide kinase (1 unit) and 3 µl water were mixed and incubated in water bath at 37 °C for 1 h. Then the reaction was heated at 68 °C for 10 min to inactivate the enzyme. 1.11 µl 3 M NaCl was added (final 30 mM) and mixed, 33.33 µl 100 % ethyl alcohol was added (final 70 %) and chilled at -20 °C for 15 min. the reaction mixture was centrifuged (14,000 rpm) for 15 min. at 4 °C. Supernatant was discarded, pellet was washed 3 times with 70 % ethanol, air dried and 10 µl H2O was added.

2.3.8 DNA polymerization reaction in the presence of RNA

A total of 5 µl reaction that contains 1 µl of 100 nM 5´-labeled DNA primer 21.1(final 20 nM) and 0.5µ l of 2 µM DNA template 55.1 (final 200 nM) were mixed with 0.5 µl buffer (10 mM Tris-HCl, 10 mM MgCl2, 50 mM NaCl, 1 mM dithiothreitol, pH 7.9), 0.2 µl of each dNTP. The final concentration of each dNTP was as follows: dATP - 240 nM (0.2 µl from 6 µM stock), dTTP - 60 nM (0.2 µl from 1.5 µM stock), dCTP- 200 nM (0.2 µl from 5 µM stock), and dGTP - 180 nM (0.2 µl from 4,5 µM stock). Total 5 µl reactions also contain various amount of *E.coli* total RNA. Reaction 1 contained no RNA (2 µl water added), reaction 2, 3, 4, 5, and 6 contained 10 ng (1 µl from 50 ng/µl stock and 1 µl water), 20 ng (2 µl from 50 ng/µl stock), 50 ng (0.5 µl from 1 µg/ul stock and 1.5 µl water), 100 ng (1 µl from 1 g/µl stock and 1 µl water), and 200 ng (2 µl from 1 µg/µl stock) total *E.coli* RNA, respectively. 0.2 µl DNA polymerase I was added to each reaction and incubated at 37 °C for 30 min. DNA polymerase I, Klenow fragment, wild

type and mutant, and all other polymerases were purchased from New England Biolab (USA) and RNA ladder from Ambion biotechnology (USA).

2.3.9 TLC analysis

TLC plates of 10 µM layer thickness purchased from micron technology, USA. The recation materials of amount 0.2 - 0.5 µl were placed at the bottom of the TLC plate with corresponding controls. The bottom of the plate was submerged in the buffer keeping the loading place one inch above the buffer layer. The chromatographic plates were allowed to soak for 30 - 45 minutes at room temperature keeping the chamber air tight. The buffers were mixed solution of isopropyl alcohol, ammonium hydroxide and water with ratio 5:4:2 or 6:3:1, respectively.

2.3.10 FPLC analysis

A total 150 µl reaction consists of 200 ng/µl *E. coli*, 100 µM dATP, were mixed with buffer reaction buffer (10 mM Tris-HCl, 10 mM MgCl2, 50 mM NaCl, 1 mM dithiothreitol, pH 7.9). A 50 µl aliquot was removed which was regarded as "zero minute" (without enzyme). KF pol was added to the rest to 150 nM (100 µl) concentration (final) and incubated at 37 ºC for 30 min and 50 µl aliquot was removed and placed in -20 °C. This aliquot was referred to as "30 min". The remaining 50 µl reaction was incubated for another 30 min which was called "1 hr" reaction. All three reactions were analyzed by separating the reaction products by loading onto HiTrap Q HP 5 ml (Amersham bioscience) anion exchange column. The column was washed with 10 column volumes (CV) of buffer A (10 mM sodium phosphate, pH 7.8) and impurities were eliminated with washing 10 CV of buffer B (10 mM sodium phosphate, pH 7.8, 1M NaCI) with a flow rate 1 ml/min. The column was equilibrated with 10 CV buffer A and each 50 µl reaction was

injected into column. After sample injection, the column was washed with 5 CV of buffer A. A 100 ml buffer B with gradient (0 – 100%) was applied to the column at the flow rate 1 ml/min. Different fractions of the reaction products were eluted by the gradient of buffer B. The retention time of dATP, dADP or dAMP were determined by the run of each component separately and by co-injection of each component with the reaction mixture. The amount of substrate (dATP) and product (dAMP) in each run were appreciated by the UV absorption spectra set at 259 nM and from retention time in continuous increasing gradient of buffer B. Peaks of the RNA or Pol I were also determined from the separate run.

2.3.11 Gel shift assay

Gel shift assay was performed to determine the binding constants of DNA polymerase I with RNA. The 5'-end of 55-mer the RNA labeled with ^{32}P by using standard method described elsewhere. A of total of 20 μL reaction, for each enzyme concentration, contained 100 nM RNA (final) mixed with 10 -100 pM ^{32}P- labeled of the same RNA (5'-end) mixed with 20 nM, 40 nM, 60 nM, or 80 nM DNA polymerase I and and binding buffer (10 mM KCI, 1 mM DTT, 5 % glycerol, pH 7.0, final) and incubated at room temperature for 30 minutes. The mixtures were then placed at 4 °C for overnight. The reaction materials were mixed with gel loading dye (10 mM KCI, 1 mM DTT, 5 % glycerol, 0.001 % xylene blue (W/V), final) and loaded on 10 % non denaturing polyacrylamide gel. The composition of running buffer was 5 mM tris chloride, 10 mM EDTA and pH 7.5 adjusted with acetic acid. Before loading samples the gels were pre-run for 1hr to remove ammonium per sulfate (APS). The gels were run with a constant voltage (250 volts) for one hour in 4 C° cold room. Gels were fixed with 7% acetic acid, dried, scanned, and

bands were quantified using a PhosphorImager. Images were also taken by exposing on X-ray film.

2.3.12 Bacterial growth study

Chemically competent *E.coli* cells (Top10) was purchased from imvitrogen. A vial of competent cell was mixed with 10 pmol pUC19 plasmid (purchased from invitrogen). In each tube H_2O, RNA (50 ng/µl), DNA polymerase I (80 ng/µl), dNTP (10 µM), RNA and DNA polymerase I , mixture of RNA, DNA polymerase I and dNTP, mixture of RNA, DNA polymerase I , and rNTP, or mixture of RNA, DNA polymerase I , dNTP, and rNTP (10 nM) was added. The tubes were kept on ice for 30 minutes and the cells were heat shocked for 45 sec. at 42 °C and spreaded on Lb-ampicillin plate. The plates were incubated at 37 °C over night and in the following day the growth of the cells were observed visually.

2.3.13 Mass spectrometry analysis

The dAMP peak at 4 minutes retention time from FPLC run (section 3.10) was collected. The sample was desalted by desalting column and dAMP was further purified by HPLC using Carbon-13 column (C-13, hydrophobic column). A gradient 40 % acetonitrile was used to elute dAMP from C-13 column. Elute from C-13 column was lyophilized and dissolved in water to concentration 10 µM. A 20 µl of the sample was sent to Core facility, Department of Chemistry, Georgia State University for high resolution mass spectrometry analysis. The dAMP peak was observed with a molecular mass 330 ($[M - H]^-$).

2.3.14 Kinetic analysis: There were total nine different DNA polymerases have been used for kinetic study.The reaction conditions were as the same as degradation reaction described in section 3.4. A total of 20 µl reaction material was prepared in determining reaction rate for each dATP concentration. At 0, 0.5, 1, 3, 5, 7, and 10 minute's interval 2 µl of the reaction material was removed and reaction were terminated by immediately mixed with loading buffer (contained 7 M urea) and placing in ice. The '0' minute refers to control which was separated before adding DNA polymerase and the same amount of water added instead. There were 100 nM to 100 µM substrate were used for determining reaction rate for each DNA polymerase. All DNA polymerases were purchased from New England Biolab.

2.4 Results and discussions

Investigations on *Escherichia coli* DNA polymerase I have been carried out over many decades. A wealth of information of this DNA primer-template directed DNA polymerase remain in our repertoire that arises from extensive structural, mutagenesis, and kinetic studies. In our present study we have found a novel function of DNA polymerase I. We found that in the presence of RNA, the DNA polymerase I degrades dNTP into dNMP and PPi *in vitro*. The reaction can be described as follows:

$$\text{dNTP} \xrightarrow[\text{DNA polymerase I}]{\text{RNA}} \text{dNMP} + \text{PPi}$$

2.4.1 Klenow fragment hydrolyzes of dCTP into dCMP and PPi in presence of RNA

In order to determine the role of DNA polymerase I and RNA in the deoxyribonucleotide degradation pathway *in vitro*, α-^{32}P-dCTP was incubated with or without Klenow fragment and RNA. After incubation at 37 ºC for 1 hr, the reaction mixtures were placed on TLC plates and the results were analyzed from co-spots of dCTP, dCDP, dCMP, and α-^{32}P-dCTP for the presence of product α-^{32}P-dCMP and substrate α-^{32}P-dCTP. It has been found that degradations of α-^{32}P-dCTP into α-^{32}P-dCTP and PPi have been taken place when the reactions contained both Klenow fragment and RNA. In addition to total RNA from *E.coli*, RNA from other sources, such as, yeast (Figure 1, lane-9), human (Figure 1, lane-10), RNA marker (Figure 1, lane-11), and 24 base-long short synthetic RNA (Figure 1, lane-12) were examined. RNA of different sources and of different length has found to activate Klenow fragment. The hydrolysis did not caused by RNA or KLenow DNA polymerase alone as there were no hydrolysis observed in the absence of any of them (Figure 1, lane- 7, 8). These observations suggest that RNA could interact with Klenow fragment and this activation enable Klenow fragment to hydrolyze dCTP into dCMP and inorganic pyrophosphate.

Hydrolysis of dCTP by Klenow DNA polymerase in the presence of RNA from various sources

α-^{32}PdCTP	-	+	+	+	+	-	+	+	+	+	+	+	+	+	-
dCTP	+	+	-	-	-	-	-	-	-	-	-	-	-	-	-
dCDP	-	-	-	-	-	-	-	-	-	-	-	-	-	+	+
dCMP	-	-	-	-	+	+	-	-	-	-	-	-	-	-	-
RNA(*E.coli*)	-	-	-	+	+	-	-	+	-	-	-	-	+	+	-
RNA(Human)	-	-	-	-	-	-	-	-	-	+	-	-	-	-	-
RNA(Yeast)	-	-	-	-	-	-	-	-	+	-	-	-	-	-	-
RNA24.1	-	-	-	-	-	-	-	-	-	-	-	+	-	-	-
RNA marker	-	-	-	-	-	-	-	-	-	-	+	-	-	-	-
Klenow(exo+)	-	-	-	+	+	-	+	-	+	+	+	+	-	+	-
Klenow(exo$^-$)	-	-	-	-	-	-	-	-	-	-	-	-	+	-	-
EDTA	-	-	-	-	-	-	-	-	-	-	-	-	-	+	-

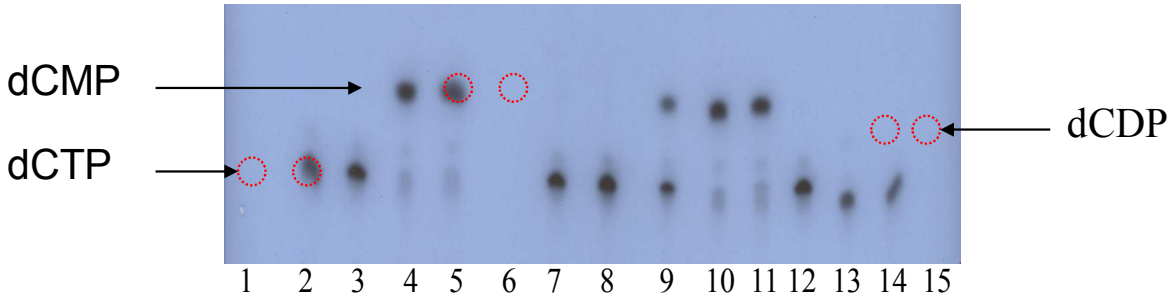

Figure 1. Degradation of dCTP by the Klenow fragment in the presence of RNA from different sources.

Figure 1. Degradation of dCTP by the Klenow fragment in the presence of RNA from different sources.

A 5 µL reaction containing 0.2 µL α-^{32}P-dCTP (final 184 nM) incubated with or without 0.2 µL DNA polymerase I Klenow fragment (final 144 nM). Each reaction supplemented with 2 µL RNA (200 ng) or with 2 uL water and 0.5 ul 10X buffer 2[10 mM Tris-HCl, 10 mM MgCl2, 50 mM NaCl, 1 mM dithiothreitol (pH 7.9)]. Finally, 2.1µl water was added in each reaction to reach the volume 5 µl. Reactions were incubated in water bath at 37 °C for 1 h. 1 µl of reactants loaded on the TLC plate and ran in saturated ammonium solution (isopropyl alcohol: ammonium hydroxide: water, 5:3:2) for 1 h. After air drying plates were wrapping with thin saran wrap and location of dCDP, and dCTP were visualised under UV light. Plates were then exposed to film and autoradiographed. Location of the radioactive substrate or product was determined by comparing with the cold dCTP or dCMP on the TLC plate. Degradation α-^{32}P-dCTP,s observed in the presence of both RNA and Klenow fragment (lane- 5) but not observed in the absence of either RNA (lane- 7) or Klenow fragment (lane- 8). Degradation also observed when α-^{32}P-dCTP incubated with Klenow fragment and RNA isolated from yeast (lane- 9) or human (lane- 10) or RNA from commercial RNA marker (lane-11). But very little degradation was observed when shorter-length RNA (24-mer) was present at this time (lane- 12). When mutant Klenow fragment (exo^{-}) substituted for wild-type Klenow fragments very little degradation was observed (lane-13). This enzymatic reaction was Mg^{+2} dependent as no degradation was observed when EDTA (20mM) was added in the reaction (lane- 14).

2.4.2 Klenow fragment hydrolyzes of dATP into dAMP and PPi in presence of RNA

We observed in Figure 1 that the Klenow fragment hydrolyzes pyramidine nucleotide (dCTP) in the presence of different kinds of RNA. Enzymes are very specific for substrate selection due to specific configuration in their active site. As dCTP is one of the precursors of DNA from pyramidine nucleotides, we examined purine nucleotide to observe whether Klenow fragment could also hydrolyze dATP activated by RNA. We incubated dATP with Klenow fragment and RNA and we observed that dATP was hydrolyzed into dAMP and PPi (Figure 2a, lane- 4, 7, 11, 14, and 17, Figure 2b, lane- 4, 7, and 14). It also observed that hydrolysis did not occur in the absence of RNA (Figure 2b, lane- 17, 18) or in the absence of Klenow fragment (Figure 2a, lane- 6, 9, 13, 16, 19, Figure 2b, lane- 6, 9, 13, and 16), the same results we observed in Figure 1. We used wild type and mutant Klenow fragment (exo^-) where in the later the 3'---> 5' exonuclease function has been abolished by D424A point mutation. It also has been observed the Klenow fragment (exo^-) was less efficient in dydrolyzing dATP in the presence of RNA (Figure 2a, lane- 5, 8, 12, 15, 18, Figure 2b, lane- 5, 8, 12, and 15). These observations indicated that the Klenow fragment interacting with RNA hydrolyzed dATP, the purine precursor of DNA.

Hydrolysis of dATP by Klenow DNA polymerase in the presence of RNA from various sources

(a)

	Human			Yeast			*E. coli*			HH WT			HH Mu		
RNA	+	+	+	+	+	+	+	+	+	+	+	+	+	+	+
Klenow (exo^+)	+	-	-	+	-	-	+	-	-	+	-	-	+	-	-
Klenow (exo^-)	-	+	-	-	+	-	-	+	-	-	+	-	-	+	-

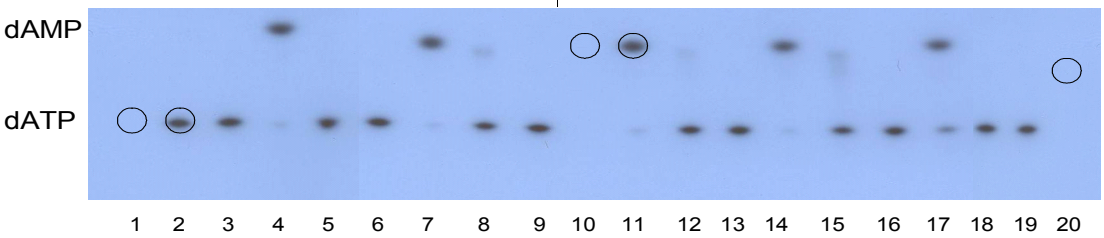

1 2 3 4 5 6 7 8 9 10 11 12 13 14 15 16 17 18 19 20

(b)

	Marker			23s r			55 b			24 b				
RNA	+	+	+	+	+	+	+	+	+	+	+	+	-	-
Klenow (exo^+)	+	-	-	+	-	-	+	-	-	+	-	-	+	-
Klenow (exo^-)	-	+	-	-	+	-	-	+	-	-	+	-	-	+

1 2 3 4 5 6 7 8 9 10 11 12 13 14 15 16 17 18

Figure 2: Degradation of dATP by Klenow DNA polymerase in the presence of RNA from various sources.

Figure 2: Degradation of dATP by Klenow DNA polymerase in the presence of RNA from various sources.

^{32}P - α labeled dATP incubated with KF pol (exo $^{+}$ or exo $^{-}$) or RNA or both. (a). RNA from human, yeast, *E. coli,* hammerhead ribozyme (HH) (WT -wild type) and HH – mu (mutant). (b). RNA marker (100b – 1 kb), 23S ribosomal RNA, 55-nts RNA, 24-nts RNA. Hydrolysis of dATP occurred only when both RNA and Klenow fragment were present (Figure a, lane- 4, 7, 11, 14, and 17) and Figure b, lane- 4, 7, 11, and 14. But hydrolysis was not observed when only RNA (Figure a, lane- 6, 9, 13, 16 and 19) and Figure- b, lane 6, 9, 13, and 16) or only polymerase (Figure b, lane- 17 and 18) was present. Klenow fragment (exo^{-}) which have point mutation at D424A hydrolyzed none or very little dATP in the presence of RNA (Figure a, lane- 5, 8, 12, 15, and 18, Figure b, lane- 5, 8, and 12, and 15).

2.4.3 Anion exchange chromatographic analysis showed dAMP as a product of RNA dependent dATP hydrolysis by DNA polymerase I

In Figure 1 and 2, we observed that RNA activated Klenow fragment hydrolyzed dNTP into two products, dNMP and PPi. The presence of the ^{32}P-α-dNMP (product) and ^{32}P-α-dNTP (substrate) on the TLC plates were determined by comparing the R_f (retention factor) of non-radioactive dNMP or dNTP as reference. In this procedure, non-radioactive dNMP or dNTP was placed on the same level as radio labeled on the TLC plate and after run the plates were illuminated under UV light and the position of the references were marked. After radiographing the TLC plate, the X-ray film was compared to the marks and the positions of ^{32}P-α-dNMP or ^{32}P-α-dNTP was determined. We also conducted anion exchange chromatography (AEC) to determine the

presence of product dAMP in the hydrolysis reaction. Anion exchange column (DEAE - sephadex) was used to separate the product dAMP from the mixture of dAMP and dATP based on the net charge differences between them. In anion exchange chromatography compounds are separated on the basis of net negative charge. At pH 7.8, dAMP and dATP have, two and four negative charges, respectively. Therefore, in DEAE – sephadex column dATP would retain longer time, as it has more negative charges than dAMP, which could be eluted at different time by NaCI gradient. In our experiment we incubated the substrate dATP with DNA polymerase I in the presence of *E.coli* total RNA for different time periods and analyzed by FPLC using anion exchange column. We analyzed three sets of reactions, "0 min", "30 min", and "1 hour". The "0 min" reaction contained only dATP (substrate) and *E.coli* total RNA but without DNA polymerase I. The "30 min" and "1 hour" reactions contained dATP (substrate), *E.coli* total RNA and DNA polymerase I and incubated for 30 min and 1 hr, respectively. The profiles were presented in Figure 3. When the "0 min" reaction was subjected to chromatography by anion exchange column, only dATP peak was observed with retention time 11.34 min with the UV intensity 3.5 mAU (blue).

Anion exchange chromatography showed dAMP is the product in RNA dependent dATP hydrolysis by DNA polymerase I

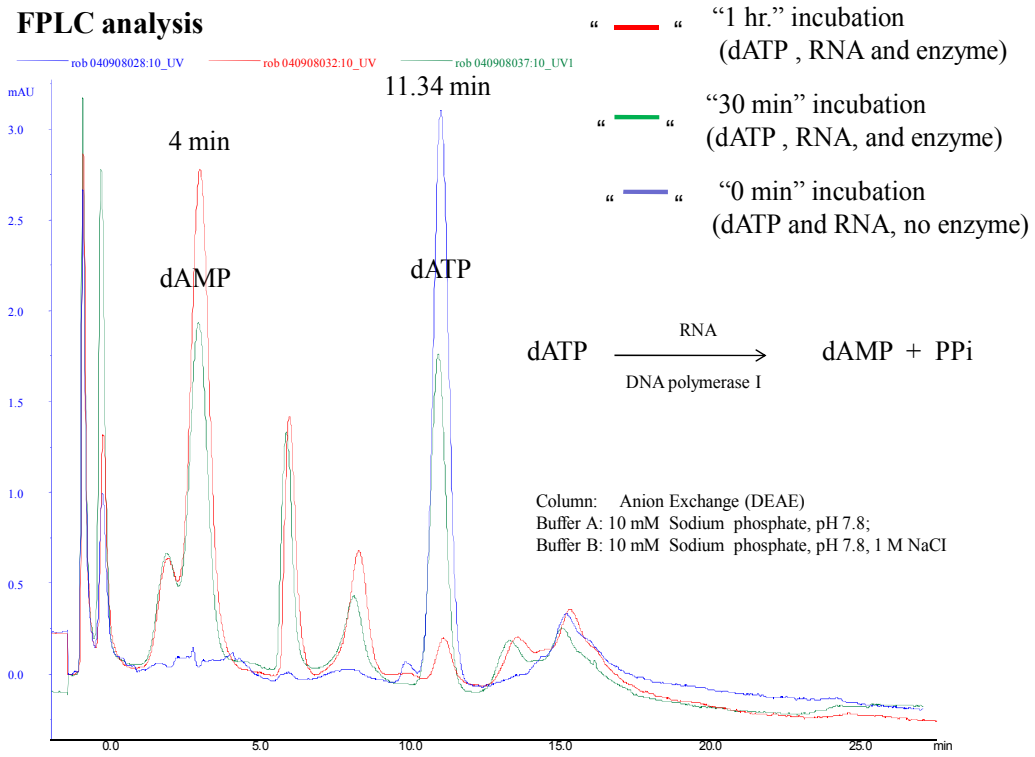

Figure 3: FPLC analysis showing the generation of dAMP as a product of dATP hydrolysis by DNA polymerase I in the presence of *E.coli* total RNA.

Figure 3: FPLC analysis showing the generation of dAMP as a product of dATP hydrolysis by DNA polymerase I in the presence of *E.coli* total RNA.

The substrate dATP was incubated with DNA polymerase I in the presence of *E.coli* total RNA for different time periods and analyzed by anion exchange column. Blue -"0 min", *E.coli* total RNA and dATP (without DNA polymerase I), only dATP peak at retention time 11.34 min with UV intensity 3.5 mAU was observed and no peak showed up at 4.0 min retention time. Green - *E.coli* total RNA, dATP, and DNA polymerase I incubated for 30 min. The dATP peak was reduced to 2.75 mAU and simultaneously dAMP peak appeared at 4.0 min retention time with UV intensity 2.0 mAU. Red - *E.coli* total RNA, dATP, and DNA polymerase I incubated for 1 hr. The 11.34 min dATP peak totally disappeared and the dAMP peak at 4.0 min retention time and UV intensity was increased from 2.0 mAU to 2.75.

Retention time profiles of dAMP and dATP in chromatographic analysis

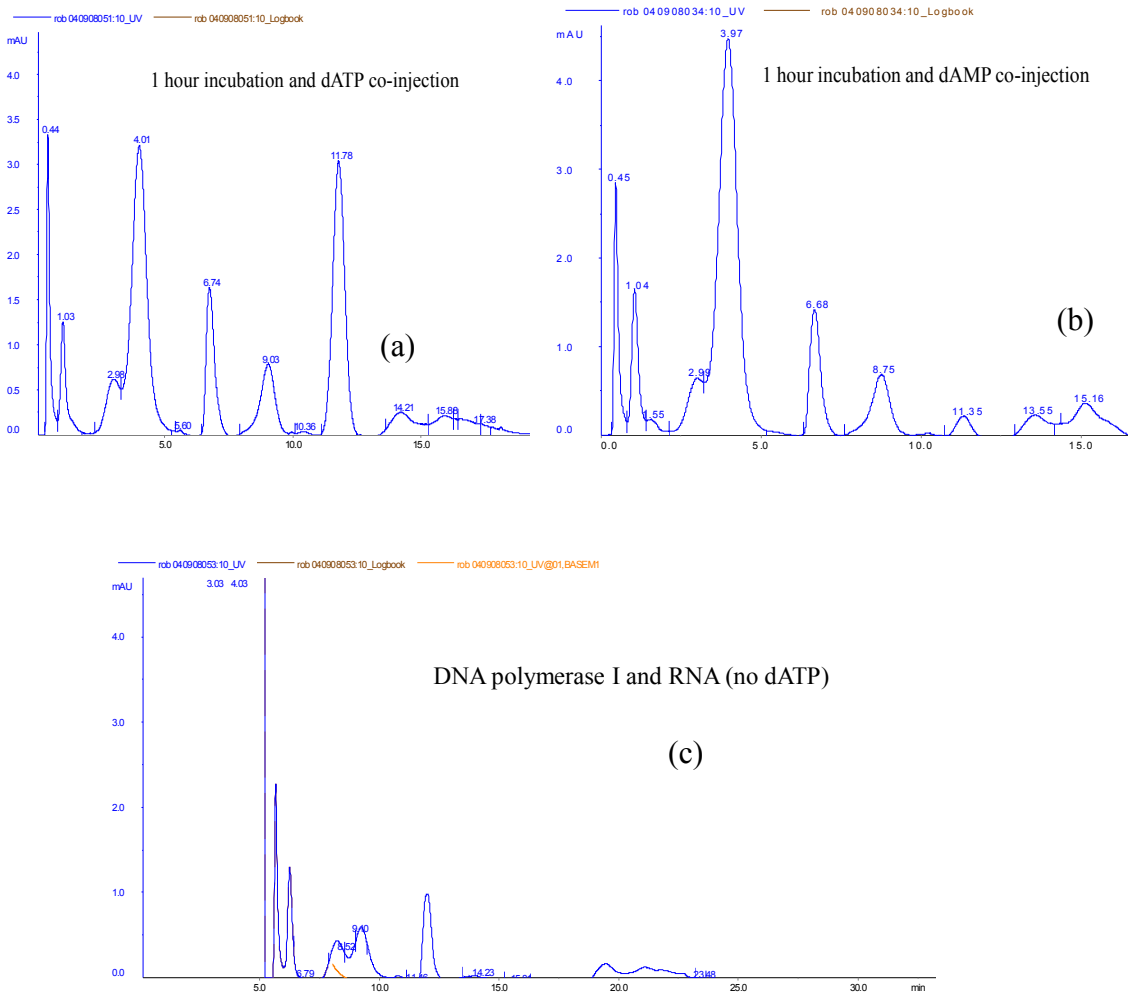

Figure 4. FPLC analysis showing the retention time of dAMP and dATP eluted from anion exchange column.

Figure 4. FPLC analysis showing the retention time of dAMP and dATP eluted from anion exchange column.

(a) dATP was mixed with the reaction (dATP, RNA, and Klenow DNA polymerase) that has incubated for 4 hours. The resulted mixture was injected into anion exchange column. The UV intensity of dATP peak at retention time 11.34 has increased (comparing with "red" in figure 3). (b) dAMP was mixed as the same as in (a) following same procedure. The peak at retention time 4.0 min was raised from UV intensity 3.0 mAU to 4.3 mAU. (c) RNA and Klenow DNA polymerase were incubated for 1 hour (without substrate dATP) and was injected into anion exchange column following the same procedure. There was no peaks were observed at 4 min (dAMP) and 11.34 (dATP) min that have seen in (a) and (b).

When the same reaction mixture was incubated for 30 min by the addition of DNA polymerase I, the same dATP peak was observed but with decreased UV intensity (2.75 mAU). This "30 min" incubation reaction has generated the products dAMP that can be visualized at retention time 4 min (green) with UV intensity 2.0 mAU. After incubating the same reaction for one hour, all the products (dATP) were hydrolyzed, as a result there was no dATP peak was visualized at retention time 11.35 min (red). This disappearance of the substrate was due to the hydrolysis of dATP that can be observed as conversion to dAMP that appeared at the retention time 4.0 min with higher UV intensity. It was also noticeable that in "0 min" (blue) there was no peak for dAMP but at "30 min" (green) the dAMP peak appeared with UV intensity 2.0 mAU which was increased to 2.75 mAU by "1 hr" incubation (red). So the anion exchange chromatographic results has proven the presence of the product dAMP in the reaction mixture that contained the substrate dATP, DNA polymerase I, and RNA. The retention time of dAMP and dATP, 4.0 min and 11.34 min, respectively, was confirmed by mixing dAMP or dATP with 1 hr incubation mixtures and were analyzed using the same procedure described in Figure 3. It could be observed that in "1 hr" reaction where all the dATP was hydrolyzed (red, Figure 3), by the addition of the dATP in the same reaction, the UV intensity was re-appeared at the same retention time 11.34 min (Figure 4b). So it was very much clear that the peak at retention time 11.34 min in Figure 3 was for the substrate dATP. In the same manner the peak at 4 min in Figure -3 (red) which was increased from the UV intensity 2.75 mAU to 4.5 mAU by the addition of dAMP was for the product dAMP (Figure 4b).

2.4.4 Mass spectrometry showed dAMP as a product in RNA dependent dATP hydrolysis by DNA polymerase I

In order to confirm further the dAMP as a product of dATP hydrolysis by RNA dependent DNA polymerase I, we analyzed the reaction product by mass spectrometry. The dAMP peak (Figure 3, retention time 4 min) from anion exchange column which has been incubated for one hour (red, Figure 3) was collected. The sample was desalted by desalting column and dAMP was separated by HPLC using C-13 column (hydrophobic column). A gradient 40 % acetonitrile was used to elute dAMP from C-13 column. Elute from C-13 column was lyophilized and analyzed by mass spectrometer. Results is shown in Figure 5 and dAMP peak was observed with a molecular mass 330 ($[M-H]^-$). This mass spectrometry analysis provided the evidence that dAMP was the product of dATP hydrolysis by DNA polymerase I in the presence of RNA.

Mass spectrometry shows dAMP as a product in RNA-dependent dATP hydrolysis by DNA polymerase I

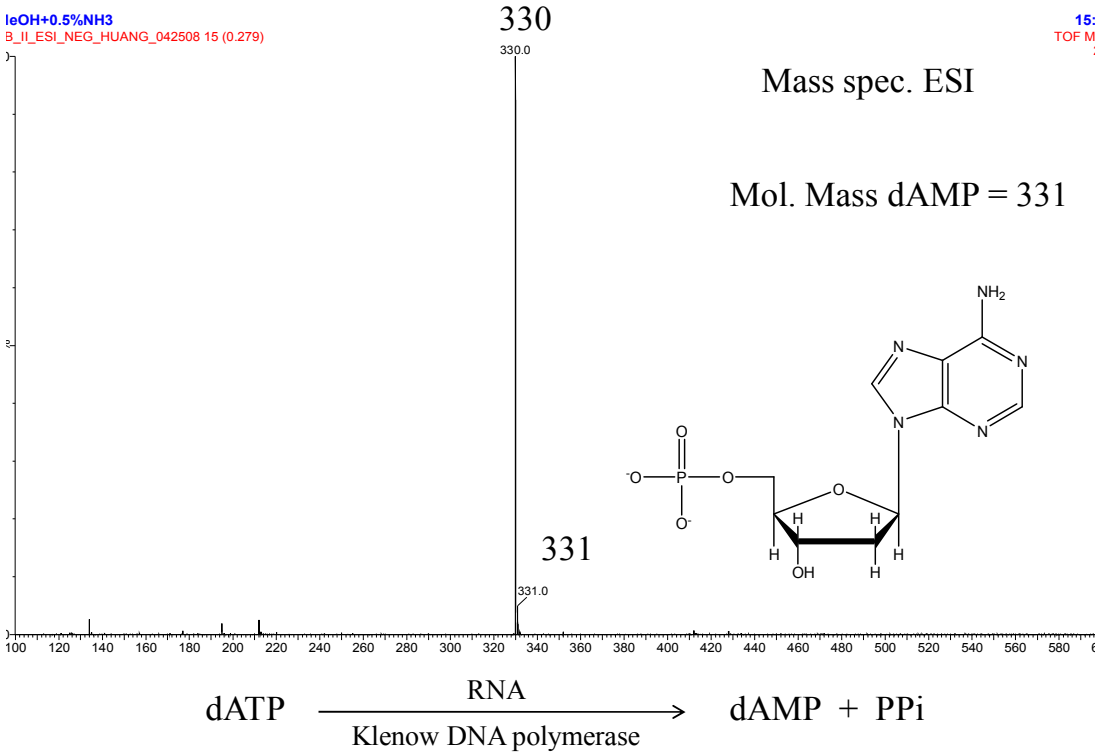

Figure 5. Mass spectrometry analysis showing dAMP as a product in RNA-dependent dATP hydrolysis by DNA polymerase I.

The MS was analyzed by electrospray ionization method $[M-H]^-$. The molecular mass of dAMP is 331and removing one proton the mass appeared as 330 for major species.

2.4.5 The second product of dATP hydrolysis was pyrophosphate (PPI) in RNA-dependent catalysis by DNA polymerase I

Deoxyribonucleoside triphosphates (dNTP) were found to hydrolyze into two products, deoxyribonucleoside monophosphates and inorganic pyrophosphate, by DNA polymerase I in the presence of RNA (Figure 1, 2). The product dAMP was confirmed by placing cold dAMP as reference and co-spot with reaction that produced dAMP. The presence of dAMP was further established by FPLC (Figure 3) and mass spectrometry analysis (Figure 5). In order to proof the PPi as another reaction product of RNA dependent dATP hydrolysis, ^{32}P-γ--dATP was incubated with DNA polymerase I and RNA. In ^{32}P-γ-dATP, the terminal gamma phosphate was radio-labeled and upon hydrolysis into dAMP and PPi, only the PPi, but not dAMP, would be visualized on radiogram when run on the TLC plate. First, a marker was developed by partially hydrolyzing γ-^{32}P-ATP with 10 mM NaOH (90 ºC, 1 hr incubation), to generate pyrophosphate, monophosphate, and non-hydrolyzed γ-^{32}P-ATP. The marker was used to detect the relative positions of the products generated from ^{32}P-γ--dATP hydrolysis by DNA polymerase I in the presence of RNA. The alkali hydrolysis of γ-^{32}P-ATP produced three bands, ^{32}PPi (bottom), ^{32}Pi (middle), and nonhydrolyzed ^{32}P-γ-ATP (Figure 6, lane-1). The position of nonhydrolyzed ^{32}P-γ-ATP was confirmed by placing intact ^{32}P-γ--ATP (Figure 6, lane-3) and ^{32}PPi by hydrolyzing it with inorganic pyrophosphatase enzyme. The partially alkali hydrolyzed reaction was neutralized by10 mM HCL and the reaction was treated with inorganic pyrophosphatase. By this enzyme,^{32}PPi was hydrolyzed to ^{32}Pi and as a result the ^{32}PPi was disappeared and accumulated as ^{32}Pi in lane- 2 (Figure 6). The intensity of ^{32}Pi band in lane- 2 (Figure 6) became stronger than in lane- 1 (Figure 6).

^{32}P- γ -dATP hydrolysis showed pyrophosphate (PPI) was the second product in RNA-dependent catalysis by DNA polymerase I

^{32}P- γ-dATP	-	-	-	-	+	+	-	+
^{32}P-γ- ATP	+	+	+	+	-	-	+	-
Pyrophosphatase	-	+	-	+	-	+	-	-
RNA (*E. coli*)	-	-	-	-	+	+	+	-
DNA pol I	-	-	-	-	+	+	+	-
NaOH	+	+	-	-	-	-	-	-

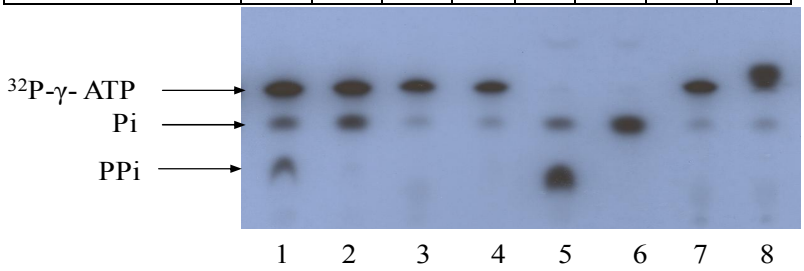

Figure 6. Generation of pyrophosphates during the hydrolysis of γ-^{32}P-dATP by the DNA polymerase I in the presence of RNA.

Figure 6. Generation of pyrophosphates during the hydrolysis of γ-^{32}P-dATP by the DNA polymerase I in the presence of RNA.

Ladder was generated by partial hydrolysis of ^{32}P-γ- ATP heated with 10 mM NaOH (final) at 90 °C for 30 min. Three species ^{32}P-γ- ATP, Pi, and PPi were observed on TLC plate (lane-1). Same amount of sample from lane 1 was neutralized to pH 7.0 by HCL, and further incubated with the enzyme pyrophosphatase for 30 min at 37 °C to digest PPi into Pi that placed on lane- 2. All PPi converted in Pi (lane- 2). γ-^{32}P-dATP incubated with the DNA polymerase I in the presence of RNA loaded on lane 5, mostly PPi and little amount of Pi were produced. Equal amount of sample from lane 5 incubated with pyrophosphatase, all PPi converted into Pi (lane-6). ^{32}P-γ- ATP was incubated with DNA polymerase I and RNA and no hydrolysis was observed (lane- 7) (Lane- 3 and lane- 8, only ^{32}P-γ- ATP and ^{32}P-γ- dATP, respectively).

When the reaction containing ^{32}P-γ- dATP, DNA polymerase I, and *E.coli* total RNA was incubated for hydrolysis, inorganic pyrophosphate (^{32}PPi) was produced that can be seen in Figure 6, lane-5 (bottom band). The product dAMP was not visualised in X-ray film as the α-phosphate of dATP was not labeled with ^{32}P. In order to determine the presence of ^{32}PPi, equal amount of the reaction product (Figure 6, from lane- 5) was incubated with pyrophosphatase. The inorganic pyrophosphate was hydrolyzed into ^{32}Pi and Pi as a result ^{32}PPi disappeared and appeared as monophosphates (Figure 6, lane- 6). These observations indicated that inorganic pyrophosphate was produced by enzymatic hydrolysis of dNTPs by the DNA polymerase I in presence of RNA along with dAMP.

2.4.6 The substrate of DNA polymerase I in RNA dependent hydrolysis was only the deoxyribonucleotides (dNTP's)

The substrate of DNA polymerases are deoxyribonucleotides in DNA polymerization reaction. Binding of dNTP to the Klenow DNA polymerase occurs through the interactions of several positively charged residues on the enzyme with the negatively charge on the phosphate oxygen of tri-phosphate nucleotides. The residues Lys-758, Arg-682 and His-734 on the "O" helix interact with the β and γ phosphates and anchor the nucleotide tri-phosphate on the enzyme. It has been proposed that DNA polymerase I employ several mechanisms to incorporate correct nucleotide into the growing DNA chain. At the first defense the steric gate build by the residues Glu-710 and Tyr-766 prevents ribonucleotides to enter into the active site. It has been suggested that Glu-710 is hydrogen-bonded to the γ-OH of the invariant tyrosine at the C terminus of the O-helix (Tyr-766), with the consequence that the aliphatic carbons of the Glu side chain are

positioned such that they could exclude the 2'-OH of an incoming rNTP (figure 8) (*100-102*). Other two approaches have proposed unambiguously that distinguish a correct or an incorrect nucleotide. First, noncomplementary nucleotides bind to the polymerases in the ground state more weakly than a complementary dNTP (*103*). Second, it is believed that only a complementary nucleotide allows a rapid conformational change to form a ternary complex that aligns the nucleotide and 3'-OH of the primer in the correct orientation for the formation of a phosphodiester bond (*2, 63*). By these precise and elaborate mechanisms DNA polymerases prevent non-canonical substrates from incorporating into the DNA growing chain.

In RNA-dependent catalysis, Klenow fragment uses dNTP as a substrate

α -^{32}P dCTP	+	-	+	-	+	-	+	-	-	-	-	-	-	-	-	-
α -^{32}P rCTP	-	+	-	+	-	+	-	+	-	-	-	-	-	-	-	-
α -^{32}P dATP	-	-	-	-	-	-	-	-	+	-	+	-	+	-	+	-
α -^{32}P rATP	-	-	-	-	-	-	-	-	-	+	-	+	-	+	-	+
RNA (*E.coli*)	+	+	-	-	+	+	-	-	+	+	-	-	+	+	-	-
RNA (Human)	-	-	-	-	-	-	+	+	-	-	-	-	-	-	+	+
Klenow frag.	-	-	+	+	+	+	+	+	-	-	+	+	+	+	+	+

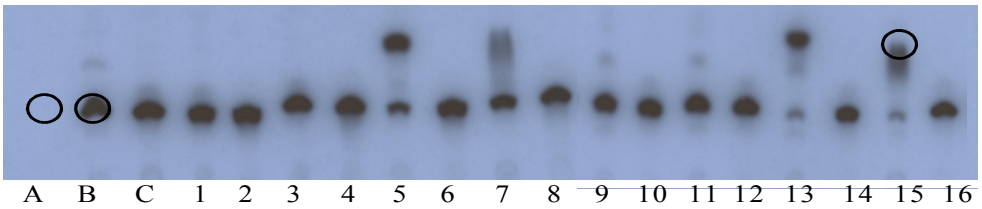

Lane- 1. dCTP and RNA, lane- 2. RNA and rCTP, lane- 3. dCTP and Klenow fragment, lane- 4. rCTP and Klenow fragment Lane- 5. dCTP, RNA, and Klenow fragment, lane- 6. rCTP, Klenow fragment and RNA, lane- 7. dCTP, RNA and Klenow fragment, lane- 8. rCTP, RNA (human), and Klenow fragment, lane- 9. dATP and RNA, lane- 10. rATP and RNA, lan- 11. dATP and Klenow fragment, lane- 12. rATP and Klenow fragment Lane- 13. dATP, RNA, and Klenow fragment, lane- 14 rATP, RNA, and Klenow fragment, lane- 15. dATP, RNA (human), and Klenow fragment, and co-spot with dCMP, lane- 16. rATP, RNA (human), and rATP Klenow fragment. A.Cold dATP, B. Co-spot of cold dATP and ^{32}P-α- dATP, C. ^{32}P-α- dATP by itself; RNA (*E.coli*): E.coli total RNA; RNA (human): Human total RNA; Klenow frag.: Klenow fragment

Figure 7: In RNA-dependent catalysis Klenow fragment used dNTP as a substrate but not rNTP.

Figure 7: In RNA-dependent catalysis Klenow fragment uses dNTP as a substrate but not rNTP. Two deoxy- (dATP, dCTP) and two ribo- (ATP, CTP) nucleotides were used as substrate in the hydrolysis reaction to observe substrate preference by the Klenow fragment in RNA dependent catalysis. dCTP,s were used in lane- 1, 3, 5, and 7 and we monitored its hydrolysis by various combinations. In presence of Klenow fragment and *E.coli* RNA (lane- 5) or human RNA (lane-7) dCTP's were hydrolyzed. But in the presence of only RNA (lane- 1) or in the presence of only enzyme (lane- 3), dCTP was not hydrolyzed. In lane- 9, 11, 13, and 15 dATP substrate was examined. In presence of Klenow fragment and *E.coli* RNA (lane-13) or human RNA (lane-15) dATP's were hydrolyzed. But in the presence of only RNA (lane-9) or in the presence of only enzyme (lane-11), dATP's were not found to hydrolyze. But the CTP or ATP was not observed to hydrolyze in the presence or absence of RNA or Klenow fragment.

Active site of Klenow fragment designed to prevent rNTP from incorporating into DNA growing chain

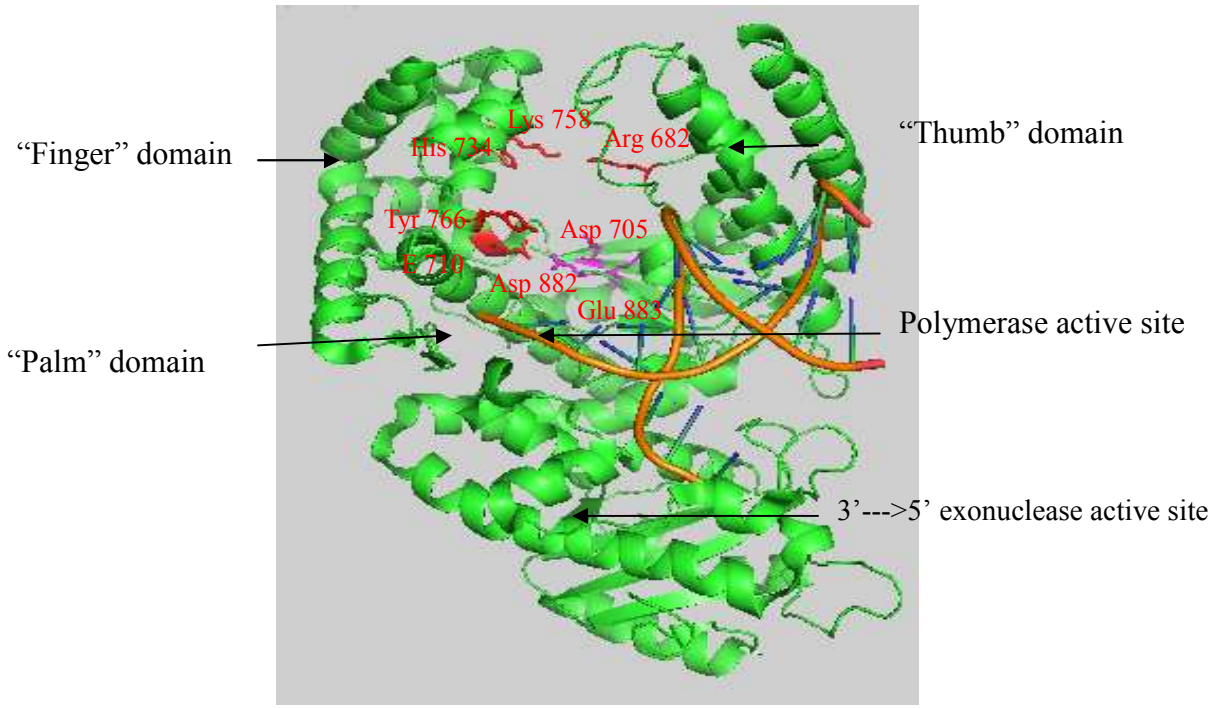

Ollis, D. L., Brick, P., Hamlin, R., Xuong, N. G. & Steitz, T. A. (1985) *Nature (London)* **313,** 762–766. (PDB: 1KLN)

Figure 8: Cartoon diagrams of Klenow fragment complex with dsDNA. The important amino acid residues involved in dNTP binding, so-called steric gate and polymerase active site. Residues Lys-758, Arg-682, Arg-754, and His-734 interact with β and γ phosphate of dNTP. The uncharged portion of dNTP, deoxyribose ring, interacts with Phe762. Glu-710 makes "steric gate" with Phe 762 which prevents rNTP to enter into active site. Asp 705, Asp 882, and Glu 883 on the "palm" domain coordinates with the metal ions in the active site. The 3'-end of the primer DNA is in 3'-5' exonuclease active site.

The X-ray crystallographic structure of Klenow fragment is presented in Figure 8. Two active sites are present in Klenow fragment, namely, polymerase and 3'--->5' exonuclease active site. The incoming dNTP anchored on the "finger" domain and the oxygen atoms on β and γ phosphate of dNTP electrostatically interact with the residues Lys-758, Arg-682, Arg-754, and His-734. Upon binding of dsDNA on the "thumb" domain the resulted conformational change of the enzyme allows dNTP to enter into the active site. On route to polymerase active site located on the palm domain, so called "steric gate" created by the Glu-710 prevents rNTP to enter. The side chain of glutamate repulses the 2'-OH of the ribose sugar and this is one of the intrinsic properties of Klenow fragment that maintain the fidelity in DNA synthesis. Our RNA-dependent dNTP hydrolysis by DNA polymerase I suggests the same phenomenon might restrict the rNTP to enter into the active site. Because we observed that Klenow fragment hydrolyzes only dNTP that depend on RNA. We found that deoxy-ribonucleotide from both purine (Figure 2) and pyramidine (Figure 1) were hydrolyzed by DNA polymerase I in the presence of RNA. It is established that the DNA polymerase I prefers dNTP as a substrate for DNA polymerization over rNTP. We extended our study to observe whether rNTP could be utilized by DNA polymerase I as a substrate for hydrolysis activated by RNA. We incubated rCTP or rATP with Klenow fragment and the results were presented in Figure 7. It was observed that neither rCTP (Figure 7, lane -6, 8) nor rATP (Figure 7, lane-14, 16) was hydrolyzed by Klenow fragment in the presence of *E.coli* (Figure 7, lane -6, 14) or human (Figure 7, lane - 8, 16) RNA. On the other hand dCTP (Figure 7, lane - 5, 7) or dATP (Figure 7, lane -13, 15) was hydrolyzed in the presence of E.coli (Figure 7, lane -5, 13) or human (Figure 7, lane - 7, 15) RNA. From these set of results it can be concluded that the DNA polymerase I uses only dNTP as a substrate in RNA dependent catalysis.

Crystal structure of Klenow fragment complex with DNAduplex showing backbone interaction with enzyme and different sheets and helices

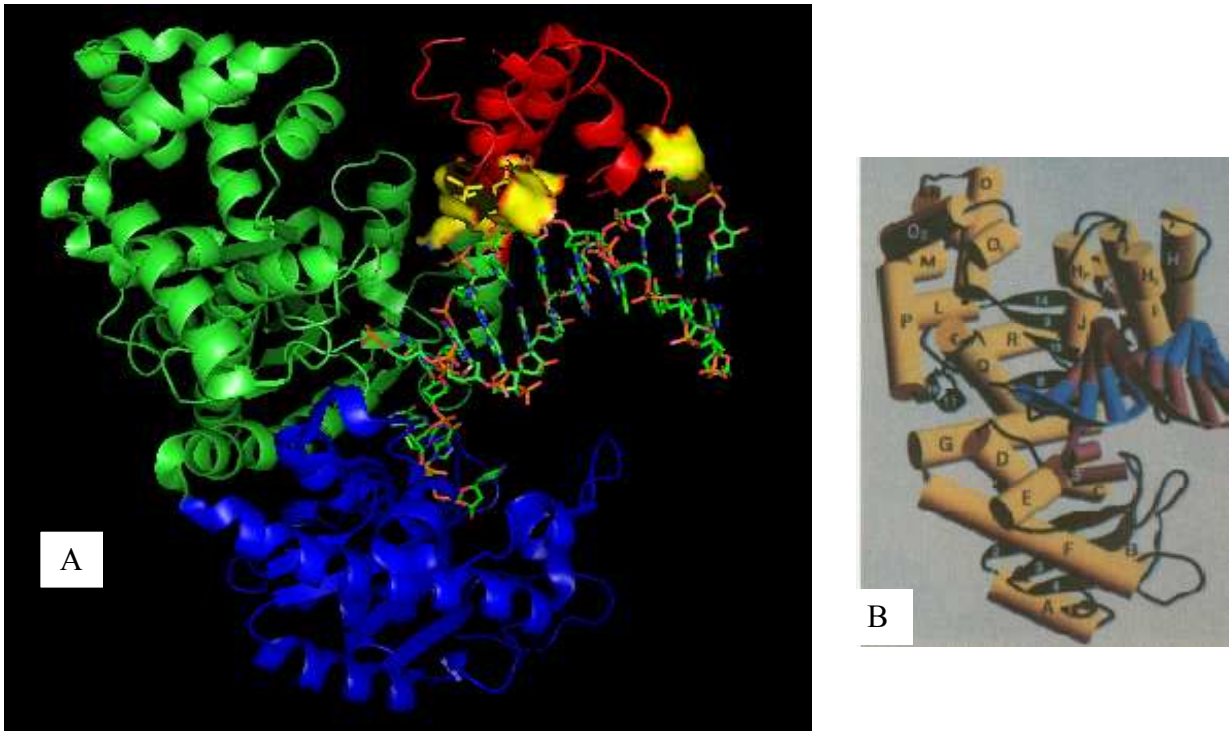

Beese,L.S., Derbyshire,V., Steitz,T.A.(1993) Structure of DNA polymerase I Klenow fragment bound to duplex DNA Science 260: 352-355, (PDB: 1KLN)

Figure 9: Crystal structure of Klenow fragment (aa 324-927) complex with DNA duplex (13nts/10 nts). Residues constitute 3'-5' exonuclease domain (aa 324-517) shown in blue. Polymerase domain (aa 518-927) shown in red. Negatively charge DNA backbone interact with the conserved amino acids Asn-575, Lys-635, Arg-631, Glu-611, Thr - 609 on the polymerase domain (conserved amino acid highlighted yellow). The 3'-end of 3-nts overhang is in the 3'-5' exonuclease active site. (b) Helices and sheets of the Klenow fragment.

Conformational change Klenow fragment upon binding of DNA duplex

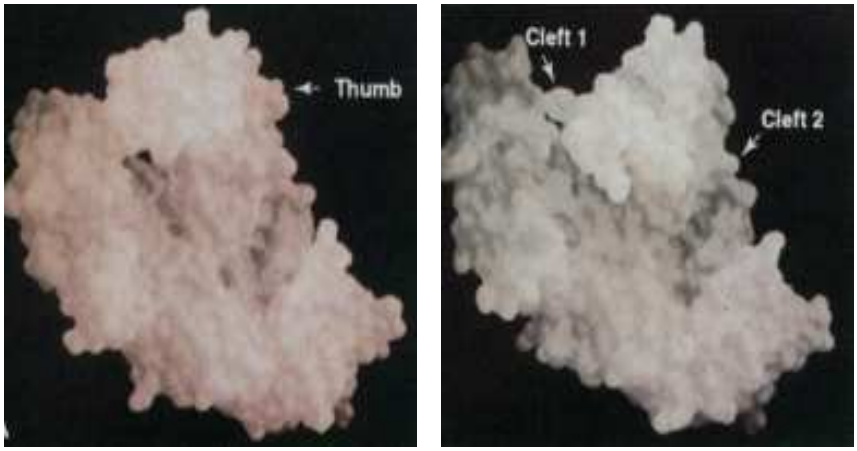

Beese,L.S., Derbyshire,V., Steitz,T.A.(1993) Structure of DNA polymerase I Klenow fragment

Figure 10. Differences in protein (Klenow fragment) conformation upon binding of DNA duplex. (a) Representation of the solvent accessible surface of apo-KF. (b) Representation of the solvent accessible surface of KF when bound to DNA. Cleft 1 contains the polymerase active site. Cleft 2 is formed upon binding duplex DNA, which it contains.

Crystal structure of Klenow fragment binding with single stranded DNA

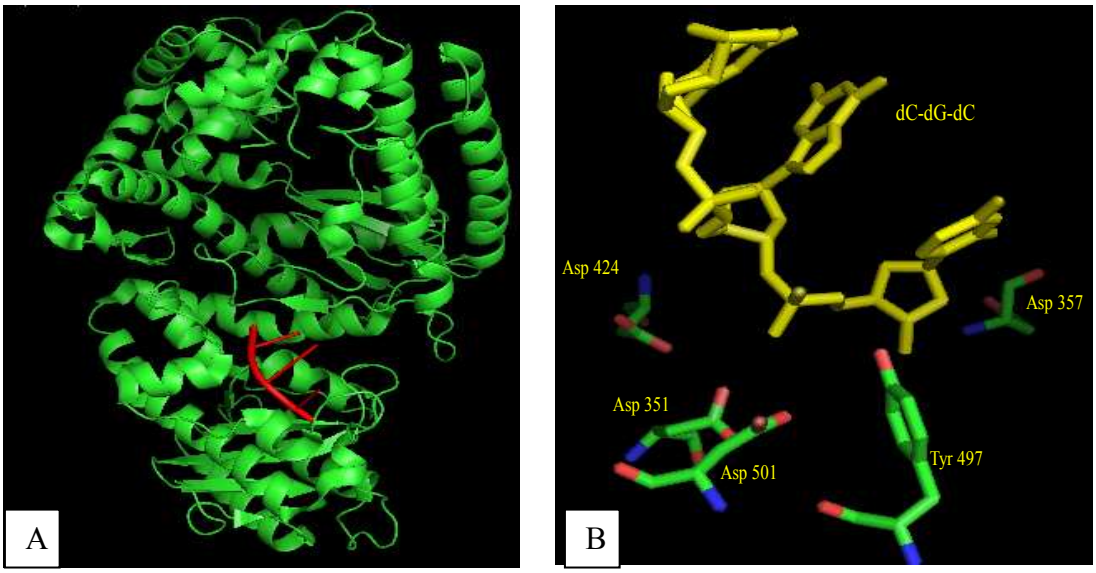

Lam WC, Thompson EH, Potapova O, Sun XC, Joyce CM, Millar DP
2002 Mar 26;41(12):3943-51.

Figure 11. X-ray crustallography structure of Klenow fragment showing (A) cartoon structure with 3-nts long single stranded DNA in 3'---->5' exonuclease active site (B) 3-nts long single stranded DNA in 3'---->5' exonuclease active site surrounded by amino acid residues involved in catalysis.

2.4.7 Binding of RNA with DNA polymerase I is fairly strong

The crystal structure of Klenow fragment complex with DNA duplex presented in Figure 9 was published in 1985 by Ollis, D. L., *et. al*. Binding of DNA duplex with Klenow fragment was found to create a conformational change in the protein. Comparison of the apo and DNA complex structures showed that a conformational change occurs in a thumb-like region of the protein that makes direct contacts with the duplex portion of the DNA (Figure 10). Residues 558 to 637, including two long helices, H and I (Figure 9B), move toward the 3' to 5' exonuclease domain to interact with the DNA. The DNA-induced conformational change in Klenow fragment produces an obvious second cleft between the thumb and the exonuclease domain into which the duplex DNA binds. Binding of duplex DNA are made exclusively through protein interactions with the DNA phosphate backbone. The side chains of the residues Asn-575, Lys-635, Arg-631, Glu-611, Thr – 609 which are conserved in DNA polymerase I make interaction with O-atoms on the backbone phosphates. Dissociation constant (K_d) of Klenow fragment and duplex DNA showed very tight binding with a K_d 1.4 nM (*102*) that has been observed from gel-shift assay.

Gel shift assay for binding of DNA polymerase I with RNA

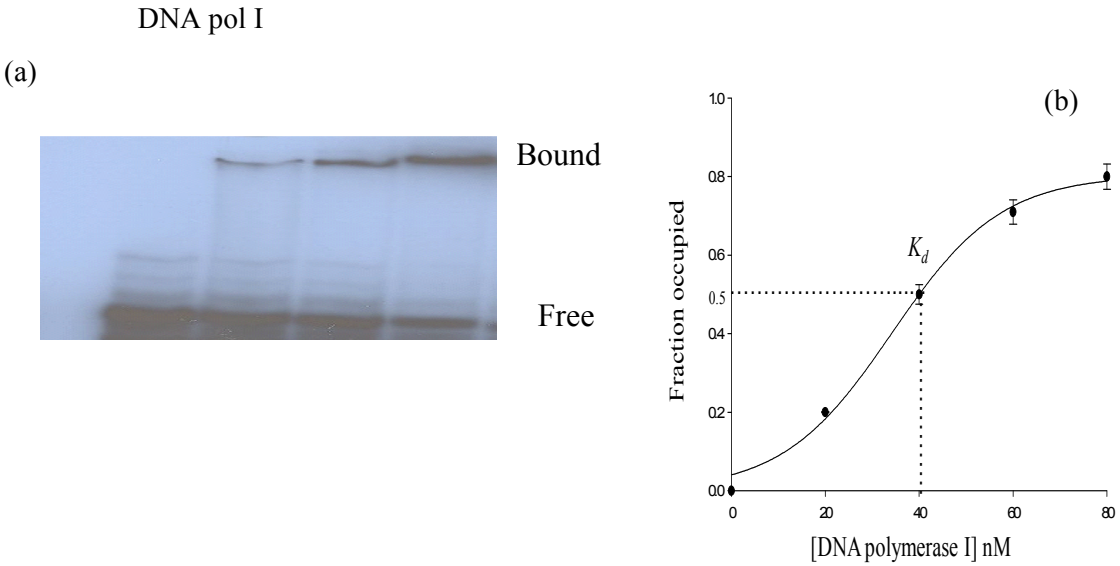

Figure 12. (a) Gel shift assay for binding of DNA polymerase I with RNA. Different amount of DNA polymerase I, 0, 20, 40, 60, or 80 nM was incubated with fixed amount RNA (50 nM). Top band showing bound RNA with DNA polymerase I and bottom band contains free RNA. (b) Dissociation constant of DNA polymerase I binding to RNA. The estimated K_d is 42.8 nM.

Binding of Klenow fragment with single stranded DNA also reported. In crystal structure of three nucleotides long single stranded DNA and Klenow fragment complex, the single stranded DNA was observed in 3'--->5' exonuclease site (Figure 11A). It has been observed that the 3'-OH end was surrounded by the residues involved in 3'--->5'exonuclease catalysis (Figure 11B). The biochemical and kinetic studies showed that the 3'--->5'exonuclease function of Klenow DNA polymerase hydrolyzed single stranded DNA from the 3'-end in DNA duplex containing 3'-end overhang. Until recently, there was no study have been made in the perspective of RNA interaction with Klenow DNA polymerase.

In our present study we observed the interaction of RNA with Klenow fragment causing hydrolysis of NTP. We speculated that this interaction must be occurred through the binding of RNA with Klenow fragment. Gel-shift assay has been conducted to examine whether the RNA binds to DNA polymerase I and from the dissociation constant of binding was determined.

For the gel shift assay ^{32}P-labeled RNA (55-nts) was mixed with cold RNA to make the final concentration 50 nM. The RNA mixed with 20 nM, 40 nM, 60 nM, or 80 nM DNA polymerase I in binding buffer (10 mM KCI, 1 mM DTT, 5 % glycerol, pH 7.0, final) and incubated at room temperature for 30 min. The mixtures were then placed at 4 °C for overnight. Before loading on the gel, the reaction materials were mixed with gel loading dye (10 mM KCI, 1 mM DTT, 5 % glycerol, 0.001 % xylene blue (W/V), final) and loaded on 10 % non-denaturing polyacrylamide gel. The composition of running buffer was 5 mM tris chloride with 10 mM EDTA and pH was adjusted to 7.5 with acetic acid. Before loading samples the gels were pre-run for 1hr to remove

ammonium per sulfate (APS). The gels were run with a constant voltage (250 volts) for one hour in 4 C° cold room. Gels were fixed with 7% acetic acid, dried, scanned, and bands were quantified using a PhosphorImager. Image was also taken by exposing on X-ray film. Results were shown in figure 12. The amount of complex formed at equilibrium was estimated from the ratio of band intensities of free RNA to the intensity of the band without the addition of polymerase. This analysis allows measurement of the amount of complex formed in solution before it was loaded on the gel and the neglect of the slight amount of dissociation of RNA-protein complexes which occurs in the gel. The fraction of RNA bound was plotted against enzyme concentration and K_d (the concentration at which 50% of the RNA is bound) was determined by interpolation. The estimated K_d of DNA polymerase I binding to RNA was 42.8 nM. This is the first time reporting of binding single stranded RNA to DNA polymerase I although the single stranded DNA binding with Klenow fragment has been reported.

2.4.8 dNTP hydrolysis depend on RNA concentration

Activation of enzyme requires for many catalysis. Those enzymes activity is sensitive to the presence of specific substances that bind to the enzyme and causes conformational change in the enzyme. In allosteric regulation an activator binds to the regulatory site of the enzyme (other than the enzyme active site) causes conformational change so that enzyme can bind to substrate efficiently. In this circumstance the enzyme activation regulation also obey the Michaelis-Menten kinetics. If the enzyme concentration remains constant, the addition of excess activator will not bring any change in the rate of catalysis. In our present study we provided ample data that shown the DNA polymerase I hydrolyzes dNTP if RNA present in the reaction media. At this time point we were not certain how RNA binds and regulates the enzymatic activity of DNA polymerase I. We have conducted study by increasing RNA concentration gradually while keeping the enzyme and substrate concentration constant. The aim of this experiment was to understand whether the RNA concentration has any effect on dNTP hydrolysis.

We observed from the gel-shift assay (Figure 12) that the fraction of RNA bound to DNA polymerase I increased as the enzyme concentration increases. It also means that the fraction of DNA polymerase I bind to RNA is depending on RNA concentration. This effect we monitored by incubating dNTP at different RNA concentrations while keeping the enzyme concentration constant (50 nM). Fixed amount of dCTP (500 nM) was incubated with DNA polymerase I and 10-160 nM RNA (Figure 13). It has been observed that hydrolysis of dCTP increased with the increasing in RNA concentration. But after certain RNA concentration (60 nM, lane-7, Figure 13a) the hydrolysis did not increased significantly although the RNA concentration has been increased (lane 8-12, Figure 13a). The reason we did not observed the significant differences in

hydrolysis might be the RNA binding site of Klenow DNA polymerase (50 nM) saturated with the 50 nM RNA. This observation indicated that each molecule of RNA interacts with the same number of enzyme molecule which does not obey the Michaelis-Menten kinetic principle.

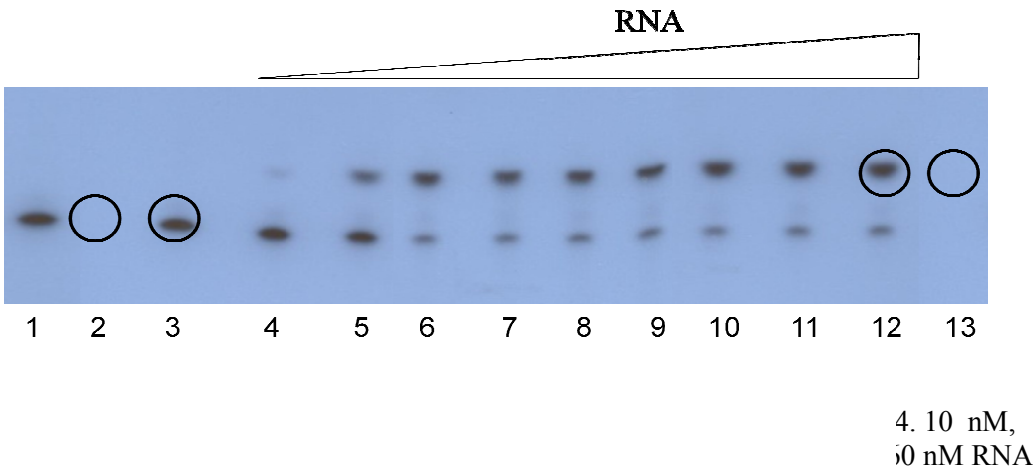

Figure 13. Degradation of α-^{32}P-dCTP in presence of DNA polymerase I and different amount of RNA. dCTP (500 nM, final) incubated with DNA polymerase I (50 nM, final) and 10, 20, 40, 60, 80, 100, 120, 140 or 160 nM of 55-nts RNA (lane 4-12). 1 µCi of α-^{32}P-dCTP added to cold dCTP to visualize on the X-ray film and phoshoimager plate. In lane 2, RNA was replaced with H_2O in reaction and referred to as "0" RNA. All reactions were incubated at 37 °C for 30 minutes. The presence of hydrolysis product dCMP visualized by exposing X-ray film and by comparing with the corresponding reference spots (lane-13) and co-spot (lane-12) of cold dCMP under UV light. It was found that dCTP degradation started at 10 nM RNA concentration (lane 4) and reached maximum at 60 nM RNA concentrations (lane-7) which was 80 %. The amount of dCTP hydrolysis was not observed to increase further as with increasing RNA concentrations. (b) Graphical representation of the dCTP hydrolysis by placing RNA concentration on X-axis and % hydrolysis on Y-axis.

2.4.9 Hydrolysis of dNTP inhibits DNA polymerization

In the course of our study we observed that *in vitro* DNA polymerase I hydrolyze dNTP in the presence of RNA. The estimated amount we learn from time course analysis was 800 nM dCTP in an hour (Figure 1). We also identified DNA polymerase I hydrolyzed both purine and pyramidine deoxynucleotide with the same preference (Figure 1 and 2). These observations lead us to appreciate whether the hydrolysis of DNA precursors in the presence of RNA bears any significant effect in DNA synthesis. We annealed DNA template (55-nts) with DNA primer (21-nts) and polymerization was initiated by adding DNA polymerase I, buffer (10 mM Tris-HCl, 10 mM MgCl2, 50 mM NaCl, 1 mM dithiothreitol, pH 7.9), and dNTP. The dNTP concentration was maintained to 10 mM, which was more than enough to support DNA synthesis under present primer-template concentration. To observe the effects of RNA, various amount of RNA were added to the polymerization reactions. The reactions were incubated for 30 min at 37 °C containing 0, 10, 20, 40, 80, 100, 150, or 200 nM RNA (final). It can be observed when the RNA concentration increased in the polymerase reaction the DNA synthesis decreases (Figure 14, lane- 3-7). Maximum DNA synthesis occurred in absence of RNA (Figure 14, lane-2) whereas maximum inhibition was observed at 200 nM RNA (Figure 14, lane-7, 88%) in comparing with the negative control (Figure 14, lane-2). These results suggest that the dNTP hydrolysis by the DNA polymerase I caused dNTP depletion from the dNTP pool. Since from from the hydrolysis the dNTP level falls below threshold concentration, it could no longer supported the DNA synthesis.

Inhibition of DNA polymerization via dNTP hydrolysis by DNA polymerase itself

(a)

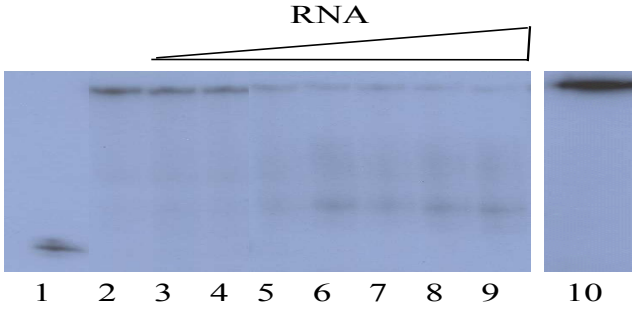

Lane 1. Primer, lane 2. No RNA, lane 3. 10 nM, lane 4. 20 nM, lane 5. 40 nM, lane 6. 80 nM, lane 7. 100 nM, lane 8. 150 nM, 9. 200 nM, RNA, 10. Template

(b)

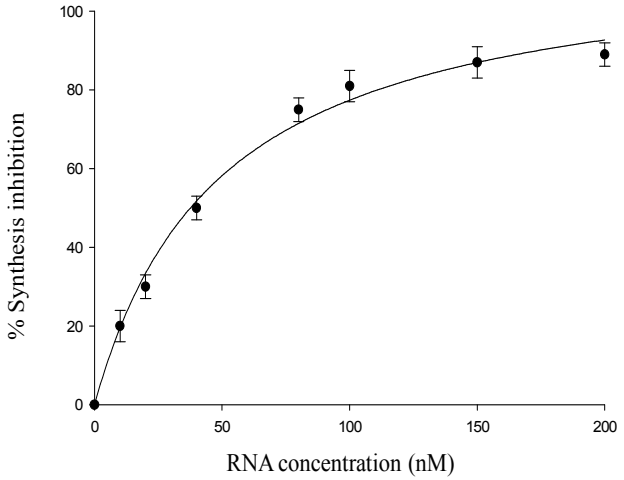

Figure 14: Inhibition of DNA polymerization via dNTP hydrolysis by DNA polymerase I itself.

Figure 14: Inhibition of DNA polymerization via dNTP hydrolysis by DNA polymerase I itself. (a) DNA template (55-mer) annealed with 5´- labeled primer (21-mer) and incubated with DNA polymerase I, RNA, and dNTPs. After 30 min incubation at 37 °C the reaction products were loaded onto 15% urea-polyacrylamide gel, dried after 2 h electrophoresis and autoradiographed. Lane-1, 5´-labeled primer; lane 2-7, polymerase reaction in the presence of RNA, 0, 10, 20, 40, 80, 100, 150, and 200 nM, respectively. It can be observed when the RNA concentration increased in the polymerase reaction, the DNA synthesis decreases. Maximum DNA synthesis occurs in absence of RNA (lane-2) and maximum inhibition occurred at 200 nM RNA (lane-7, 88%) in comparing with the negative control (lane-2). (b) Graphical representation of DNA synthesis inhibition by dNTP hydrolysis.

2.4.10 Pyrophosphate inhibits dNTP hydrolysis by Klenow DNA polymerase in the presence of RNA

Pyrophosphorylosis or PPi exchange reactions could occur in DNA polymerase I active site in addition to polymerization. These series of reactions in DNA polymerase I active site that might happened was first established by Deutscher and Kornberg in 1969. Pyrophosphorolysis is the reverse of the polymerization reaction in which pyrophosphate reacts with the 3'-nucleotide monophosphate (NMP or dNMP), which is removed from the oligonucleotide to release the corresponding triphosphate (dNTP from DNA, or NTP from RNA). Excising chain terminators by HIV reverse transcriptase (RT) using PPi or ATP is the most thoroughly investigated phenomenon (*104*) Certain HIV strains become resistant to drugs, such as AZT, which acts as a chain terminator during reverse transcription. Due to mutation in reverse transcriptase the organism able to enhance pyrophosphatase activity which add PPi in the chain terminator and remove the drug and become self replicative (*105*).

Pyrophosphorylosis $DNA_n + PPi \rightleftharpoons DNA_{(n-1)} + dNTP$

PPi exchange $DNA + dN\text{-}P\text{-}P\text{-}P + -*P\text{-}P \rightleftharpoons DNA + dN\text{-}*P\text{-}P\text{-}P + -P\text{-}P$

Inhibition of dCTP hydrolysis by pyrophosphates

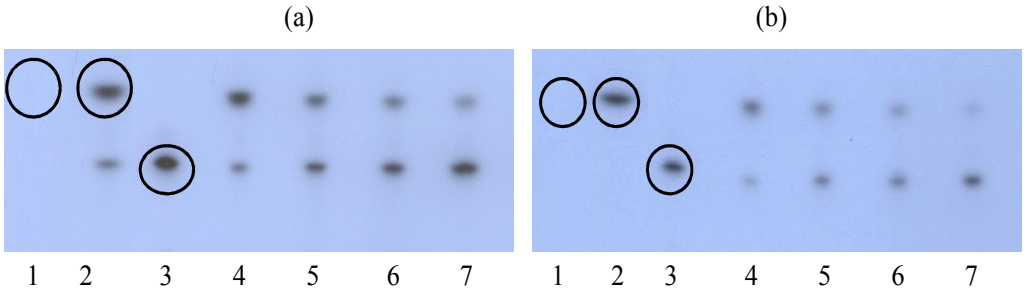

(a) 30 min incubation with PPi, (b) 1 hr incubation with PPi. Lane 1. Cold dCMP; lane 2. reaction with no added PPi and co-spot with cold dCMP; lane 3. Co-spot of cold dCTP and ^{32}P-α-dCTP; lane 4. 0.2 µM ; lane 5. 0.4 µM; lane 6. 0.8 µM ; lane 7. 1 µM, PPi.

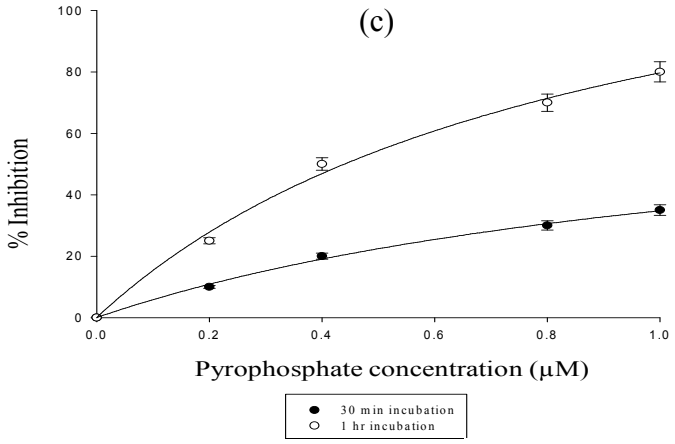

Figure 15. Inhibition of dCTP hydrolysis by pyrophosphates.

Figure 15. Inhibition of dCTP hydrolysis by pyrophosphates

A total 40 µl reaction containing RNA , dCTP, and Klenow fragment incubated with different amount of pyrophosphate at two different time periods (procedure same as in Figure 1 and 2). The reaction mixture of RNA, dCTP, and Klenow fragment with buffer distributed into 2 sets, 5 tubes in each set. Each tube contained 5 µl of the reaction materials. In each tube 0 (H_2O supplemented for PPi), 10 nM, 20 nM, 40 nM, or 60 nM pyrophosphates (final concentration) was added. One set incubated for 30 minutes and another for 1 hour. After incubation, the reactions were terminated by adding 1 mM EDTA and placing on ice. Each reaction was loaded onto TLC plate as described in methods and materials. The results showed that the dCTP hydrolysis by DNA polymerase I inhibited in both 30 min (a) and 1hr (b) incubations with pyrophosphate. Lane 2 (a and b) were incubated at the same time but H_2O was supplemented for pyrophosphate. It has been found that dCTP hydrolysis was inhibited where pyrophosphates were present (lane - 4-7). The inhibition observed was PPi concentration and time dependent. It was not observed without pyrophosphates (lane- 2). In 30 min incubation (a) 5 (lane- 4), 20 (lane- 5), 35 (lane- 6), and 40 (lane- 7) % and in 1 hr incubation (b) 15 (lane- 4), 45 (lane- 5), 70 (lane 6), and 80 (lane- 7) % inhibitions occurred by 0.2 µM, 0.4 µM, 0.8 µM, or 1 µM PPi, respectively, in comparing to the control (C, graph).

Pre-steady-state kinetic experiments showed that in Klenow fragment active site nucleotide insertion into DNA primer strand involves a number of sequential steps. It has been proposed that in the open conformation the Klenow fragment can bind to the primer terminus after which it is converted to the closed conformation by the incoming dNTP. Upon formation of a new phosphodiester bond, pyrophosphate is released, and the DNA polymerase returns to the open conformation, allowing for translocation of the enzyme to the new primer terminus. Binding of dNTP to the Klenow fragment occurs through the interactions of few positively charged amino acids located on "thumb" and "finger" domains. The residues are Lys-758, Arg-682, Arg-754, and His-734 which interact with β and γ phosphate of dNTP whereas the uncharged portion of dNTP, deoxyribose ring interacts with Phe762 (Figure 8) (*106*). Pyrophosphate was found to be interacting with the same residues as dNTP's do. It has been suggested that PPi binding site overlaps the dNTP binding site in the ternary complex and PPi acts as a competitive inhibitor in the polymerase reaction (*107*). We pursued our experiments to observe whether PPi could be the inhibitor in the dNTP hydrolysis reaction by Klenow fragment in the presence of RNA. We incubated the reactions containing RNA, dCTP, and Klenow fragment with different amount of pyrophosphate for 30 minutes (Figure 15a) and 1 hr (Figure 15b). For each set of time a total of four concentrations, 0.2 μM, 0.4 μM, 0.8 μM, or 1 μM PPi, were added. Each reaction was loaded onto TLC plate and visualized by exposing on the X-ray film and the location of products and substrates were detected from co-spot and each spot was quantified (see methods and materials for details). The inhibitory effect of PPi was determined by plotting the percent inhibition against PPi concentrations from interpolation by considering the reaction without PPi (Figure 15 a,b, lane- 2) as negative control (Figure 15c). It has been observed that PPi caused

significant amount of inhibition in dCTP hydrolysis in 30 min and 1 hr reaction periods in a dose dependent manner. The highest inhibition was observed in 1 hr at 1 μM PPi concentration which was 80% in comparing with control (Figure 15c). The concentration of Klenow fragment 50 nM and dNTP 0.5 μM were maintained in the reaction. It has been observed that the hydrolysis inhibited gradually with increasing PPi concentrations and dependent on time (Figure 15a,b, lane 4-7). It was also noticeable that the dCTP hydrolysis was not completely inhibited even the PPi concentrations were large excess to the substrate concentration (Figure 15 a,b, lane- 6,7). As the inhibition was depending on inhibitor concentration and time, it suggested that there was competition between inhibitor and substrate in binding to enzyme. The pyrophosphorylosis reaction also could happen that converted the product (dCMP) back into substrate by reacting with the inhibitor PPi. This also suggested that the similar reaction could ensue in the Klenow fragment enzyme reaction by interacting with RNA instead of primer-template.

A comparison of primer-template DNA bound to four DNA polymerases

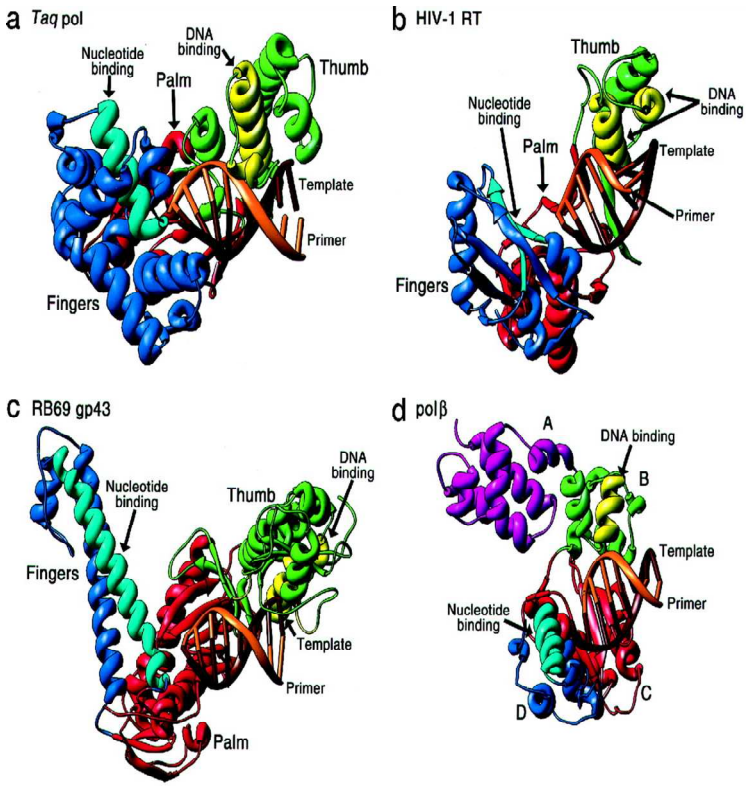

jbc

Figure 16: A comparison of primer-template DNA bound to four DNA polymerases.

Figure 16: A comparison of primer-template DNA bound to four DNA polymerases.

The complexes shown in A, B, and D are co-crystal structures, whereas the complex in C is a homology model. These four structures have been similarly oriented with respect to each other by superposition of the first two base pairs at the primer terminus. The primer strand and template strand are labeled. A, Taq DNA polymerase bound to DNA. As with the other three structures shown in this figure, the DNA stacks against the fingers and is contacted across the minor groove by the thumb domain. B,the binary complex of HIV-1 RT and DNA . This structure does not have a nucleotide-binding α-helix in the fingers domains. Instead, a β-hairpin probably performs this function. C, the model of DNA bound to RB69 gp43. A likely DNA-binding α-helix has been highlighted. It appears that the thumb domain would have to move toward the primer terminus to bind DNA analogously to the other polymerases.D, the ternary complex of rat pol β with DNA and dideoxy-NTP. Domain D plays the role of the fingers and presents an α-helix at the primer terminus. Domain B is analogous to other polymerase thumb domains and binds the minor groove of the duplex substrate

RNA dependent dATP hydrolysis by different DNA polymerases (1)

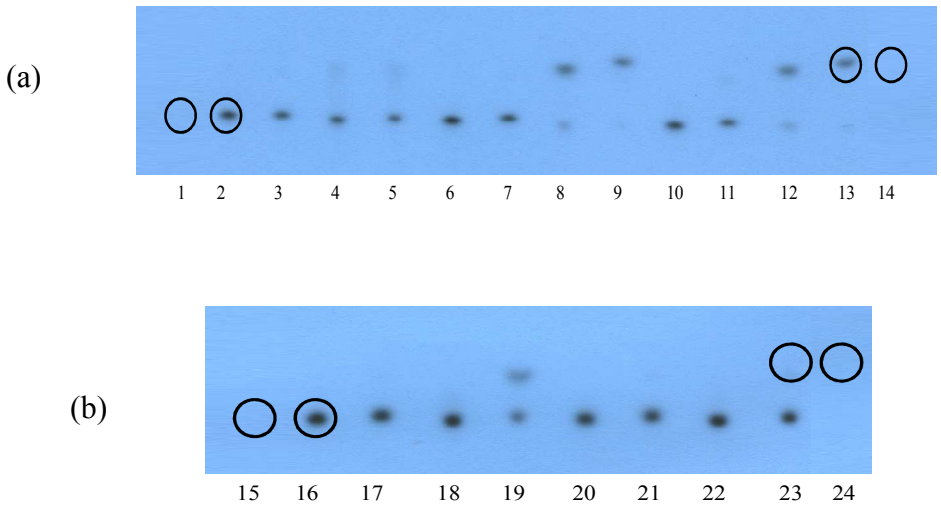

(a)

Lane -1. Cold dATP; lane -2. No RNA, KF (exo$^-$), α -^{32}P-dATP and co-spot with cold dATP;. lane -3. RNA, No Enz, α -^{32}P-dATP; lane- 4. RNA, KF (exo$^-$), α -^{32}P-dATP; lane-5. RNA, KF (exo$^-$), α -^{32}P-dCTP; Lane -6. No RNA, KF (exo$^+$) , α -^{32}P-dATP; lane -7. RNA, No Enz, α -^{32}P-dATP; lane- 8. RNA, KF (exo$^+$), α -^{32}P-dATP; lane- 9. RNA, KF (exo$^+$), α -^{32}P-dCTP; lane -10. No RNA, Pol I, α -^{32}P-dATP; lane -11. RNA, No Enz, α -^{32}P-dATP; lane- 12. RNA, Pol I, α -^{32}P-dATP; lane -13. RNA, Pol I, α -^{32}P-dCTP and co-spot with dCTP; lane- 14. cold dCTP;

(b)

Lane -15. Cold dATP; lane. 16. No RNA, Pol β, α -^{32}P-dATP and co spot with cold dATP; lane -17. RNA, No enz., α -^{32}P-dATP; lane- 18. RNA, Pol β, α -^{32}P-dATP; lane -19. RNA, Pol β, α -^{32}P-dCTP; Lane -20. No RNA, Pol III, α -^{32}P-dATP; lane -21. RNA, No Enz., α -^{32}P-dATP; lane- 22. RNA, Pol III, α -^{32}P-dATP; lane- 23. RNA, Pol III, α -^{32}P-dCTP and co-spot with cold dCMP; Lane 24. Cold dCMP

Figure 17: Hydrolysis of dNTP by different DNA polymerases in the presence of RNA. (a) Klenow fragment (exo-) (lane- 2-5), Klenow fragment (lane- 6-9), DNA polymerase I (lane- 10-13). (b) DNA polymerase β (human) (lane- 16-19), DNA polymerase III (polymerase subunit) (lane- 20-23). All enzymes are showing dNTP hydrolytic activities in the presence of RNA. In the absence of RNA or enzyme no hydrolysis was observed.

RNA dependent dATP hydrolysis by different DNA polymerases (2)

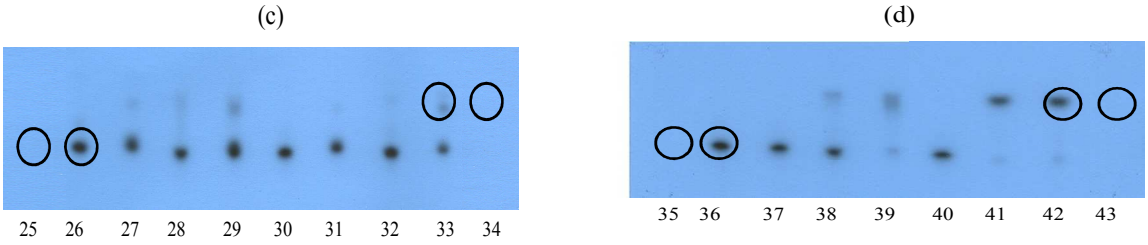

(c)

Lane -25. Cold dATP; lane -26. No RNA, Taq, α -^{32}P-dATP and co-spot with cold-dATP; lane -27. RNA, No enz., α -^{32}P-dATP; lane- 28. RNA, Taq, α -^{32}P-dATP; lane- 29. RNA, Taq, α -^{32}P-dCTP; lane -30. No RNA, RT, α -^{32}P-dATP; lane -31. RNA, No Enz., α -^{32}P-dATP; lane- 32. No RNA, RT, α -^{32}P-dATP; lane- 33. RNA, RT, α -^{32}P-dCTP and co-spot with cold-dCMP; lane -34. Cold dCMP.

(d)

Lane 35. Cold dATP; lane -36. RNA, No enz. α -^{32}P-dATP and co-spot with cold dATP; lane -37. No RNA, Vent (exo$^-$), α -^{32}P-dATP; lane -38. RNA, Vent (exo$^-$), α -^{32}P-dATP ; Lane -39. RNA, Vent (exo$^-$), α -^{32}P-dCTP ; lane -40. No RNA, Vent (exo$^+$),), α -^{32}P-dATP ; Lane 41. RNA, Vent (exo$^+$), α -^{32}P-dATP ; lane -42. RNA, Vent (exo$^+$), α -^{32}P-dCTP and co-spot with cold dCMP; lane -43. Cold dCMP.

RNA - *E. coli* total RNA, No enz. –No enzyme: KF (exo $^-$) - Klenow DNA polymerase (exo $^-$), KF (exo$^+$) – Klenow DNA polymerase (exo$^+$), Pol I - DNA polymerase I, Pol β - DNA polymerase β (human), Pol III – DNAPolymerase III (polymerase domain), Taq – Taq DNA polymerase, RT - Reverse transcriptase,Vent (exo$^-$)-Vent DNA polymerase (exo$^-$), Vent (exo$^+$)-Vent DNA polymerase (exo$^+$)

Figure 18: Hydrolysis of DNTP by different DNA polymerases in the presence of RNA. (c) Taq DNA polymerase (lane 26-29), reverse transcriptase (lane 30-33), (d) Vent DNA polymerase (exo-) (lane 37-39), Vent DNA polymerase (exo+) (lane 40-42). All enzymes are showing dNTP hydrolytic activities in the presence of RNA. In the absence of RNA or enzyme no hydrolysis was observed.

2.4.11 All DNA polymerases interact with RNA and hydrolyze dNTP

All DNA polymerases those structures are known presently, appear to share a common overall architectural feature that can be compared with a right hand and have been described as consisting “thumb,” “palm,” and “fingers” domains. In Figure 16, the crystal structure of four DNA polymerases is shown. The overall common features can be appreciated. The function of the palm domain appears to catalyze the phosphoryl transfer reaction whereas that of the fingers domain includes important interactions with the incoming nucleoside triphosphate as well as the template base to which it is paired. The thumb on the other hand may play a role in positioning the duplex DNA and in processivity and translocation. In present study our observations suggested that Klenow DNA polymerase interacts with RNA that caused dNTP hydrolysis. We included some other DNA polymerases in our study to see whether those have the similar activity in interacting with RNA that cause dNTP hydrolysis. We observed that all the DNA polymerases that we brought under study have similar activities as DNA polymerase I. They interacted with RNA and hydrolyzed dNTP but with different magnitude (Figure 17, 18). It has been found that vent DNA polymerase (exo^+) has similar activity (Figure 18d, lane- 40) as Klenow fragment but the other DNA polymerases, such as, Taq DNA polymerase (Figure 18c , lane- 28), reverse transcriptase (Figure 18c, lane- 33), vent DNA polymerase (exo^-) (Figure 18d, lane- 38), DNA polymerase β (Figure17b , lane- 18), DNA polymerase III (polymerase sub unit) (Figure 17b , lane- 22) and Klenow fragment (exo^-) (Figure 17a , lane- 4,5) have lower activities. These RNA dependent dNTP hydrolysis reactions clearly demonstrated that the DNA polymerases in general could interact with RNA which enables them to hydrolyze dNTP. The RNA interacting dNTP hydrolysis property of DNA polymerases might be a common function

that could arise from the common architectural features and the presence of common key residues at proper positions.

Different functional domains of DNA polymerase I

DNA polymerase I - a model enzyme

1. Extensive studied
2. Common 3-D architechture Thumb, palm, and finger sudomain
3. Polymerase, proofreading (3'--> 5' exonuclease), and 5'--> 3' exonuclease functions present in a single polypeptide chain (103 kDa)

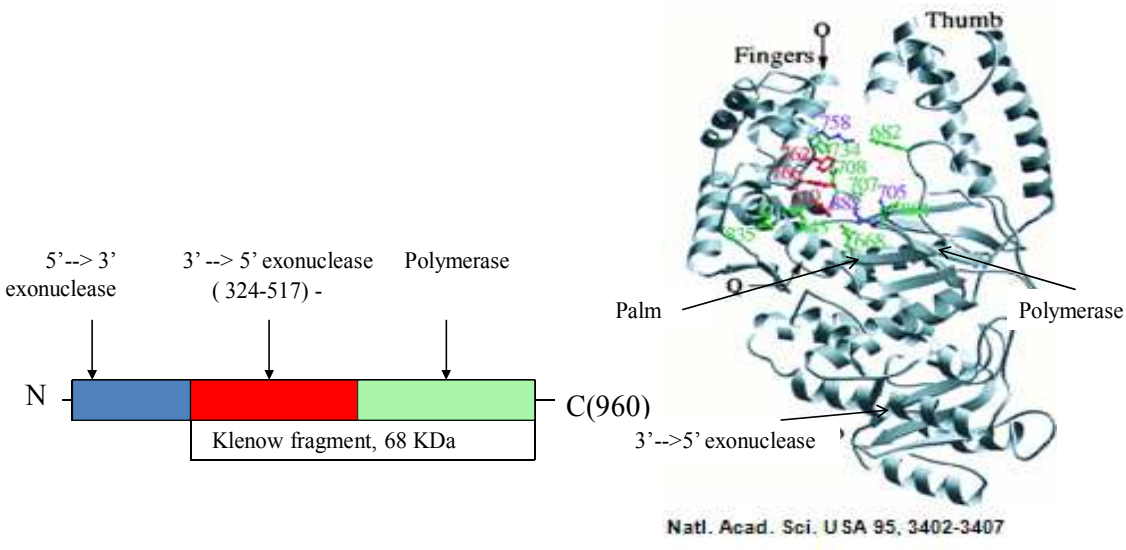

(a) DNA polymerase I (b) Crystal structure of Klenow fragment

Figure 19. Different functional domains of DNA polymerase I. (a)The DNA polymerase I is single chain polypeptide with 960 amino acid long (horizontal bar). It has three functional domains, the N-terminal 323 amino acid (blue) makes 5'----> 3' exonuclease domain, the middle 324-517 residues (red) 3'---.> 5' exonuclease domain, and C-terminal 518-960 make polymerase domain (green). (b) Crystal structure of Klenow fragment is on the right showing 3'-->5' exonuclease and polymerase domains.

2.4.12 Three active sites of DNA polymerase I involved in RNA dependent dNTP hydrolysis

DNA repair enzyme DNA polymerase I, a single chain polypeptide containing three domains, each with unique property. The N-terminal functional domain called 5'--->3' exonucleases remove nucleotide from 5' to 3' direction. This domain excises RNA primer from the lagging strand during DNA synthesis. Its role also implicated in removing pyrimidine dimer (T-T dimer) that may result from exposure of DNA to UV radiation. The 3'--->5' proofreading domain located on the middlewhich removes misincorporated nucleotide from the 3'-end of the primer in a direction opposite to polymerization. The polymerase domain at C-terminal incorporates dNTP at the primer end (Figure 19). In our present study we have examined several DNA polymerases with different functional domains (Figure 17 and 18). It has been found that the DNA polymerases those who possesess all three functional domain exhibited higher dNTP hydrolytic activities than others.It could be observed in Figure -17a (lane -12,13), DNA polymerase 1 has heighst RNA dependent hydrolytic activity as it have three functional domains. Klenow fragment (Figure 17a, lane- 8,9) and Vent DNA polymerase (exo^+) (Figure 18d, lane- 41,42) has also higher activity because they have two catalytic domains. Klenow fragment (exo^-) (Figure 17a, lane- 4,5) and Vent DNA polymerase (exo^-) (Figure 18d, lane- 38,39) which have only one active site remain showed lower activities. DNA polymerase III, Taq DNA polymerase, DNA polymerase β, and Reverse transcriptase also exhibited lower activities. It was clear that the DNA polymerases with more functional domain have higher efficiency in RNA dependent dNTP hydrolysis.

2.4.13 Kinetic analysis showed DNA polymerases with three functional domains have higher catalytic efficiency

We have performed steady state kinetic analysis for different DNA polymerases for RNA dependent dNTP hydrolysis. We have determined K_m and K_{cat} for several DNA polymerases and the results were presented in table-1. The DNA polymerases that were examined in this kinetic analysis are all single chain polypeptides with the polymerase functionality in common and many have multiple functions in the same polypeptide unit. The 5'---->3' exonuclease function is unique to DNA polymerase I (*E.coli*) and Taq DNA polymerase among the enzymes under this study.

DNA polymerase I was the first DNA polymerase discovered was not the primary replicative polymerase, but instead involved in Okazaki fragment resolution and DNA repair, classified as class -A DNA polymerase (Pol I family). It has three 5'--->3' exonuclease, 3--->5' exonuclease (proofreading), and polymerase functional domains. The 5'--->3' exonuclease domain functions to remove RNA primer during DNA replication and short stretch of single stranded DNA during DNA repair from 5' to 3' direction, one nucleotide at a time. The other two enzymes, Klenow DNA polymerase and Klenow DNA polymerase (exo^-) were developed by eliminating 324 amino acids from the N-terminal of the same DNA polymerase I enzyme. Thus, the Klenow DNA polymerase has two a Klenow DNA polymerase (exo^-) active domains, 3--->5' exonuclease and polymerase. But in Klenow DNA polymerase (exo^-) the 3'--->5' exonuclease

function was abolished by site directed mutagenesis and only polymerase function exists. From the kinetic data it was noticeable that even all the three enzymes were catalytically active in RNA dependent dNTP hydrolysis, their activities were not the same. The DNA polymerase I which have three active sites, 5'--->3' exonuclease, 3--->5' exonuclease, and polymerase, showed more activity (K_m- 0.43 µM, K_{cat} - 12 s^{-1}, K_{cat}/K_m -28 x 10^6 $M^{-1}s^{-1}$) than to the Klenow DNA polymerase where the 5'--> 3' exonulease functional domain of the same DNA polymerase I was removed (K_m- 1.2 µM, K_{cat} - 8 s^{-1}, K_{cat}/K_m - 6.6 x10^6 $M^{-1}s^{-1}$). The enzymatic efficiency gets even lowered for the Klenow DNA polymerase (exo^-) where only the polymerase active site remains (K_m- 3.04 µM, K_{cat} - 0.14 s^{-1}, K_{cat}/K_m - 0.05 x 10^6 $M^{-1}s^{-1}$). The lower K_m signifies stronger binding to substrate and thus the dNTP binding to DNA polymerase I was stronger than the other two forms of the same enzyme. The overall efficiency (K_{cat}/Km) of RNA dependent dNTP hydrolysis of DNA polymerase I was twice than that of the Klenow DNA polymerase and 100 folds higher than the Klenow DNA polymerase (exo^-). These observations clearly demonstrated that the enzyme's exonuclease site was more efficeient and playing a major role in RNA dependent dATP hydrolysis than polymerase active site. It was consistence with the hydrolytic activities found for DNA polymerase I (Figure 17a, lane -12, 13), Klenow fragment (Figure 17a, lane -8,9), and Klenow fragment (exo^-), where the the RNA dependent dATP hydrolytic activity of Klenow fragment (exo^-) was the lowest (Figure 17a, lane-4,5).

The T7 DNA polymerase and Vent DNA polymerase have two functional domains, 3'--->5' exonuclese and polymerase, similar to Klenow DNA polymerase. In our present study it has been

found that these two enzymes have similar K_m and K_{cat} as Klenow DNA polymerase in RNA dependent dATP hydrolysis. But in Vent DNA polymerase (exo$^-$), where the function of 3'--->5' exonuclese active site was abolished by point mutation, the K_m was larger and the K_{cat} was lower than the wild type of the same enzyme. This was another indication for the exonuclease site that might have been involved more efficiently in RNA dependent dATP hydrolysis. The other DNA polymerases, Reverse transcriptase, and Dpo4 have only polymerase active site.

Although the Taq DNA polymerase have two functional domains, our study showed that its RNA dependent dATP hydrolytic activity was less efficient than DNA polymerase I or Klenow DNA polymerase. *Taq* DNA Polymerase is a thermostable DNA polymerase enzyme derived from the thermophilic bacterium *Thermus aquaticus* that possesses a 5′→ 3′ polymerase activity (1,2,3) and a 5′ flap endonuclease activity ((*108*). It is belongs to the family of DNA polymerase I enzymes (DNA Pol I), which play a role in the repair of DNA lesions in prokaryotic organisms (*109*). Taq polymerase is a single monomeric enzyme with a molecular weight of 93.9 kDa (*110*). The primary sequence of Taq polymerase is 38% identical to Escherichia coli DNA polymerase I (E. coli Pol I), an enzyme which has served as a model for the study of DNA replication by proteins of the DNA Pol I family (*111*). Like other members of the Pol I family, Taq polymerase consists of three domains: an N-terminal domain (residues 1-290) which has a 5'-3' nuclease activity, an intervening domain (residues 291-419) and a C-terminal polymerase domain (residues 420-832), which is highly homologous in primary sequence and nearly identical in structure to the large domain of the Klenow fragment of E. coli Pol I. While the intervening domain of E. coli Pol I supports a 3'--->5' exonuclease activity

(editing), the equivalent region of Taq polymerase has lost and no editing 3'--->5' exonuclease activity.

From TLC analysis it has been found that the RNA dependent dATP hydrolytic activity of Taq DNA polymerase was very low (Figure 18c, lane -28, 29) in comparing with DNA polymerase I (Figure 18a, lane 4,5) and Klenow fragment (Figure 17a, lane 8.9). The results of kinetic analysis showed the same lower efficiency for Taq DNA polymerase. It has found that the Km of Taq DNA polymerase was 25 and 10 folds higher than DNA polymerase I and Klenow DNA polymerase, respectively. The Kcat for Taq DNA polymerase in RNA dependent dATP hydrolysis was also found lower. The Kcat for Taq DNA polymerase was 0.59 μM/sec/mole enzyme whereas 8 μM/sec/mole enzyme and 5.66 μM/sec/mole enzyme for DNA polymerase I and Klenow DNA polymerase, respectively. It was clearly demonstrated that the 3'--->5' exonuclease active site, which is absent in Taq DNA polymerase, have a greater effect in RNA dependent dATP hydrolysis by DNA polymerases.

The structural and functional properties of DNA polymerases have been reviewed by T. A. Steiz. It has been proposed that DNA polymerases have common structural similarities and have several conserved key amino acid residues involve in dNTP binding, DNA binding, and in coordination with metal ions in active sites. In this RNA dependent dNTP hydrolysis study we included two enzymes, Reverse Transcriptase, and Dpo4, from different polymerase familily to observe whether these DNA polymerases have the similar RNA dependent dATP hydrolytic activities. Reverse Transcriptase is an RNA-dependent DNA polymerase with two functional domains, polymerase and RNase H. It synthesizes a complementary DNA strand initiating from

a primer using either RNA (cDNA synthesis) or single-stranded DNA as a template. Reverse Transcriptase lacks 3′ → 5′ exonuclease activity. We found that the Reverse Transcriptase also interacts with RNA and hydrolyzes dATP but with lower efficiency.

Reverse Transcriptase is an RNA-directed DNA polymerase. This enzyme synthesize a complementary DNA strand initiating from a primer using either RNA (cDNA synthesis) or single-stranded DNA as a template, it contains RNase H activity and like other reverse transcriptase it lacks 3′ → 5′ exonuclease activity (*112*). In our study we have been using M-MuLV Reverse Transcriptase having a molecular mass 78 Kda with functional RNase H domain. During kinetic study it has been observed that RNA dependent dATP hydrolysis by reverse transcriptase was very slow. It was produced dADP (K_m- 13.2 μM) as product in addition to dAMP (K_m- 10.24 μM). The K_{cat} of reverse transcriptase was 10 times lower than tht of DNA polymerase I.

We included another enzyme called DNA polymerase IV (Dpo4) isolated from the bacteria *Sulfolobus solfataricus* belongs to Y-family DNA polymerase (*113-115*) family polymerases are able to bypass a variety of DNA lesions that impede high-fidelity replicative DNA polymerases. Such bypass polymerases exhibit a higher error rate and lower processivity on undamaged DNA templates, and can extend from mismatched base pairs. Y-family DNA polymerases are temporarily recruited to overcome blocks to replicative polymerases (*116, 117*). In the crystal structure (Figure 20) it has been shown that the Dpo4 enzymes makes fewer contacts with the deoxyribonucleotide triphosphate in compare with the Klenow fragment (Figure 8).

As there were fewer contacts have been observed with the deoxyribonucleotide triphosphate by Dpo4, we examined the RNA dependent dATP hydrolysis by this enzyme. The kinetic analysis habe been performed and it was observed that the K_m, which reflects the binding affinity, was 55 μM which was about 100 folds higher than DNA polymerase I. The Dpo4 enzyme also produced dADP as a product where the K_m was 100 μM. The generation of two kinds of products might be due to the flexible binding of dATP in the active site where the both α or β phosphate was accessible to the nucleophilic attack. These observations might be consistence with the facts that the Y-family polymerases have more spacious and solvent-accessible active sites. These solvent-accessible natures of the active site and the smaller number of contacts of the template-primer DNA with the polymerase enable Dpo4 to accommodate unusual DNA structures, such as modified DNA template or primer and modified DNA bases.

Crystal structure of *Sulfolobus solfataricus* Dpo4 enzyme complex with double stranded DNA

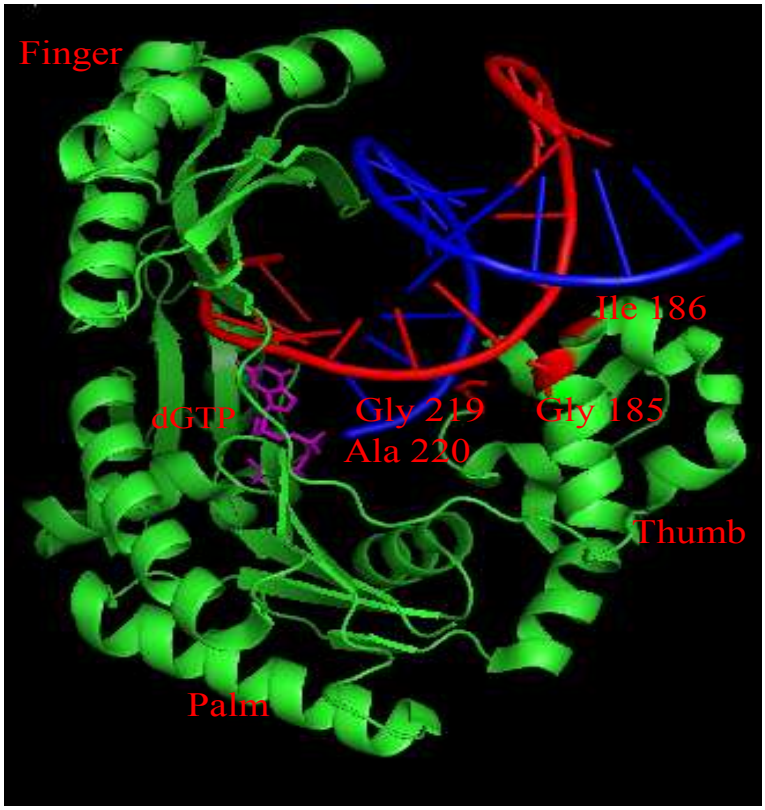

Ling, H., Boudsocq, F., Woodgate, R., Yang, W. (2001) Cell, 107: 91-102 (PDB:1JXL).

Figure 20: Crystal structure of *Sulfolobus solfataricus* Dpo4 enzyme complex with primer, template and dGTP

Figure 20: Crystal structure of *Sulfolobus solfataricus* Dpo4 enzyme complex with primer, template and dGTP. The Dpo4 enzyme also consists of "thumb", "palm", and "finger" domains. The primer (blue) makes contact with Gly-185 and Ile- 186, and the template (red) makes contact with Gly- 219 and Ala-220. The dGTP (magenta) located in the active site in the "palm" domain.

Steady - state enzyme kinetics of DNA polymerases (1)

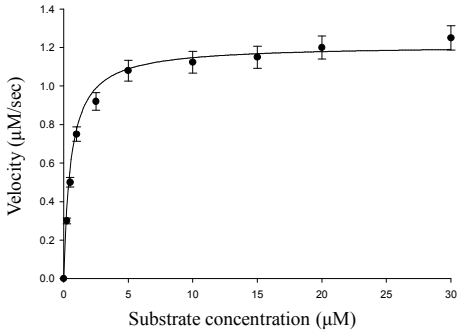

a. DNA polymerase I, K_m- 0.43 μM

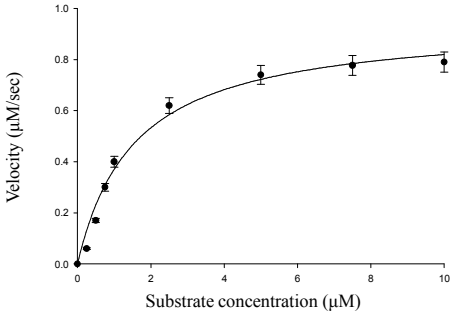

b. Klenow fragment K_m- 1.2 μM

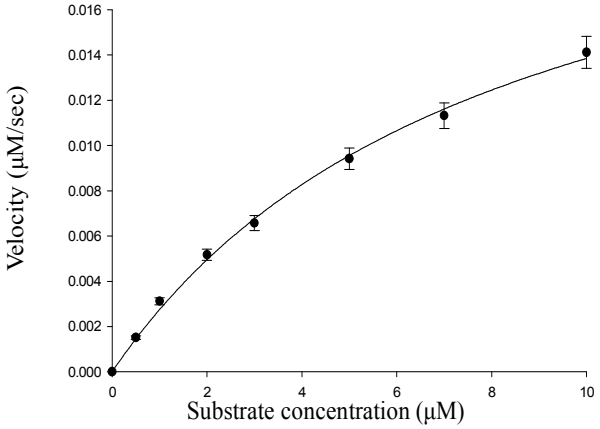

c. Klenow fragment (exo$^-$), K_m -3.04 μM

Figure 21. Steady state kinetic analysis of different DNA polymerases in RNA dependent dNTP hydrolysis.

Figure 21. Steady state kinetic analysis of different DNA polymerases in RNA dependent dNTP hydrolysis.

The K_m of each enzyme is shown. a. DNA polymerase I, Km- 0.43 μM, b. Klenow DNA polymerase, Km- 1.2 μM, c. KlenowDNA polymerase (exo$^-$), K_{m-}- 3.04 μM. The 3'--->5' exonuclease active site of Klenow DNA polymerase (exo$^-$) is mutated and the K_m is the heighst among the three enzymes are compared.

Steady - state enzyme kinetics of DNA polymerases (2)

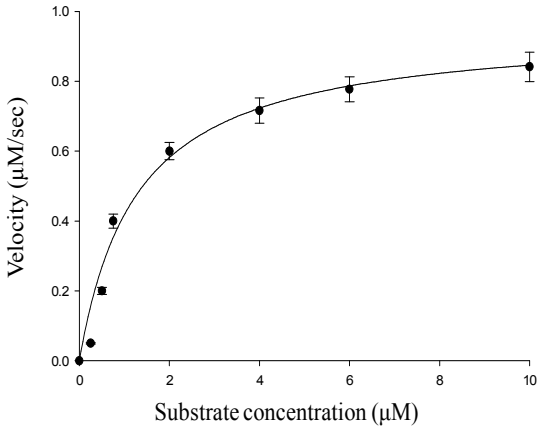

a. T_7 DNA polymerase, K_m- 1.03 μM

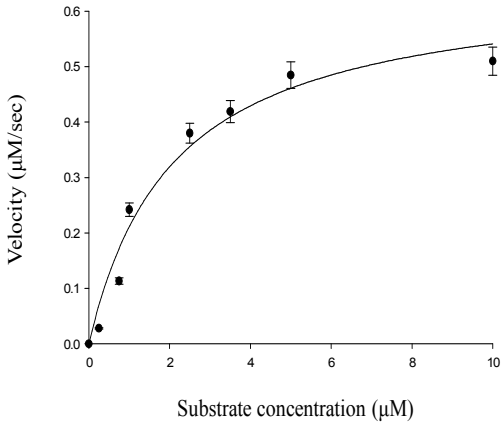

b. Vent DNA polymerase, K_m- 1.34 μM

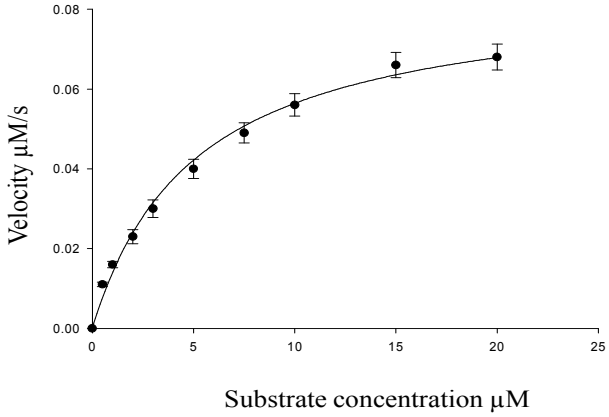

c. Vent DNA polymerase (exo$^-$), K_m- 3.65 μM

Figure 22. Steady state kinetic analysis of different DNA polymerases in RNA dependent dNTP hydrolysis

Figure 22. Steady state kinetic analysis of different DNA polymerases in RNA dependent dNTP hydrolysis.

The K_m of each enzyme is shown. a.T_7 DNA polymerase, K_m- 1.03 μM, b. Vent DNA polymerase, K_m- 1.34 μM, c.Vent DNA polymerase (exo$^-$), K_m- 3.65 μM. The 3'--->5' exonuclease active site of Vent DNA polymerase (exo$^-$) is mutated and the K_m is the heighst among the three enzymes are compared.

Steady - state enzyme kinetics of DNA polymerases (3)

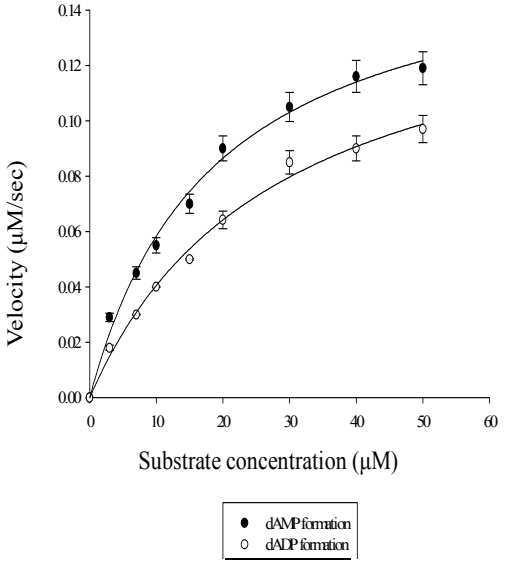

a. Reverse Transcriptase, K_m- 10.24 μM (dAMP), K_m- 13.2 μM (dADP)

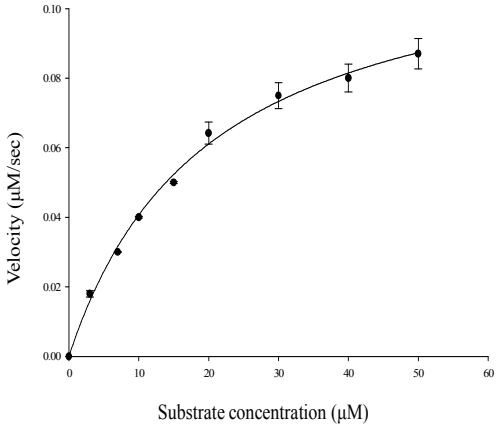

b. Taq DNA polymerase, K_m-10.67 μM

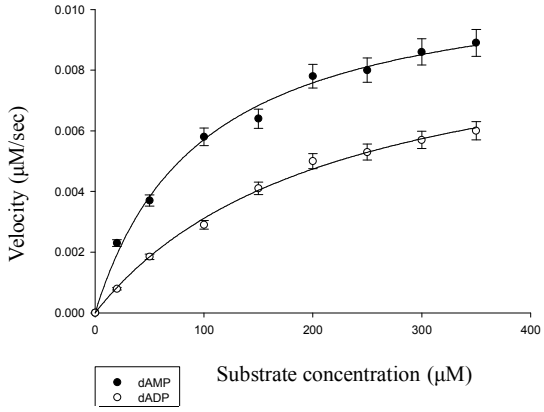

c. Dpo4, K_m- 55 μM (dAMP), K_m- 100 μM (dADP)

.

Figure 23. Steady state kinetic analysis of different DNA polymerases in RNA dependent dNTP hydrolysis.

Figure 23. Steady state kinetic analysis of different DNA polymerases in RNA dependent dNTP hydrolysis. The K_m of each enzyme is shown. Taq DNA polymerase produced only dAMP whereas reverse transcriptase and Dpo4 enzymes produced dAMP and dAMP in RNA dependent dATP hydrolysis; a. Reverse Transcriptase, K_m- 10.24 μM (dAMP), K_m- 13.2 μM (dADP) b. Taq DNA polymerase, K_m-10.67 μM c. Dpo4, K_m- 55 μM (dAMP), K_m- 100 μM (dADP)

Table1. Steady state kinetic parameters of different DNA polymerases in RNA dependent dATP hydrolysis

Parameters / Enzyme	5'-3' Exonu-clease	3'-5' Exonu-clease	Polyme-rase	Product	K_m (μM)	V_{max} (μM/s)	K_{cat} (s^{-1})	$Kcat/Km$ (x 10^6 $M^{-1}s^{-1}$)	dNTP,s Insertion K_m (μM)
DNA polymerase I	+	+	+	dAMP	0.43	1.2	12	28	1 – 2 [a]
Klenow fragment	-	+	+	dAMP	1.2	0.8	8	6.6	2[b]
Klenow (exo-)	-	-	+	dAMP	3.04	0.014	0.14	0.05	-
T7 DNA polymerase	-	+	+	dAMP	1.03	0.85	8.5	7.08	18[c]
Vent DNA polymerase (WT)	-	+	+	dAMP	1.34	0.54	5.4	4.5	40[d]
Vent DNA polymerase (exo-)	-	-	+	dAMP	3.65	0.066	0.66	0.31	60[d]
Reverse Transcriptase	-	-	+	dAMP/ dADP	10.24 / 13.2	0.12/ 0.09	1.2/ 0.9	0.11/ .07	18[c]
Taq DNA polymerase	+	-	+	dADP	10.67	0.09	0.9	0.06	13[d]
Dpo4	-	-	+	dAMP/ dADP	55.0/ 100	0.009/ 0.006	0.09/ 0.06	1.63 x 10^{-3}/ 6 x 10^{-4}	140[e]

a. McClure, W.R. and Jovin, T.M. (1975) *J. Biol. Chem.,* 250, 4073–4080
b. Polesky, A.H., Steitz, T.A., Grindley, N.D.F. and Joyce, C.M. (1990) *J. Biol. Chem.,* 265, 14579–14591
c. Patel, S.S., Wong, E. and Johnson, K.A. (1991) *Biochemistry,* 30, 511–525.
d. Kong, H.M., Kucera, R.B. and Jack, W.E., (1993) *J. Biol. Chem.,* 268, 1965–1975

Table1: Steady state kinetic parameters of RNA dependent dATP hydrolysis by different DNA polymerases.

Table1: Steady state kinetic parameters of RNA dependent dATP hydrolysis by different DNA polymerases.

DNA polymerase I which have three active domains showed heighst performance in RNA dependent dATP hydrolysis. The K_m of the enzymes in RNA dependent dATP hydrolysis is also compared with the K_m values for dNTP insertions during DNA synthesis obtained from published literatures.

Effect of RNA dependent dNTP hydrolysis by DNA polymerase I on *E. coli* growth

a. *E.coli* total RNA b. Yeast total RNA c. Human total RNA

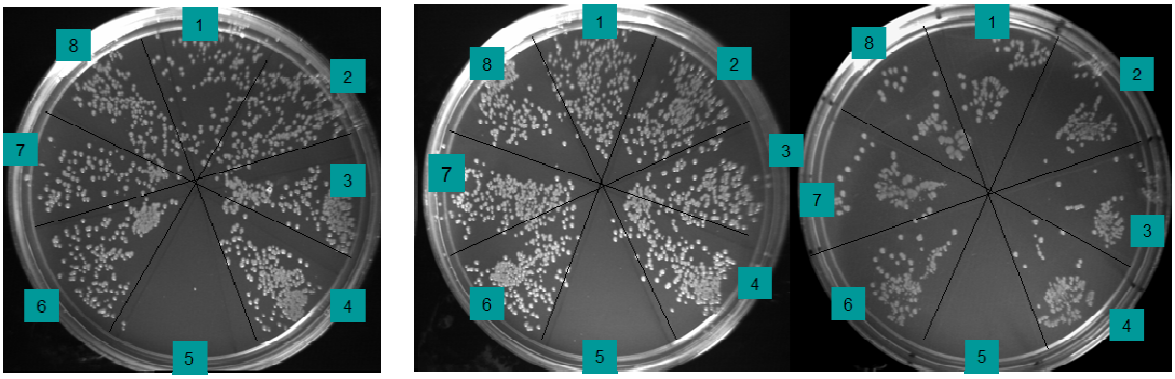

Compartment:

1. H_2O, 2. RNA, 3. DNA polymerase I, 4. dNTP, 5. RNA and DNA polymerase I
6. RNA, DNA polymerase I, and dNTP, 7. RNA, DNA polymerase I, and rNTP.
8. RNA, DNA polymerase I, dNTP, and rNTP

Figure 24. Effect of RNA dependent dNTP hydrolysis by DNA polymerase I on *E. coli* growth

Figure 24. Effect of RNA dependent dNTP hydrolysis by DNA polymerase I on *E. coli* growth. Chemically competent *E.coli* cells (Top10) with pUC19 plasmid DNA was mixed with H_2O (compartment 1), RNA (compartment-2, 50 ng/µl, final), DNA polymerase I (compartment-3, 80 ng/µl, final), dNTP, RNA and DNA polymerase I (comptartment- 4) , mixture of RNA, DNA polymerase I (compartment- 5), mixture of dNTP, RNA, DNA polymerase I (compartment- 6) , mixture of rNTP, RNA, DNA polymerase I (compartment-7) , and mixture of dNTP, rNTP, RNA, and DNA polymerase I (compartment- 8). Total RNA from three sources, E.coli (a), Yeast (b), and human (c) were used. All sources of RNA have similar results and it has been found that in compartment-5, where RNA and DNA polymerase I was added, E.coli growth has been inhibited.

2.4.14 RNA-dependent dNTP hydrolysis by DNA polymerase I cause bacterial (*E.coli*) growth inhibition

In our study we observed that dNTP, the building block of DNA, could be hydrolyzed by DNA polymerase in the presence of RNA. This section of study was performed to observe whether the RNA-dependent dNTP hydrolysis by DNA polymerase have any effect on living organism. We carried out the transformation reaction of *E.coli* with plasmid DNA along with RNA and DNA polymerase I. It has been found that the *E.coli* growth was completely inhibited when RNA and DNA polymerase I were present in the transformation reaction (Figure 24, compartment- 5). This could happen as excess RNA and DNA polymerase I were taken up during transformation reaction which caused dNTP hydrolysis inside the cell that became unsupportive for DNA replication or repair. This phenomenon was supported by the fact that the E.coli growth was found to restore by the supplementation of dNTP in the same transformation reaction (Figure 24, compartment- 6). But we have not observed any growth inhibition with RNA, DNA polymerase I, and rNTP (Figure 24, compartment-7). As rNTP is not the precusur of DNA and it was very likely that growth inhibition could occur with presence of RNA and DNA polymerase whether or not rNTP was present. It might have one possibility that the rNTP also taken up by the bacteria and the rNTP get converted to dNTP by the ribonucleotide reductase enzyme raising the dNTP pool despite of the higher rate of dNTP hydrolysis. The ribonucleotide reductase catalyzes the *de novo* synthesis of dNTP and allosterically control the relative level of dNTP,s in the cellular system (*118, 119*).

Hypothetical catalytic pathway of RNA dependent dNTP hydrolysis by DNA polymerase I

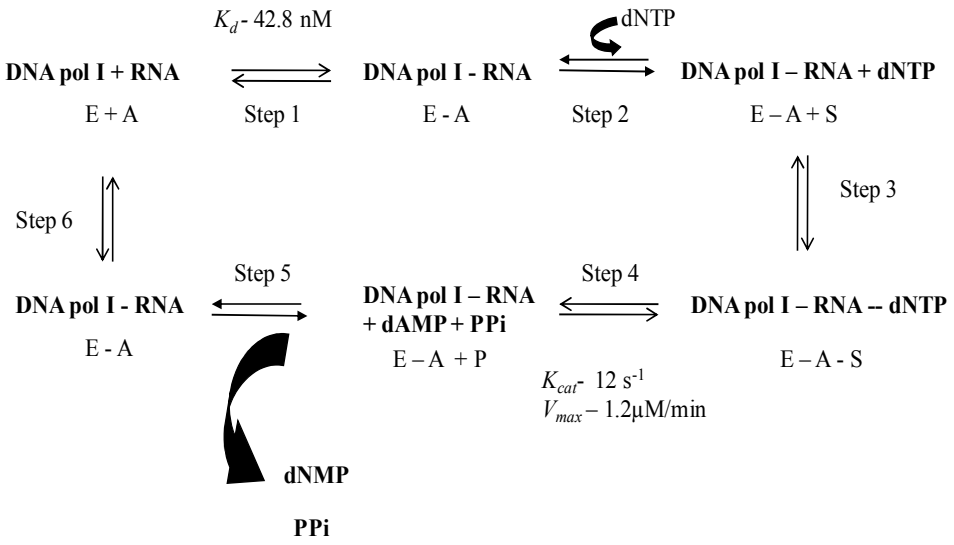

Scheme1. Hypothetical catalytic pathway of RNA dependent dNTP hydrolysis by DNA polymerase I. (E: enzyme, DNA polymerase I; A: activator, RNA; P: product, dNTP).

We are proposing that the catalytic pathway of RNA dependent dNTP hydrolysis by DNA polymerase I occurs in six steps. The hypothetical scheme has illustrated in Scheme 1. In the first step RNA (A, activator) binds to DNA polymerase I (E, enzyme) with dissociation constant (K_d) 42.8 nM (section 2.4.7, Figure 12), which is fairly strong, forming enzyme - RNA (E-A) complex. From RNA titration study (section 2.4.8, Figure 13) we are assuming that the stoichiometric ratio of DNA polymerase I and RNA is 1:1. The substrate dNTP (S, substrate) binds to E – A complex in step 2 forming DNA polymerase I – RNA - dNTP (E-A-S) complex. The K_m of DNA polymerase I in this RNA dependent dNTP hydrolysis was 0.43 μM (Table 1) which is very similar to K_m (1-2 μM) of dNTP insertion during DNA synthesis (*97*). In step 4, which is transition stage, the substrate became converted into products with a catalytic rate 12/s and with V_{max} 12 μM/min (Table 1). From our experimental result described in section 2.4.10 it has been found that this step was a reversible step and rate limiting. In the next step the products were dissociate from the complex and the cycle repeats.

2.4.15 Summary

DNA polymerase I Klenow fragment is a DNA binding protein. During DNA synthesis this enzyme binds to minor groove produced by Watson-Crick base pairing of primer and template. The ternary complex has formed upon binding of dNTP at the polymerase active site. It also binds to single stranded DNA and remove dNMP from 3′-end by 3′-5′ exonuclease active sites as it was found in enzymatic digestion of Okazaki fragment(*120*). RNA binding with DNA polymerase, however, is not been reported. In our biochemical approaches, we found that dNTPs were degraded into dNMPs and pyrophosphates (Figure 1, lane-4, 9, and 10) in the presence of Klenow fragment and RNA. Although the DNA polymerase I is the enzyme, RNA could also participates in catalysis which is familiar as ribozyme. In order to determine whether RNA itself participated in catalysis, the dNTPs were incubated with only RNA and no degradation was observed (Figure 1, lane-7, and 8). dNTPs were also incubate with Klenow fragment without RNA to figure out whether Klenow fragment alone was enough to degrade the dNTPs. Likewise, no degradation was taken place (Figure 2, lane-1, 9). This catalytic role of the Klenow fragment as a dNTP degradation enzyme was further strengthening by the observations that dNTPs were not found to be hydrolyzed when the heat inactivated enzyme (heating at 68 °C for 10 min) was used (data not shown). From these observations it can be concluded that the role of RNA is not catalytic but regulatory while the Klenow fragment acts as a hydrolytic enzyme. In addition to total RNA isolated from *E.coli*, RNA from eukaryotic cells, such as, human and yeast, RNA ladder (100-700 bases), and short synthetic 24-mer RNA were used and the same interactions have been observed for all RNA.

The polymerase and the 3′-5′ exonuclease active sites of Klenow fragment are very specific for substrate selection. The substrate dNTPs were found to hydrolyze by the Klenow fragment in primer-template free reaction in the presence of RNA, we further examined whether any discrimination is maintained by Klenow fragment in selecting rNTPs as a substrate. In doing so reactions were carried out with the same components and conditions, except rNTPs were replaced for dNTPs. It has been found that neither α-^{32}P-rCTP (Figure 2, lane-6) nor α -^{32}P-rATP (Figure 2, lane-14) were hydrolyzed. Also the same results were obtained in reaction where Klenow fragment (for α-^{32}P-CTP, Figure 2, lane-2; for α-^{32}P-ATP, Figure 2, lane-10) or RNA (for α-^{32}P-rCTP, Figure 2, lane-4; for α-^{32}P-rATP, Figure 2, lane-10) was absent. These observations prompted us to conclude that ribonucleotides are not the substrates for Klenow fragment in dNTP degradation reaction.

The polymerase active site of DNA polymerase I Klenow fragment is arranged to bind and align dNTP in such a way so that the terminal 3′-oxygen of the growing nucleotide chain can make nucleophillic attack on the α-phosphorous of the incoming dNTP. On the other hand, the 3′-5′ exonuclease active site is to remove any wrong mononucleotide that has already been covalently bonded at the 3′-end of the primer. Both active sites prohibit rNTP to enter. But in the 3′-5′ exonuclease active site rNTP can enter if that rNTP is the last added nucleotide at 3′-end of the primer terminus because the sugar at the 3′-end is 2′-endo (*100*). In this perspective, the free dNTP may enter into the hydrophobic pocket of the active site where it may hydrolyze into dNMP and PPi through the activation of RNA. It has also been noticed that degradation did not occur, or in some cases partial degradation, when mutant Klenow fragment (exo⁻) that have

point mutations at D356A and E358A was used (Figure 1, lane -13). This result indicated that the 3′-5′ exonuclease domain may responsible for dNTP hydrolysis.

As dNTPs were degrading from solution in a timely manner and also dependent on RNA concentration, we try to determine if the DNA precursor degradation have any effect on DNA synthesis *in vitro* by incubating different concentration of RNA with primer, template, and DNA polymerase I (Figure 13). It has been observed that the dATP hydrolysis dependent on RNA concentration. All DNA polymerases have similar structural configurations that have been reviewed by T. A. Steitz, we suspected that DNA polymerases other than Pol I might have the same RNA interacting dNTP hydrolytic properties. We examined different DNA polymerases from different polymerase family. Interestingly, all DNA polymerases under study showed the RNA interacting property that caused dNTP hydrolysis. We found that the activity was not the same for all DNA polymerases. The DNA polymerases that have the 3'---->5' exonuclease active site were more efficient in catalysis. These observations suggested that the 3'---->5' exonuclease active site might involve in catalysis. We examined the impact of RNA dependent dNTP hydrolysis by DNA polymerase I in bacterial system. It has been found that *E. coli* could not survive when transformation reaction carried out in the presence of DNA polymerase I and RNA. This observation suggests that excess RNA and DNA polymerase I taken up by *E.coli* during transformation which caused dNTP hydrolysis inside the cell. As the dNTP hydrolyzed and reached below the level that no longer supports the DNA synthesis which results in cell death.

The kinetics of RNA dependent dNTP hydrolysis by several DNA polymerases has been explored. It has observed that the DNA polymerases in general have the ability to interact with RNA and to hydrolyze dNTP. The K_m, K_{cat} and V_{max} of the DNA polymerases were determined by steady state kinetics (Table 1). It has found the DNA polymerases I has the lowest K_m and heighst K_{cat}. This could be due to the presence of three functional active sites. The lowest performance was observed for the Dpo4.

This enzyme is classified as a lesion bypass enzyme and it has a broader selection of dNTP which has arise from flexibility of substrate binding in the active site. Also Dpo4 enzyme does not have any exonuclease domain which is more likely to involve in RNA dependent dNTP hydrolysis.

2.4.16 Conclusions

E.coli DNA polymerase I is a repair enzyme and constitutively express in a cell at a definite concentration. Organism maintains dNTPs pool in all phases of cell cycle but in different concentration. RNA is ubiquitous and its interaction with protein is well documented. Interaction occurs mainly through conserved amino acid sequence of protein with particular structure that may arise from secondary, tertiary, or three dimensional structure of single stranded or double stranded RNA. This is the first time report of RNA and DNA polymerase I interactions that lead to dNTP degradation. This finding may lead us to make some predictions that as the RNA (from different sources) stimulate the DNA polymerase I to degrade dNTP without any base discrimination, this could be one of the regulation in maintaining dNTP pool and can be consider as a fine tuning. If we can identify the specific base sequence of the single stranded RNA, on which the DNA polymerase I interacts, that specific base sequence of RNA can be manipulated to degrade dNTPs in rapidly proliferative cells. DNA polymerase β, the human counterpart of DNA polymerase I, also constitutively expressed and the same phenomenon could be occurred.

Chapter 3

Kinetic Analysis of RNase H (BH) Enzyme with Native and Modified DNA Templates

3.1 Abstract

The physical and chemical details of the mechanisms by which enzymes catalyze chemical reactions are still a matter of some controversy. X-ray crystallographic structure brought clarity in many ways in understanding the mechanisms. The crucial problem of this approach 'the phase problem' has been circumvented by introducing selenomethionine in peptide sequence owing to the anomalous scattering effect of selenium. The X-ray crystal structure of nucleic acid - protein complex by introducing selenium in nucleic acid has been solved for the first time by Zhen Huang laboratory. The crystal structure of selenium modified DNA, where the selenium has been introduced in 6-position of the base guanine (G), RNA, and RNase H (BH) protein complex showed very interesting details about the interaction of protein and nucleic acid. It has been observed that due to selenium introduction the base pair $d^{Se}G$….C shifted 0.3 Å. This base pair shifting causes the scissile bond closer to the active site and the catalytic rate of RNase H (BH) enhances by thousand folds in comparing with the native duplex. Our present data suggest a novel approach by which the catalytic rate of an enzyme could be enhanced by introduction of selenium into nucleic acid.

3.2 Introduction

Selenium belongs to the same group in the periodic table as oxygen (O) (100, 101). It also called oxygen family and the other members are sulfur (S), selenium (Se), tellurium (Te), the radioactive polonium (Po), and the synthetic ununhexium (Uuh). Selenium was discovered in 1818 by Swedish chemists Jons Jakob Berzelius (1779-1848) and J. G. Gahn (1745-1818). Selenium is a member of the chalcogen family. The chalcogens are elements in Group 16 (VIA) of the periodic table. Other chalcogens are oxygen, sulfur, tellurium, and polonium.The name chalcogen comes from the Greek word *chatkos,* meaning "ore." The first two members of the family, oxygen and sulfur, are found in most ores. The elements in a group have similar configurations of the outermost electron shells of their atoms and the most chemical properties are dominated by the orbital location of the outermost electron(*121*). As being in the same group, in nature, selenium has been found to replace oxygen or sulfur in many naturally occurring chemical compounds such as selenomethionine and selenocysteine (*122-125*). In selenocysteine, also called the 21st amino acid, the oxygen of the amino acid serine is substituted by selenium (*126-129*).

Selenium is now established as an essential trace element from bacteria to mammals, it has been found to be incorporated into the active sites of many proteins primarily in the form of selenocysteine by deliberate and distinctive mechanism (*130-132*). The majority of selenoproteins whose function is known are oxidation-reduction enzymes using selenocysteine in

the active site having antioxidant properties (*133-136*). The chemical structure of selenocysteine differs from cysteine only by the selenium instead of the sulfur atom; however, the electronic structure of the selenium atom renders the selenolate anion, the conjugated base of selenocysteine, more stable than the corresponding cysteine thiolate. The selenol proton is thus more acidic than in the cysteine thiol (pKa of 5.2 versus 8.5for the thiol), hence ionization of selenocysteine (Sec) occurs at physiological pH (*137-139*). Sec differs from Cys by a single atom (selenium *versus* sulfur) and has similar chemical properties, but the lower pK_a value (5.3) and stronger nucleophilicity of Sec make it much more reactive (*137*). The identification of novel amino acid selenocysteine (Sec) in proteins was reported on 1973 (*140*), another breakthrough appeared in the mid-1980s (*131, 141*). A number of research groups found that selenocysteine does not exists as a free amino acid that might be incorporated into protein in a classical way (*142*). During translation, on the other hand, the selenocystine (Sec) synthesized on the selenocysteins t-RNA (tRNASec) that recognize UGA stop codon on the m-RNA transcript (*143-148*). The first step of its biosynthesis starts with the charge of serine on the specific tRNASec by the conventional seryl-tRNA synthetase. The serine on the Ser-tRNASec is next converted into Sec tRNASec by selenocysteine synthase that utilizes monoselenophosphate as the substrate. This compound is produced from sodium selenite or more likely selenide by a reaction catalyzed by selenophosphate synthetase (*149-153*)

Selenium is currently one of the most hotly studied agents in cancer prevention, according to the National Cancer Institute, there are four phase III cancer prevention trials under way that involve selenium for the prevention of cancers of the prostate, colon, and lung (*154-157*). The role of

selenium has also been implicated in p53 dependent DNA repair inhibitory effect on HIV in vitro through antioxidant effects of glutathione peroxidase and other selenoproteins (*158-161*).

In nature sulfur replacement by selenium at γ-position of methionine has been identified around 1950 that had been termed as selenomethionine (Se-met). It has been found that selenomethionine could stably incorporate into protein and the biological functions do not alter significantly, unless Se-met replaces Met in the vicinity of the active site (*162*). Because the CH3-Se group of Se-met is more hydrophobic than the CH3-S-moiety of Met, substrate access to the active site may be affected, could altering the kinetic parameters (*163, 164*). Sel-met formation is specific to strains of *Saccharomyces cerevisiea*, *Candida albicans*, *Escherichia coli*, rumen bacteria, marine algae, and cereal and forage crops. Sel-met formations in that living system depend on the level of selenium available in the growing media. Higher animals have no efficient mechanism for Met synthesis, they are also unable to synthesize Se-met its incorporation into protein depends upon its availability in the cellular system (*165*).

Introducing recognizable "heavy" atoms for structure solve either using an *ab initio* approach (direct methods) or the Patterson method now became a routine work (*166, 167*). Selenomethionine introduced proteins have been using in x-ray crystallography to determine the structure of the protein since 1980 (*168*). In order to generate electron density maps by Fourier synthesis structure factor amplitude of reflection including temperature factor and the phase angle are required. Unfortunately, only intensities (which are the amplitudes squared) can be measured during a diffraction experiment. This missing piece, the phases (the displacement of the crest from the origin), called phase problem, made solution of crystal structures extremely difficult and time-consuming until the early 1980s (*169-172*). The phase problem has been

overcome with the *ab initio* approach (direct methods) or the Patterson method, which relies on having several recognizable "heavy" atoms in the structure (*173*). This, the method of multiple isomorphous replacements (MIR), entails the trial and-error preparation of heavy-atom derivatives and it is frequently limited by lack of isomorphism. Another alternate *de novo* approach has been move forward in solving phasing of macromolecular crystal structure. This approach uses the 'anomalous scattering' properties of some heavy atoms on the tunable synchrotron radiation. When the passing x-ray photon has the same energy as one of the atoms electron (near the k-edge absorption) the induced vibrations resonate with the intrinsic atomic oscillations and the electron can be rejected from the shell (*169*). This ejection affects both the degree of scattering and timing of scattering events. That is, there is a delay in the time it takes to scatter the photon. The contribution of the anomalous scattering of the atom to the diffraction pattern shifts amplitude and phase as a whole which depends on the wavelength of the X-ray to illuminate the crystal. By collecting data at several wavelengths near the absorption edge of an element in the crystal, one can obtain phase information analogous to that obtained from MIR. This technique is called MAD, for multiple-wavelength anomalous dispersion. One popular way to use MAD is to introduce selenomethionine in place of methionine residues in a protein (*174-177*) The selenium atoms (which replace the sulfur atoms) have a strong anomalous signal at wavelengths that can be obtained from synchrotron X-ray sources and proven as an effective center for MAD phasing (*169*).

X-ray crystal structure determination suffers the phage problem as proteins. Methods that have been developed to solve the phase problem in protein, such as, heavy-atom soaking and co-

crystallization is found to be less effective for nucleic acid structure determination. The heavy-atom soaking and co-crystallization methods, which are usually powerful for protein crystallography, have proven to be less successful in nucleic acids crystal structure determination, probably due to the lack of the specific binding sites for the cations and the problem of the backbone cleavage by the metal cations.

Proteins crystal structures determination has been using selenium by MAD phasing since 1988 (*177*). The inherent anomalous diffraction properties of selenium have been using to solve nucleic acid crystal structure by Huang laboratory since 1998 (*178*). In this pioneering methods site specific replacement of the O-atom by selenium and their X-ray crystal structures provided numerous novel insights. It has observed that selenium could stably substituted at various chemical environments of nucleic acid while the nucleic acids maintain their classical properties, such as, secondary structure and duplex formation (*179*) catalytic property (ribozyme) (*180*), and enzyme recognition (*181*). Crystal structures of nucleic acid– protein complexes by the selenium derivatized nucleic acid also determined at 1.80 Å resolution and C 2 space group (*179*). In this crystal structure selenium modified DNA base paired with RNA co-crystallized with C-terminal (61-196 aa) mutant (D132N) truncated RNase H from Bacillus halodurans (mut-tr-RNase H (BH)). This crystal structure of the ternary complex provided a very interesting set of information's on enzyme mechanism and interaction with nucleic acid. The Bacillus halodurans RNAse H became a model enzyme in mechanism study owing to its easy expression and purification, enzyme stability, and easy to grow crystal.

RNase H is an endonuclease that specifically hydrolyzes the RNA in a RNA-DNA hybrid. This enzyme was first discovered in 1969 by Peter Hausen's laboratory (*182*). It has been implicated to function in many organisms from virus to mammals (*183-186*). The first RNase H gene from E.coli was cloned and characterized in 1983 (*187*). It is classified as type-1 RNase H (RNase H 1) encoded rnhA gene it requires Mg^{2+} for their activity and cleavage products are 5'-phosphate and 3'-OH. E.coli RNase HI is composed of a single polypeptide chain of 155 aa with two distinct structural domains (*187*). The major domain constituted from four α helices and one large *β* sheet composed of three antiparallel *β* strands at the N-terminus as well as two parallel *β* strands. The minor domain consists of one α helix with roughly two turns and a following loop composed of about 10 residues (*183, 188, 189*).

The novel fold of RNase HI, which consists of a five stranded β sheet flanked on both faces by α helices and the two key active site aspartates (Asp 10 and Asp 70), were later identified to be common among the integrase superfamily, which includes retroviral integrases, transposases, RuvC, and Argonaute. Four conserved acidic residues D10, E48, D70, and D134 located in the *β* sheet constitute catalytic active site (*169-171, 173*).

The bacillus halodurans RNase H enzyme 196 aa long composed of hybrid binding domain (1-58 aa) and catalytic domain (59-196 aa). The truncated enzyme (catalytic domain) is more active than that of wild type enzyme. The tertiary structure of the catalytic domain consists of a mixed β sheet with three antiparallel (*182, 187, 190, 191*) and two parallel (*191*) strands and three α helices (A, B, and D) arranged like a letter "H" on one side of the sheet. Helix A runs between

strands 3 and 4, and helices B and D run between strands 4 and 5. Together they form the αβα Rossmann-like fold. C-helix that present in E.coli is missing in bacillus halodurans RNase H (*77*). The active site is formed by four conserved (D71, E109, D132, and D192) and one non-conserved (E188) acidic amino acids coordinated with two Mg+2 ions.

RNase H (BH) recognizes DNA/RNA duplex by interacting directly with both DNA and RNA strand. In DNA/RNA duplex, DNA adopt B-form (3'-exo) and RNA adopt A-form (2'-exo) conformations and this mixed conformation duplex recognized by RNase H. The enzyme makes direct contact with DNA and RNA strands through the face of the RNase HC containing the active site has two grooves separated by 8.5 Å. The minor groove width of DNA/RNA duplex is 8.5 Å which perfectly fit into the enzyme active site. The RNA strand is recognized by the direct contacts with five consecutive 2′-OH groups. The catalytic carboxylates E109, D132(N), and their immediate neighbors (N106 and Q134) make hydrogen bonds with two 2′-OH groups immediately 5′ to the scissile phosphate. S74 and G76 adjacent to D71 (the other active-site residue) contact the two 2′-OH groups 3′ to the scissile phosphate. The DNA binding groove, which comprises the N terminus of helix αA and the loops between helices αB and αD and between the β1 and β2 strands is accentuated by a phosphate binding pocket composed of T104, N106, S147, and T148 (*192, 193*). The active site of RNase H is located in the groove that accommodates the RNA strand. The phosphate binding pocket probably plays a role in anchoring the B form DNA and contributes to the specificity for an RNA/DNA hybrid (*194*).

A two-metal-ion catalysis mechanism was proposed by Steitz and Steitz in 1993 (*195*). In this mechanism one metal ion activates the hydroxyl nucleophile and the other stabilizes the

pentacovalent intermediate. Based on stereochemical studies, it has been proposed that reactions catalyzed RNase H enzymes occur by a one-step S_N2-like (bimolecular nucleophilic substitution) mechanism accompanied by a pentacovalent intemediate and inversion of the phosphate stereo configuration (*192, 193*). The two metal ions, A and B, are coordinated by the active site residues. The metal ion A is coordinated by D192 and E188 and metal ion B by D109 and D132 where D71 interacts with the both metal ions. The residue D192 also make interactions with the *Pro-*S_p oxygen and nucleophile water molecule and acts as a general acid –base catalyst. The residue D192 which interact with metal ion A abstract one proton from water molecule and the resulting -OH (hydroxyl ion) ion makes nucleophilic attack on the phosphate forming pentacovalent intermediate releasing H-atom in the solvent. The transition state is stabilized by A metal ions by coordinating with *Pro-*R_p oxygen and 2'-OH group of the sugar immediate 5' of the sessile phosphate atom. As the attack occurs from *Pro-*S_p oxygen side and proceeded through a one-step S_N2-like mechanism, the bond on the 3' side of the phosphate get cleaved forming 5'-phosphate and 3'-OH products (*193*).

The crystal structures of mut-tr-RNase (H) with 6-mer DNA/RNA hybrids provided detail information's about the enzyme and nucleic acid interactions (*192*). These structures are solved by heavy atom soaking using MAD phasing method. Crystal structure of the same ternary complex was solved by Huang laboratory by MAD phasing. But selenium functionality has introduced in the DNA base guanine at 6-position by replacing O-atom instead of native solved by Wei et. al. (*192*). In 6-mer DNA selenium modified DNA the selono-G was placed at 3rd and 6th place of the DNA from 5'-end. There were several advantages and novel insights have been

noticed by this selenium introduction. The crystal grew in very short time (about a week) than the native duplex (several months) and the resolution was 1.8 Å instead of 2.8 Å for the native. By superimposing the native DNA /RNA on the selenium modified DNA/RNA structure it has been observed that the global or local structure ^{Se}DNA/RNA remain the same as native. The selenium in 6 position of G also form H-bond (6Se···H-N) with N-4 of cytosine but the bond length increased to 3.5 Å instead of 3 Å in classical G-C base pair. Due to the heavy nature of selenium atom the ^{Se}G-C base pair shifted 0.3 Å. From this selenium substitution it has also been noticed that DNA structure is flexible and can accommodate larger atom while retaining the same physical and chemical properties.

In our current study we were attempted to answer some questions that would help us to understand further the mechanism of catalysis. Selenium functionality that has been introduced into DNA may affect the protein functionality. This understanding may improve our knowledge that could be used in drug design and therapeutics.

3.3 Methods and Materials

3.3.1 Sequences used for enzymatic study

Native DNA template with 3'- OH (D_1): 5'-ATGTCG-3'

Native DNA_P template with 3'- phosphate (D_2): 5'-ATGTCG-P-3'

Single selenium (6-Seleno G) modified DNA template (D_3): 5'- $AT^{Se}GTCG$ -3'

Double selenium (6-Seleno G) modified DNA template (D_4): 5'- $AT^{Se}GTC^{Se}G$ -3'

Single sulfur (6-Sulfur G) modified DNA template (S_1): 5'- $AT^{S}GTCG$ -3'

Double sulfur (6-Sulfur G) modified DNA template (S_2): 5'- $AT^{S}GTC^{S}G$ -3'

RNA substrate (native) (R_N): 5'-UCGACA-3'

RNA substrate (Sulfur modified) (R_S): 5'-UCGA-(S)-CA-3'

Sequences used for Tm study:

Native DNA (D_{TmN}): 5'-TGTCGT GTC G-3'

Sulfur modified DNA (6-Sulfur G) (D_{TmS}): 5'-$TGTCGT^{S}GTCG$-3'

Selenium modified DNA (6-Seleno G) (D_{TmSe}): 5'-$TGTCGT^{Se}GTCG$-3

RNA (R_{Tm}): 5'-ACGACACGAC-3'

3.3.2 Gel shift assay:

Gel shift assay was performed to determine the binding constants for native or modified DNA templates base pairs with RNA substrate bind to tr-RNase H (BH). The 5'-end of the RNA substrate was labeled with ^{32}P by using standard method describe elsewhere. Native or modified DNA templates of 1 μM concentration were mixed with 1.5 equivalent of RNA substrate. On each 20 μL reaction that contained DNA/RNA duplex, 0.5 μL of ^{32}P-labeled RNA substrate was added. The mixtures were heated in water bath for 5 minutes at 85 °C and allowed to cool down to room temperature. The mixtures were then placed at 4 °C for overnight. Duplexes of 1 μM concentration of each was mixed with 1.0, 3.5, 5.5, 7.5, 9.5, 11.5, and 13.3 μM wild type RNase H (BH) enzyme with binding buffer (10 mM KCI, 1 mM DTT, 5 % glycerol, final) and incubated at room temperature for 30 minutes. The reaction materials were mixed with gel loading dye (10 mM KCI, 1 mM DTT, 5 % glycerol, 0.001 % xylene blue (W/V), final) and loaded on 21 % non denaturing polyacrylamide gel. The composition of running buffer was 5 mM tris chloride, 10 mM EDTA and pH was adjusted to pH 7.5 with acetic acid. Before loading samples the gels were pre-run for 30 minutes to remove ammonium per sulfate (APS). The gels were run with a constant voltage (250 volts) for one hour in 4 C° cold room. The gels were dried in a vacuum dryer and images were taken by phosphoimager and quantified using image quanting software. Binding study for native template was performed again using less enzyme concentrations 0.25, 0.5, 1.0, 2.0, 3.0, 4.0, 5.0 and 6.0 μM because enzyme saturation level arrived at low enzyme concentration.

3.3.3 RNA substrate 5'-labeling

A total of 20 µl reaction containing 10 pmol (10 µl of 1µM) RNA substrate, 2 µl (20 unit) of T4 polynucleotide kinase (purchased from New England Biolab), 2 µl ATP Gamma ^{32}P (20 µCi final) and 2 µl of 10X polynucleotide kinase buffer [70 mM Tris-HCl, 10 mM $MgCl_2$ and 5 mM Dithiothreitol pH 7.6 (final)] was incubated for 1 h at 37 ˚C. The ^{32}P labeled RNA was purified by precipitating with 70 % ethanol supplemented with 0.3 M NaCl (final) added prior to add ethanol. The pellet was air-dried and dissolved in 10 µl water and the final concentration of the stock became 1 µM.

3.3.4 Reaction conditions (RNase H catalysis)

A total of 20 µl reactions were prepared for each DNA template D_2, D_3, D_4, S_1 or S_2 in order to carry out time course analysis. Wild type or truncated RNase H (BH) (expressed and purified) enzyme was used to determine the apparent catalytic rate and turnover number for each template. Each reaction contained 2.5 µl of 1 µM ^{32}P RNA substrate (final 125 nM), 15 µM DNA template (final), RNase H enzyme (10 nM final) and RNase H buffer. The reaction buffer composition was 75 mM KCl, 50 mM Tris-HCl, 3 mM $MgCl_2$, pH 7.8. In each 20µ reaction 0.02 µl borane tetrahydrofuran complex (1.0 M solution in THF, 1 mM final) was added prior to add RNase H enzyme. During time course aliquot of reaction materials was taken out before adding RNase H (referred to '0' min). After adding RNase H enzyme aliquot was taken at 0.5, 1, 3, 5, and 10 minutes that carried out at 37 °C and the reactions were quenched by adding DNA loading dye (contained 7 M urea) and placing on ice.

3.3.5 Urea-polyacrylamide gel analysis

The reaction materials were loaded on 19 % urea-polyacrylamide gel and ran for 2 h at 250 volts. The gel was dried and quantified using phosphoimager (Storm 860 Molecular Imager) and also exposed to X-ray film to obtain gel images.

3.3.6 Separation of sulphur modified RNA substrate diesteromers

The two diesteromers were separated by FPLC using anion exchange column. 10 column volumes of elution buffer (buffer B) containing 1 M NaCI was allowed through the column to remove impurities, if any. After equilibrating the column by 30 column volume of buffer A, 20 mM sodium phosphate, pH 7.5, 20 μ mole of the sulphur modified RNA substrate was injected onto the column. After loading, the sample was washed with 10 column volume of buffer A with a flow rate 1 ml/min. The diesteromers were eluted with 30 column of elution buffer (buffer B) with 0-100 % gradient using a flow rate 1 ml/min and the two diesteromers , dr1 and dr 2, were eluted at 30 % and 33 % gradient, respectively. The collected samples, 1 ml of each, were lyophilized by adding 1 mM borane tetrahydrofuran complex to prevent dimer formation, dissolved in dH_20 and quantified by UV-vis. Both diesteromers (dr_1 and dr_2) were labeled at 5'-end by using the same procedure described earlier and used as substrate.

3.3.7 Reaction conditions for the sulfur modified substrates

The reactions were carried out in several different conditions. Those were with or without manganese supplemented in the reaction buffer (reaction buffer compositions stated earlier) and with different enzyme concentrations. The dr_1 or dr_2 substrates were hybridized with the different

DNA templates and the reactions were carried out in reaction buffer (contained 10 mM magnesium chloride) using two enzyme concentrations, 100 nM or 1 nM, setting the temperature at 37 °C. In reactions with Mn^{+2}, 10 mM manganese chloride was added to the reaction buffer using the same procedures as described while the enzyme concentration was kept 1 nM. The visualization procedures were the same as described.

3.3.8 Melting temperature study

In order to determine the free energy differences among the duplex with normal and modified DNA with RNA UV absorbance monitored melting temperature were performed at four concentrations ranging from 8 μM down to 0.25 μM duplex. Samples with 1:1 ratio were mixed with 1 ml melting buffer, 5 mM sodium phosphate, pH 7.0, 0.5 mM EDTA, 1 M NaCI and placed in 1.5 ml eppendroff tube. The samples were placed in water that preheated to 85 °C and kept at room temperature until the temperature down to 25 °C and the samples were then kept at 4 °C freezer for 3 hours. Samples in quartz cuvettes with 1 cm path length were placed in thermostated sample chamber of Cary win UV 300 UV-vis spectrophotometer to monitor the melting curve. The temperature was raised from 6 - 80 °C with a rise 0.5 °C/min and the UV spectra recorded in every 0.5 min at 260 nm wave length and the each process were repeated four times. The thermodynamic parameters were analysed by van't Hoff method. The van't Hoff enthalphy and entropy were determined from the dependence of Tm on DNA/RNA concentration by the following equation:

$$1/T_m = (\text{n-1})R \ln[Ct] / \Delta H^o + \Delta S^o / \Delta H^o$$

Where *Ct* was the total strand concentration, n, R, and ΔS^o denoted as molecularity, gas constant, and entropy, respectively. The plot was constructed by 1/Tm *VS* ln Ct putting on the Y-axis and X-axis, respectively. Three sets of data for native, sulfur modified, and selenium modified DNA were placed in the same graph and the slope was set equal to (n-1) R/ΔH° where n value set to 2 and intercept was equal to $\Delta S^o/\Delta H^o$. Slope and intercept of the plot were calculate using Microsoft excel. After calculation of entropy (ΔS^o) and enthalpy (ΔH^o) for each DNA, free energy of duplex formation for each duplex was determined by using the following equation:

$$\Delta G^o = \Delta H^o - T\Delta S^o, \quad \text{where T is the absolute temperature.}$$

3.3.9 Expession and purification of RNase H protein

Wild type and truncated RNase H (*B. halodurans*) constructs, pET15 and pET 42, respectively, were received from Dr. Wei Yang lab (NIH) as a gift. Protein expressions were carried out in BL21 (DE3) pLys E. coli (purchasecd from Invitrogen). The transformation was accomplished by heat shock methods. One picomole of the plasmid carrying our gene of interest was added in a vial of (50 µl) competent cell and swirl gently. The vial was placed in ice for 30 minutes and heat shock for 40 seconds at 42 °C and placed again in ice for 5 minutes. In the vial 150 µl of SOC medium was added and shaken for 1 hour at 37 °C. The bacteria then spreaded on LB-agar-ampicillin-chloramphenicol plate and kept in 37 °C incubator for overnight. A single colony was picked up and grown in LB-ampicillin-chloramphenicol broth for overnight at 37 °C by shaking.

Two liters LB-ampicillin-chloramphenicol broth was prepared and 1/50th volume of over night culture was added and grown for 2-3 hours. The protein expression was induced by adding 1 mM

IPTG when the OD600 reached 0.6 and the culture was allowed to grow for 4 hrs and the cells were harvested by centrifugation. The cell were washed twice with lysis buffer (75 mM NaCl, 40 mM NaH_2PO_4 pH 7, 0.1 mM EDTA, 1 mM dithiothreitol DTT, 5 % glycerol) and the cells were suspended in the same buffer. The cells were lyzed by sonication and centrifuzed for 30 min at 13,000 rrm and supernatant was collected. The supernatant was loaded onto the Ni affinity column and protein with his tag was eluted by 500 mM imidazole gradient buffer (40 mM NaH_2PO_4 (pH 7.0), 300 mM NaCl, 5% glycerol, 1.4 mM β-mercaptoethanol, and 500 mM imidazole). The buffer was exchanged to 40 mM NaH_2PO_4, 150 mM NaCl, 5% glycerol, 2 mM DTT, and 0.5 mM EDTA for thrombin digestion. The proteins were further purified on a Phenyl Superose column with a 2 to 0.3 M gradient of ammonium sulfate, concentrated to 15–20 mg/ml, and stored in 20 mM HEPES (pH 7.0), 75 mM NaCl, 5% glycerol, 0.5 mM EDTA, 2 mM DTT at 4°C or −20°C.

3.4 Results and Discussions:

3.4.1 Crystal structure of double selenium modified DNA base pair with RNA and tr-mut- RNase H (BH) ternary

Crystal structure of the ternary complex D_4 - R_N - tr-mutant RNase H (BH) has been resolved by X-ray diffraction (NDB ID: PH0043, 2R7Y, 2007) by Jiang, J.-S., Gerlits, O., Huang, Z. at 1.8 Å resolution. MAD phasing method was used for determining the ternary complex structure in C 2 space group (Figure 1). This is the first crystal structure of protein - nucleic acid complexes that have been determined based on Se-derivatized nucleic acids (SeNA) and MAD phasing. In this X-ray diffraction experiment truncated version of RNase H enzyme from *Bacillus halodurans* (BH) was co-crystallized. This truncated enzyme is more active enzymatically than its wild type (WT) and gave better resolution in crystal structure. The truncated RNase H (BH) was generated by removing N-terminal (1-57) amino acid residues that constitutes the hybrid binding domain (HBD). The inactive version of the truncated RNase H (BH) has a point mutation where negatively charged aspartate residue 132 (D132) was replaced by a positively charged amino acid asparagine (N). From this D132N mutation, coordination of the enzyme with the metal ion B has been abolished and the enzymatic activity of the RNase H (BH) was lost. In the duplex, the template was 6-mer selenium modified DNA (D_4: 5'- $AT^{Se}GTC^{Se}G$ -3') that form base pair with 6-mer RNA substrate (R_N: 5'-UCGACA-3'). The 6-mer selenium modified DNA template was synthesized by solid-phase methods and selenium was introduced at the 6 position of both G

(guanine) bases replacing oxygen atoms (Scheme 1). In this duplex, the DNA base A (1') and RNA base U (1) remain overhang on both sides where the other 5 bases form base pairs with their complementary bases (Figure 1a). So, the tr-mut-RNase H (BH) was 58-196 amino acids long where the N-terminal Hybrid Binding Domain (HBD) was genetically removed and only C-terminal catalytic domain (58-196 aa) was present.

Crystal structure of the ternary complex, selenium modified DNA, RNA, and tr-mut-RNase H (BH) protein

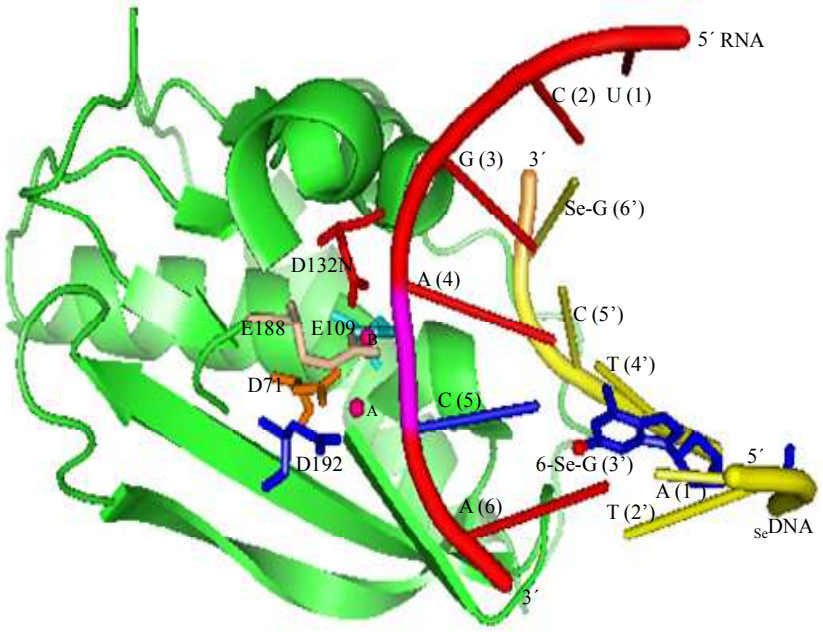

NDB ID: PH0043, 2R7Y, 2007, Jiang, J.-S., Gerlits, O., Huang, Z.

Figure 1: Crystal structure of the ternary complex, selenium modified DNA (yellow), RNA (red) and tr-mut-RNase H (BH) protein (green). The amino acids in the active site (labeled), Mg^{+2} ions A and B (hot pink balls), ^{Se}DNA (yellow), RNA (red). The 6-seleno-G (blue) with selenium (red ball) base pairs with C (5') and the cleavage bond (pink) between A (4) and C (5) on the RNA strand are shown. The amino acid residues D194 (Asp-194), E198 (Glu-198), and D132N, the catalytic triad (DDE motif) makes the active site of the enzyme. The two magnesium ions A and B located at the active site close to the scissile bond.

The co-crystal structure of selenium modified DNA, RNA, and tr-mut-RNase H (BH) protein ternary complex showed the presence of duplex formation between ^{Se}DNA and RNA (Figure 1). In this duplex 5'-A of the ^{Se}DNA (D_4, 5'- AT^{Se}GTC^{Se}G -3') and 5'-U of the RNA (R_N, 5'-UCGACA-3') remain overhang on both sides. The two selenium atoms located at the 6-positions of G's on the DNA strand. The conserved amino acid residues, D71, E109, D132N, and D192 and the non-conserved amino acid E188, forms catalytic active site. The two Mg^{+2} ions located in the active site coordinates with amino acids and water molecules. The amino acid residues D194, E198, and D132N, the catalytic triad, makes the active site of the enzyme. The two magnesium ions (red) located at the active site coordinates with the active site residues, scissile bond of RNA (pink), and water molecules. The putative scissile bond, between 3' of A (4) and 5' of C (5), of the substrate RNA located close to the active site (Figure 1).

Tertiary structure of tr-mut-RNase H (BH) showing different helices and sheets

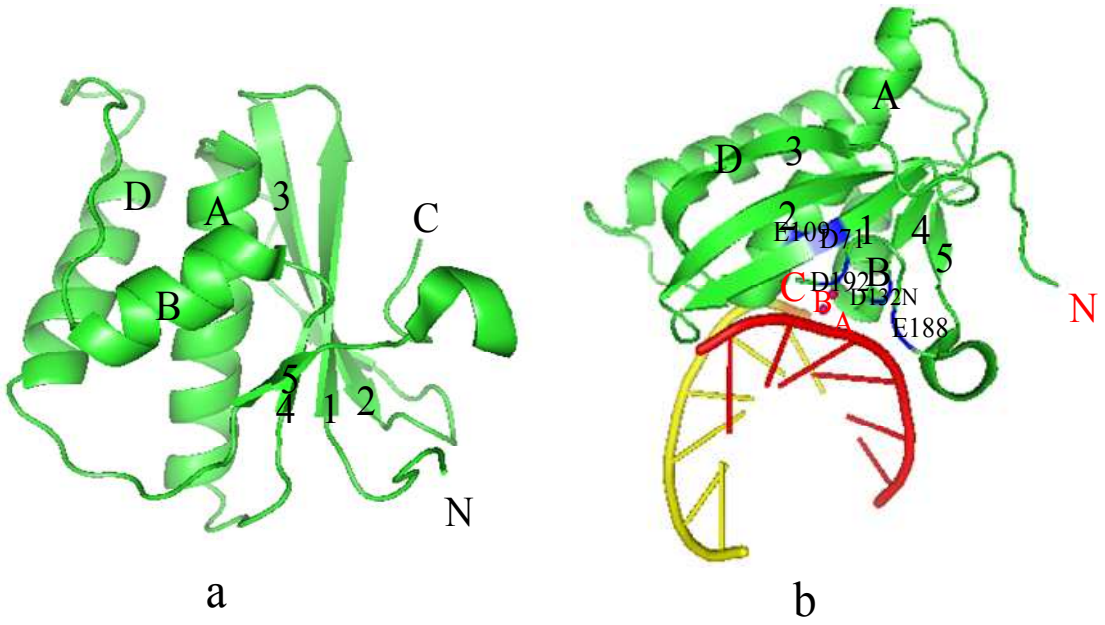

NDB ID: PH0043, 2R7Y, 2007, Jiang, J.-S., Gerlits, O., Huang, Z.

Figure 2: Tertiary structure of tr-mut-RNase H (BH) C-terminal catalytic domain residues from 61 to 193. (a) The tertiary structure showing β - strands and α-helices. This catalytic domain consists of a mixed β sheet with three antiparallel (1, 2, and 3) and two parallel (4 and 5) strands and three α helices (A, B, and D) arranged like a letter "H" on one side of the sheet. (b) Catalytic domain of tertiary structure tr-mut-RNase H (BH) with different α-helices and β - strands showing active site residues (black labeled), ^{Se}DNA (yellow)/RNA (red) duplex, and Mg^{+2} metal ions (red balls, A and B).

The tertiary structure of the catalytic domain located at the C-terminal (59-196 amino acid) consists of a mixed β sheet with three antiparallel (1, 2, and 3) and two parallel (4 and 5) strands and three α helices (A, B, and D) arranged like a letter "H" on one side of the sheet (Figure 2a). Helix A runs between strands 3 and 4, and helices B and D run between strands 4 and 5. Together they form the αβα Rossmann-like fold. In the duplex ^{Se}DNA paired with RNA. The two magnesium ions (red ball, A and B) remain in close proximity of the active site. Four conserved residues D71, E109, D132, D192 and one non-conserve residue E188 constitute the catalytic active site (Figure 2b). The residues D192 and E 188 located on the loop at the C-terminal of the chain and the residues D71 and E109 resides on the β-1 strand and on the A helix, respectively.

Crystal structure of tr-mut-RNAse H (BH) showing important residues interact with DNA/RNA duplex

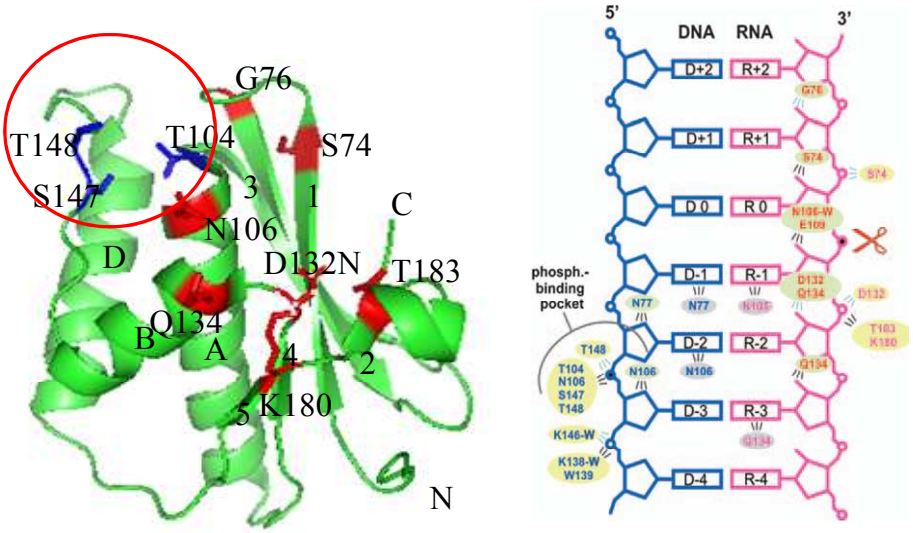

Marcin Nowotny, Sergei A. Gaidamakov, Robert J. Crouch, and Wei Yang; Cell, Vol. 121, 1005–1016, July 1, 2005.

Figure 3: DNA/RNA duplex binding to the tr-mut-RNase H (BH) enzyme showing interacting amino acid residues on different strand and helices and schematic diagram of DNA/RNA duplex. (a) The residues of the tr-mut-RNase H (BH) involved in interaction with DNA/RNA duplex are labeled. The residues that make theDNA phosphate binding pocket (residues labeled blue in red circle) interact with phosphate group of the DNA backbone. (b) Interactions between the RNA/DNA hybrid and tr-mut-RNase H (BH). Shown are the residues interacting with phosphates (yellow highlight), sugars (green highlight), and bases (gray highlight). Cyan lines indicate interactions made by the protein backbone, and black lines indicate interactions made by side chains. Water-mediated interactions are indicated by –W.

The specificity of RNase H recognition by DNA/RNA duplex accomplished through the direct contacts with five consecutive 2′-OH groups on the RNA strand (Figure 3b). The face of the RNase H (BH) containing the active site has two grooves separated by ~8.5 Å, into which the backbones of the RNA/DNA hybrid fit snugly, with the minor groove straddling the ridge in between. The DNA binding groove, which comprises the N terminus of helix αA and the loops between helices αB and αD and between the β1 and β2 strands (Figure 3a), is accentuated by a phosphate binding pocket composed of T104, N106, S147, and T148. The active site of RNase H is located in the groove that accommodates the RNA strand. The catalytic carboxylates E109, D132(N), and their immediate neighbors (N106 and Q134) make hydrogen bonds with two 2′-OH groups immediately 5′ to the scissile phosphate. S74 and G76 adjacent to D71 (the other active-site residue) contact the two 2′-OH groups 3′ to the scissile phosphate. The phosphate binding pocket probably plays a role in anchoring the B form DNA and contributes to the specificity for binding of a mixed conformation RNA/DNA hybrid.

Stereoview of the tr-mut-RNase H (BH) -substrate complex showing molecular surfaces and puckering of ribose sugars in the complex

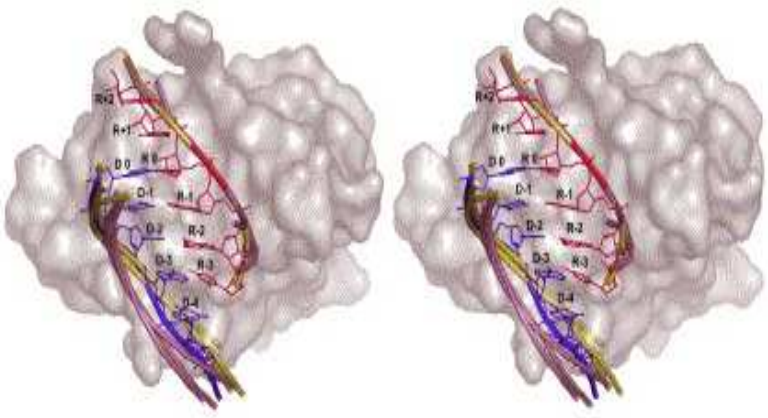

a

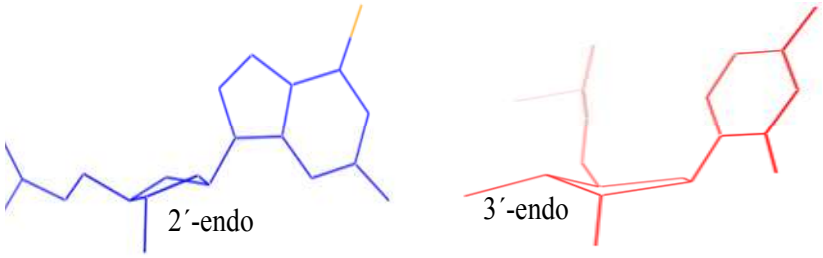

$d^{Se}G$ (3) rC (5)

(b)

Nowotny M,Yang W, (2006) EMBO J. May 3;25(9):1924-33. 6.

Figure 4: Stereoview of the tr-mut-RNase H (BH) -substrate complex showing molecular surfaces and puckering of ribose sugars in the complex.

Figure 4: Stereoview of the tr-mut-RNase H (BH) -substrate complex showing molecular surfaces and puckering of ribose sugars in the complex. (a) The molecular surface of tr-mut-RNase H (BH) is shown in pinkish gray, and the substrate RNA (red) and DNA (blue) are shown as rods (backbone) and sticks (bases). The three crystal (pink) and three NMR (yellow) structures of RNA/DNA hybrids are superimposed onto the RNase H (BH) structure. Nucleotides are numbered relative to the nucleotide at the active site and according to the polarity of the RNA strand. The face of the RNase H (BH) containing the active site has two grooves separated by ~8.5 Å, into which the backbones of the RNA/DNA hybrid fit snugly, with the minor groove straddling the ridge in between.

(b) Suger puckering of ^{Se}DNA and RNA in ^{Se}DNA/RNA duplex in binding in crystal structure with tr-mut-RNase H (BH) protein. DNA and RNA adopt 2′-endo and 3′-endo, respectively, in DNA/RNA duplex.

The RNA/DNA hybrid in the complex of RNase H (BH) adopts a mixed A and B conformation. The RNA strand is in A form with 3′-endo sugar puckers, and the DNA strand is in B form with 2′-endo or 1′-exo sugars (Figure 4b). In addition to the sugar puckers, the mixed A and B character of RNase H (BH) substrate is reflected in the minor-groove width. The average minor-groove width of three A-like crystal structures of RNA/DNA hybrids is 9.8 Å, and the average of three mixed A/B form NMR structures is 8.4 Å, that has been found in DNA/RNA complex (155). Superposition of the three crystal and three NMR structures of RNA/DNA hybrids with that of the RNase H (BH) complex reveals a near perfect alignment of the RNA strands, but the positions of the DNA strands differ (Figure 4a). The B form DNA strand with one local distortion fits the RNase HC surface perfectly, while the A-like structure does not. RNases H probably select and stabilize an RNA/DNA hybrid in the mixed A and B conformation and thereby discriminate against dsRNAs, which are invariably A form.

Superimposition of global and local structures of the 6^{Se}G-modified and native DNA/RNA duplexes of the nucleic acid–protein complex

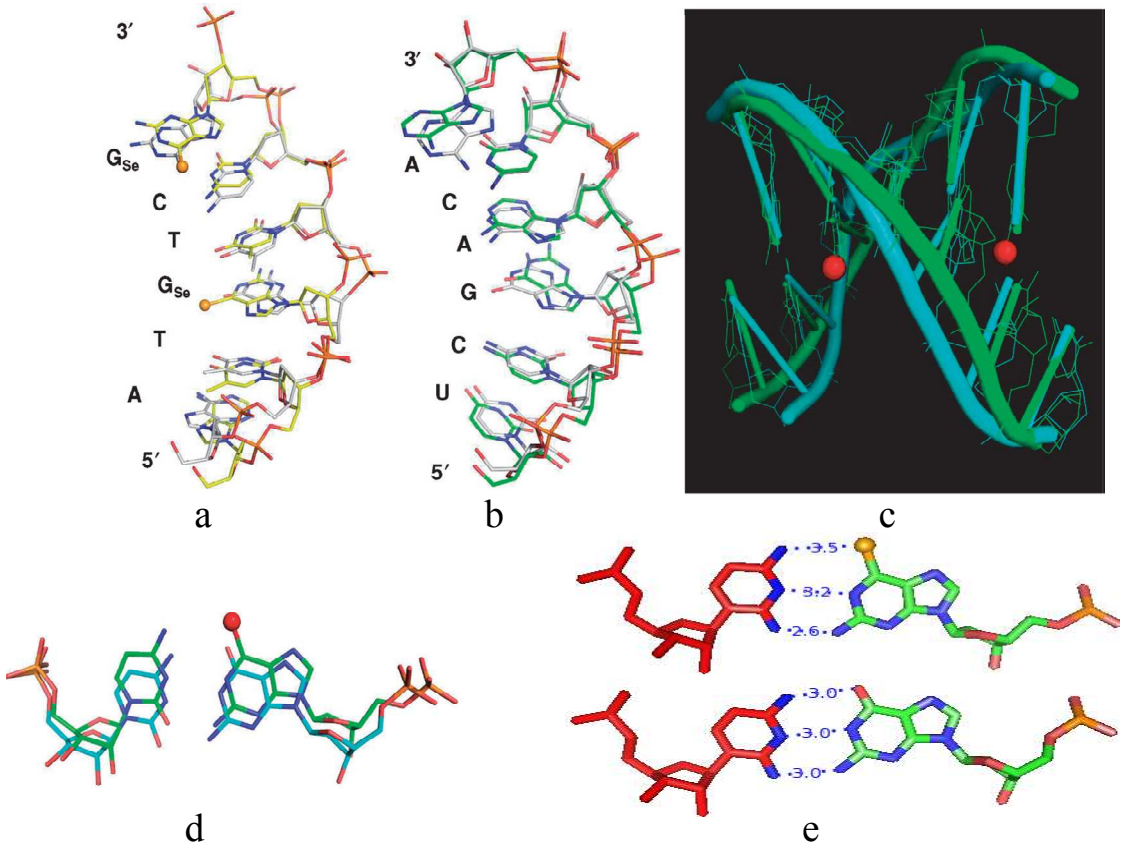

Jozef Salon, Jiansheng Jiang, Jia Sheng, Oksana O. Gerlits and Zhen Huang
Nucleic Acids Research, 2008, Vol. 36, No. 22 7009–7018

Figure 5: Seperimposition of global and local structures of modified and native DNA/RNA duplex. Superimposition of global and local structures of the 6^{Se}G-modified (2R7Y, 1.80-_ resolution) and native (2G8U, 2.70 Å resolution) DNA/RNA duplexes (R_N, 5'-ATGTCG-p-3'/D_2, 5'-UCGACA-3') of the nucleic acid–protein complex are shown.

Figure 5: Seperimposition of global and local structures of modified and native DNA/RNA duplex.

Superimposition of global and local structures of the 6^{Se}G-modified (2R7Y, 1.80-_ resolution) and native (2G8U, 2.70 Å resolution) DNA/RNA duplexes (R_N, 5'-ATGTCG-p-3'/D_2, 5'-UCGACA-3') of the nucleic acid–protein complex are shown. The red balls represent Se-atoms in the Se-derivatized DNA (D_4, 5'-AT^{Se}GTC^{Se}G-p-3'). a) The structure of the ^{Se}DNA sequence (2R7Y, in yellow) is superimposed over the corresponding native DNA (2G8U, in grey). b) The structure of the RNA sequence (2R7Y, in green) is superimposed over the corresponding native (2G8U, in grey). c) Superimposition of ^{Se}DNA/RNA (D_4/R_N) duplex on native DNA/RNA (D_2/R_N) duplex. d) Superimposition of the base pair ^{Se}G (3´)/C (5) on native G/C base pair. Due to introduction of selenium at 6-position of G caused 0.3 Å base pair shifting. e) Comparisons of H-bond lengths in ^{Se}G (3´)/C (5) base pair (2R7Y) with native G/C base pair (2G8U). The crystal structure shows three H-bonds (exo-6-Se/exo-4-NH_2, 1-NH/N(3), and exo-2- NH_2/exo-2-O) with H-bond lengths of 3.5, 3.2, and 2.6 Å, respectively, for ^{Se}G (3´)/C (5) base pair where in native G/C base pair the H-bond lengths for exo-6-O/exo-4-NH_2, 1-NH/N(3), and exo-2-NH_2/exo-2-O are 3.0, 3.0, and 3.0 Å, respectively.

The superimposed global and local structures of the 6 - ^{Se}G-modified DNA/RNA duplex (5'-AT^{Se}GTC^{Se}G-p-3'/5'-UCGACA-3') and native DNA/RNA duplexes (5'-ATGTCG-p-3'/5'-UCGACA-3') in the nucleic acid–protein complex demonstrated that the global nucleic acid structures of the native and Se-modified duplexes are very similar (Figure 5a,b). The ^{Se}G and C also form a base pair, similar to the native G/C pair, via the Se-mediated H-bond (Se· · ·H:N) exo-6-Se/exo-4-NH_2. It was noticeable that due to selenium introduction at the 6 position of G, the hydrogen bond length between exo-6-Se and exo-4-NH_2 increased to 3.5 Å which was 0.5 Å longer than its native counterpart (3.0 Å As a result of this increase, due to the presence of bigger atom, the H-bonds of 1-NH/N(3) also increased (3.2 Å) but the H-bond of exo-2- NH_2/exo-2-O (2.6 Å became shorter in comparing with the native. The shorter H-bond of exo-2- NH_2/exo-2-O (2.6 Å) may due to sustain the helical properties of the RNA/DNA duplex, such as minor groove width (8.4 Å) (Figure 4a), in order to fit itself in the enzyme binding site (Figure 5e). The introduction of larger atom selenium in place of oxygen at 6 position of G also caused shifting of the ^{Se}G:C base pair about 0.3 Å (Figure 5d). This shifting could reduce the aromatic base stacking interaction that might arise from the greater anharmonicity of the exo-6-Se/exo-4-NH_2 vibrational potential of the G in ^{Se}G/C, which arises from electronic interactions between ^{Se}G/C and adjacent bases. The lessening of base stacking interaction coupled with increase in H-bond length may bring into being decrease in stability for selenium modified DNA/RNA duplex (5'-AT^{Se}GTCG-p-3'/5'-UCGACA-3'). This phenomenon may reflect in decrease in T_m, higher in free energy of duplex formation, and binding to enzyme (-Δ*G*) that we observed in our present study (discussed later).

Although, as a whole, the stability of the selenium modified DNA/RNA duplex (5'-AT^{Se}GTCG-p-3'/5'-UCGACA-3') was substandard compare to the other duplex considered in this study, we found the reactivity of the se-modified DNA as a template was much faster used by the tr-RNase H (BH) enzyme. It is worth pointing out that this novel strategy could be used as an alternative and simple tool to study enzyme functions and enzyme mechanisms. It also could be use to enhance enzyme activities and that might have therapeutic advantages.

Active site of tr-RNase H (BH) complex with the ^{Se}DNA/RNA hybrid

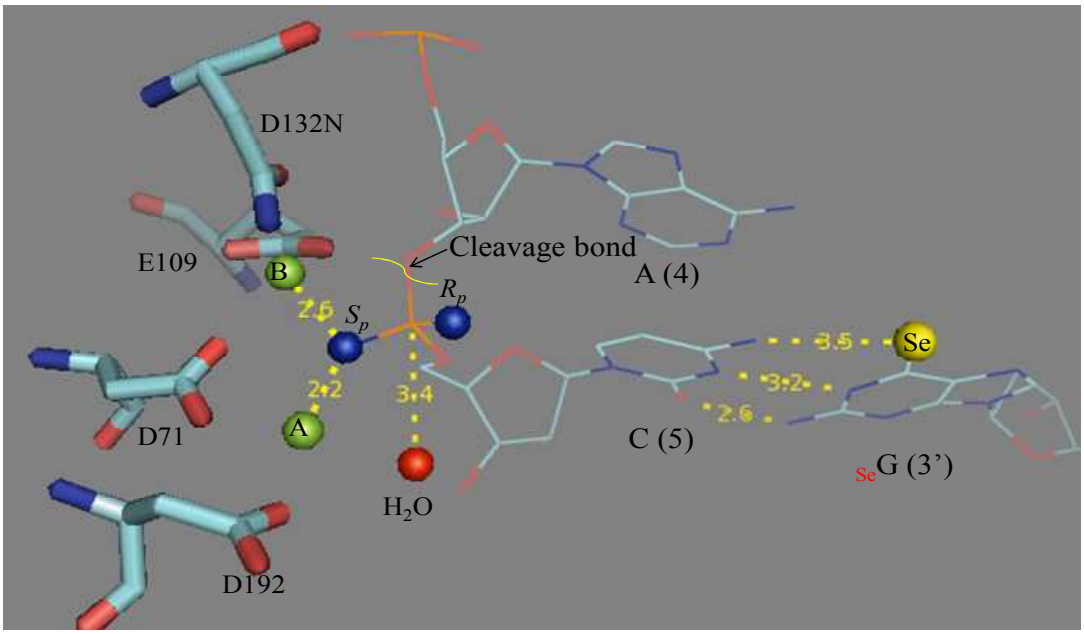

Figure 6: Active site of tr-mut-RNase H (BH) complex with the selenium modified DNA and RNA hybrid. Amino acid residues in the active site are labeled. In substrate RNA strand, cleavage bond between the base rC (5) and rA (4) are marked. In the template DNA strand selenium modified G (3') forms base pair with rC (5) in RNA strand. The water molecule positioned to attack the scissile phosphate is indicated. Metal-ions A and B are coordinated by amino acid residues are labeled. Pro-R_p and pro-S_p oxygens are labeled as R_p and S_p, respectively. The metal ions A and B also interact with pro-S_p oxygen and the distances are 2.2 Å and 2.6 Å, respectively. The nearest water molecule is 3.4 Å away from the electrophile phosphate atom.

Interactions of metal ion and water molecule with pro-S_p and pro-R_p oxygen in tr-mut-RNase H (BH) active site

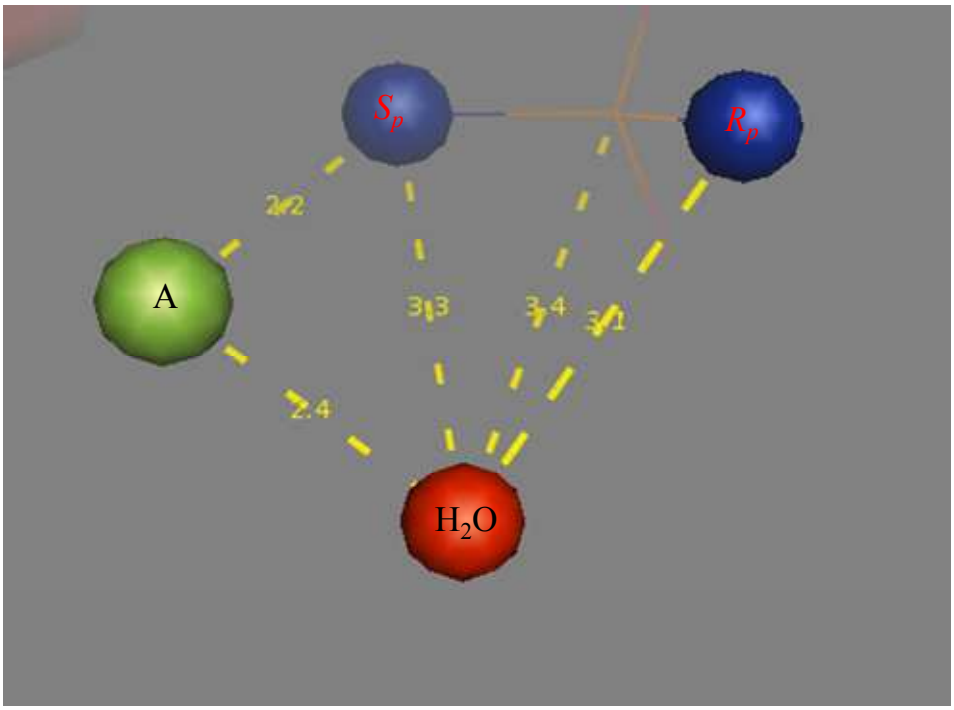

Figure 7: Interactions of metal ion and water molecule with pro-Sp and pro-Rp oxygen in tr-mut-RNase H (BH) active site. The metal ion A positioned at co-ordinating distance (2.4 Å) with pro-Sp oxygen and water molecule. The water molecule become activated by positively charged metal ion (Mg^{+2}) which makes nucleophilic attack on phosphate atom.

In nucleotidyl transfer reactions catalyzed by an RNase H-like enzyme, two metal ions catalytic mechanism have been proposed by Steitz and Steitz in 1988. In this mechanism the metal ion A activates the water molecule for nucleophilic attack and metal ion B stabilizes the pentacovalent intermediate and the product. In RNase H (BH) four conserved and one nonconserved carboxylate amino acid residues constitute the active site. The A metal is coordinated by D192, E188 (a nonconserved fifth carboxylate), the pro-S_p oxygen atom of the scissile phosphate, and the water molecules in a nearly perfect octahedral geometry (Figure 6). The metal ion A also coordinated by the first conserved carboxylate, D71, is located in the middle of the β1 strand (Figure 2) and D71 coordinates both metal ions A and B (Figure 6). One of the water molecules is 3.4 Å away from the scissile phosphate and is perfectly positioned for an in-line nucleophilic attack (Figure 7). This water molecule does not contact any protein residues, but it is only 3 Å from the pro-R_p oxygen of the phosphate immediately 3′ to the scissile bond. Replacement of this pro-R_p but not the pro-S_p oxygen with a sulfur atom reduces the k_{cat} of *E. coli* RNase H by 86%. This pro-R_p oxygen most likely orients the water for the nucleophilic attack and may even serve as a general base for deprotonation and then shuttle the proton to solvent. The B metal ion, which is proposed to stabilize the pentacovalent intermediate and the product 3′-OH, is coordinated by E109, D132 (mutated to Asn), and both bridging and nonbridging oxygen atoms of the scissile phosphate (Figure 6 and 8).

Stepwise reaction steps for RNase H catalysis

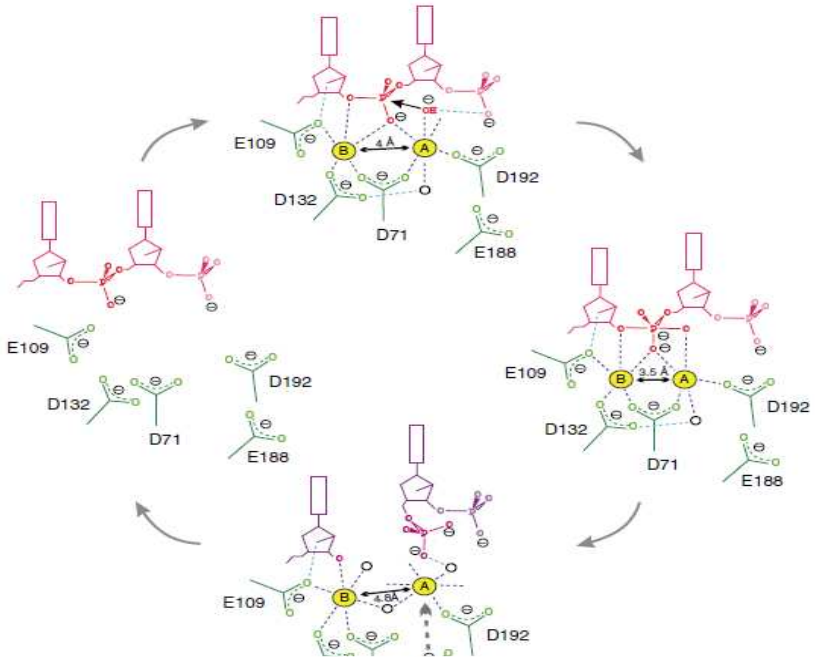

Nowotny M, Yang W, (2006) EMBO J. May 3;25(9):1924-33

Figure 8: Stepwise reaction steps for RNase H catalysis

The substrate RNA is shown in pink and products in purple. Coordination of metal ions is highlighted in dark blue and scissile phosphate in red. Selected hydrogen bonds are shown as blue lines. Blackcircles represent water molecules. The distance between the two metal ions is indicated in the enzyme–substrate, enzyme–intermediate and enzyme–product complexes.

The catalysis of RNase H (BH) occurs in severel steps showing in Figure 8. All the interactions and atomic distances are equally important for catalysis to occur. The nucleotides upstream and downstream of the cleavage bond are well coordinated. The catalysis begins with activating the water molecule, which is 3.4 Å away from sessile phosphate atom (Figure 6), is coordinated by the metal ion A and the phosphate oxygen of the nucleotide immediately 3' of the scissile phosphate. The 3'-oxygen and 2'-OH of the nucleotide upstream to sessile phosphate are coordinated by the metal ion B and E109, respectively. The 3'-oxygen interact with metal ion A and pro-R_p oxygen coordinated by both the metal ions. The optimum distance between two metal ions is 4 Å. This reaction occurs by one-step by S_N2-like (bimolecular nucleophilic substitution) accompanied by a pentacovalent intemediate and inversion of the phosphate stereo configuration. The cleavage products are 3'-OH and 5'-phosphate.

3.4.2 Free energy of duplex formation is higher for selenium modified DNA base pair with complementary RNA.

Melting temperature studies were performed in order to determine the free energy of duplex formations. This free energy determination would give information's whether selenium incorporation at 6-position of the base G has any effect on duplex formation. Three DNA sequences, native DNA (D_{TmN}): 5'-TGTCGTGTCG-3', sulfur modified DNA (6-Sulfur G) (D_{TmS}): 5'-TGTCGT^{S}GTCG-3', and selenium modified DNA (6-Seleno G) (D_{TmSe}): 5'-TGTCGT^{Se}GTCG-3, base pair with complementary RNA (R_{Tm}): 5'-ACGACACGAC-3', was selected. In each duplex nine bases would form base pair where 5'-dT and 5'-rA remain overhang on both sides. Of the two modified DNA oligos, D_{TS} has sulfur at the 6-position of G substituted for oxygen atom (O) and in D_{TSe} selenium at the same position in place of oxygen atom (O). The native DNA, D_{TN}, was selected for comparing the melting temperatures (T_m) and the free energies with modified duplexes. In establishing T_m study, D_{TmN} or G_{TS} or D_{TmSe} was mixed with R_{Tm} in equimolar ratio (1:1) in T_m buffer (5 mM sodium phosphate, pH 7.0, 0.5 mM EDTA, 1 M NaCI, 10 mM di-borane in THF). Four different concentrations for each duplex ranging from 8.74 μM down to 0.25 μM were chosen to determine the enthalpies by using van't Hoff method. The duplexes were placed in a water bath preheated to 85 °C and allowed to cool down to room temperature and placed at 4 °C freezer for 3 hours. Samples were placed in quartz cuvettes with 1 cm path length in thermostated sample chamber of Cary win UV 300 UV-vis spectrophotometer to monitor the melting curve. The temperature was raised from 6 °C - 80 °C with a rise of 0.5 °C/min and the UV spectra recorded in every 0.5 min at 260 nm wave lengths

and the each process was repeated four times. The T_m profile for the duplex D_{TmN}/ R_{Tm} is given below that has been carried out in four different concentrations. The T_m of the duplex concentration 0.25 µM, 3.08 µM, 5.92 µM, and 8.74 µM was 52.2 °C, 54.5 °C, 56.2 °C, and 58.2 °C, respectively, showed increment of T_m with the increase in duplex concentration.

Melting temperature (T_m) of the duplex D_{TmN}/ R_{Tm} at four different concentrations

D_{TmN}/ R_{Tm} : 5'-TGTCGTGTCG-3'/5'-ACGACACGAC-3'

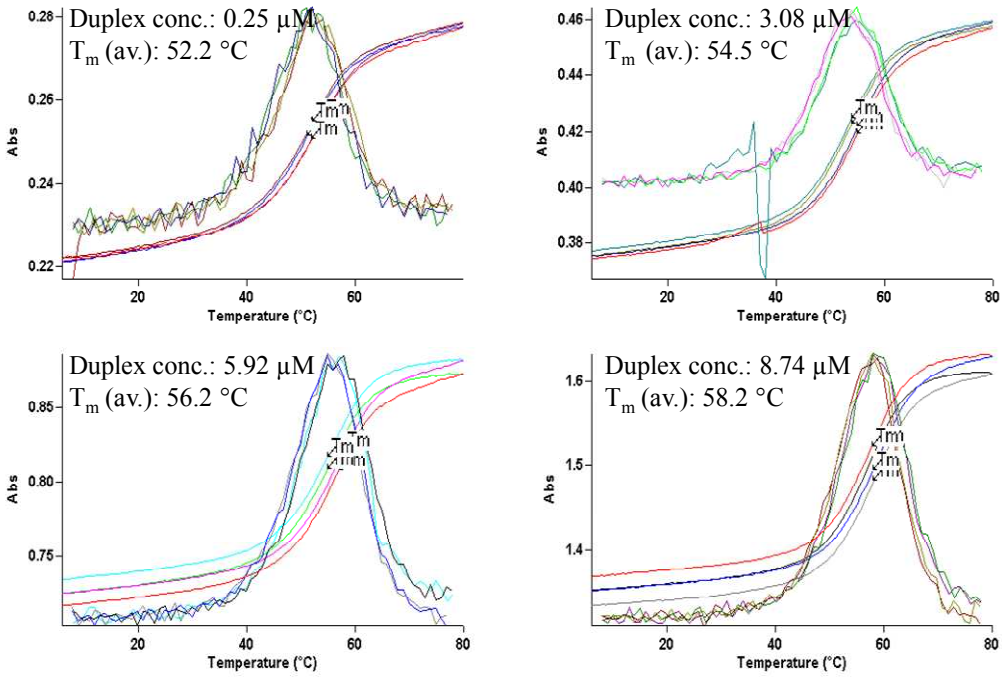

Figure 9: T_m of the duplex D_{TmN}/ R_{Tm} (5'-TGTCGTGTCG-3'/5'-ACGACACGAC-3') at four different concentrations. The measured T_m of the duplex concentration, 0.25 µM, 3.08 µM, 5.92 µM, and 8.74 µM was 52.2 °C, 54.5 °C, 56.2 °C, and 58.2 °C, respectively, showed increment of T_m with the increase in duplex concentration.

Melting temperature (T_m) of the duplex D_{TmS} / R_{Tm} at four different concentrations

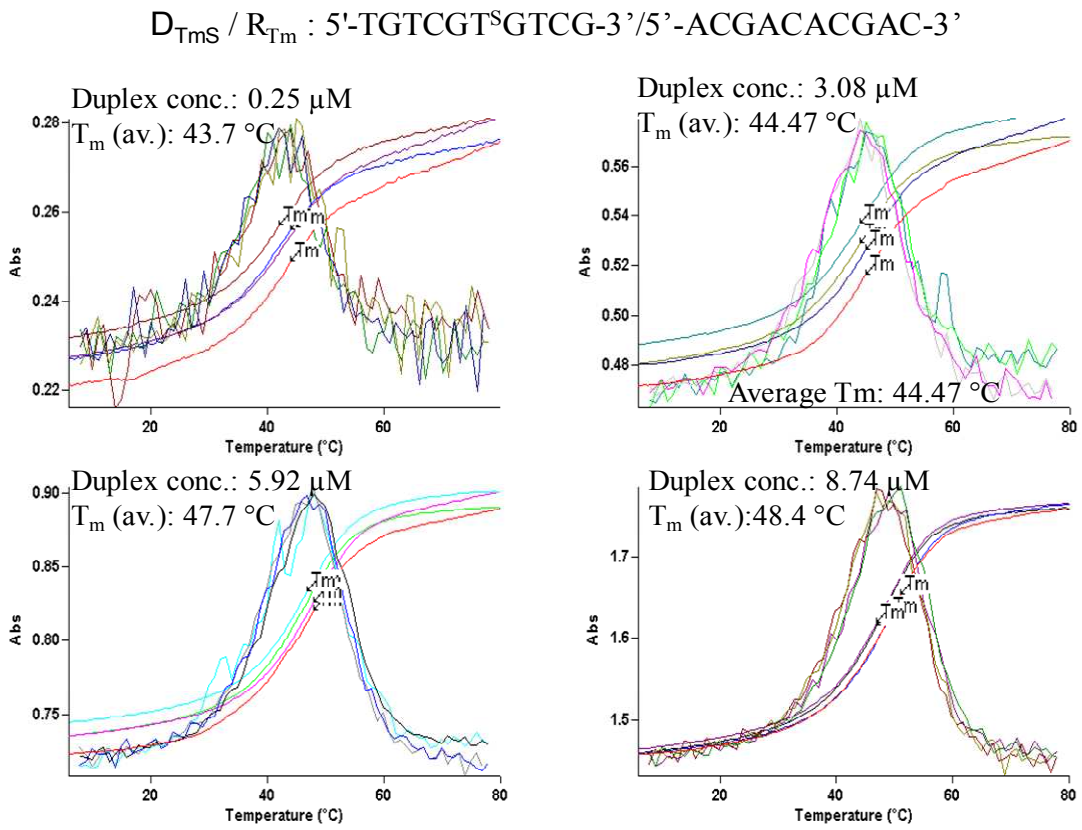

Figure 10: T_m of the duplex D_{TmS} / R_{Tm} (5'-TGTCGT^{S}GTCG-3'/5'-ACGACACGAC-3') at four different concentrations. The measured T_m of the duplex concentration, 0.25 µM, 3.08 µM, 5.92 µM, and 8.74 µM was 43.7 °C, 44.47 °C, 47.7 °C, and 48.4 °C, respectively, showed increment of T_m with the increase in duplex concentration.

Melting temperature (T_m) of the duplex D_{TmSe} / R_{Tm} at four different concentrations

D_{TmSe} / R_{Tm} : 5'-TGTCGT^{Se}GTCG-3'/5'-ACGACACGAC-3'

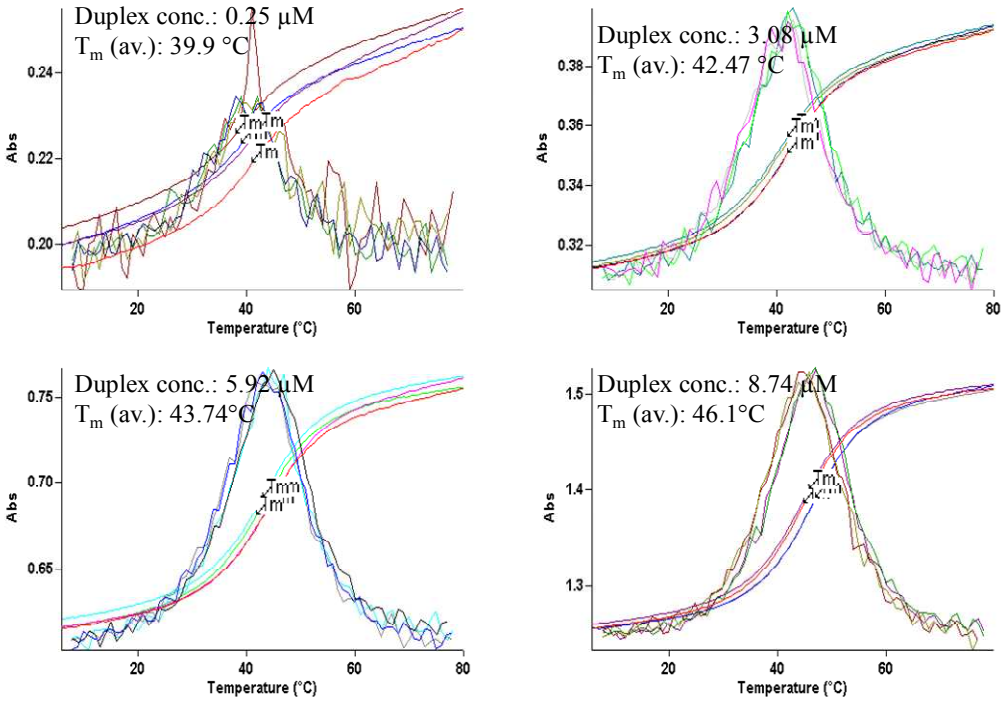

Figure 11: The measured T_m of the duplex concentration, 0.25 µM, 3.08 µM, 5.92 µM, and 8.74 µM was 39.9 °C, 42.47 °C, 43.4 °C, and 46.1 °C, respectively, showed increment of T_m with the increase in duplex concentration.

After collecting all melting temperature data the thermodynamic parameters were analyzed by van't Hoff method. The van't Hoff enthalphy and entropy were determined from the dependence of Tm on DNA/RNA duplex concentration by the following equation:

$$1/T_m = (n\text{-}1)R \ln[C_T] / \Delta H^o + \Delta S^o / \Delta H^o$$

Where *Ct* was the total strand concentration, n, R, and ΔS^o denoted as molecularity, gas constant, and entropy, respectively. The plot was constructed by 1/Tm *VS* ln C_T plotted on the Y-axis and X-axis, respectively. Three sets of data for native, sulfur modified, and selenium modified DNA were placed in the same graph and the slope was set equal to (n-2) R/ΔH° where n value set to 2 and intercept was equal to $\Delta S/\Delta H^o$. Slope and intercept of the plot were calculate using Microsoft excel. After calculating entropy (ΔS^o) and enthalpy (ΔH^o) for each DNA/RNA duplex, free energy of each duplex formation was determined by using the following equation:

$\Delta G^o = \Delta H^o - T\Delta^\circ S^o$, where T is the absolute temperature.

van't Hoff plot for native and modified DNA/RNA duplex ($1/T_m$ vs ln C_T)

Figure 12: van't Hoff graphical representation of reciprocal melting temperature ($1/T_m$) and natural log of total strand concentrations (ln C_T) plotted on Y- and X-axis, respectively. The symbol "◆", "◇" and "▼" in the graph represents the T_m of duplex $D_{TmSe}/R_{Tm,}$ D_{TmS}/R_{Tm}, and D_{TmN}/R_{Tm} at various concentrations, respectively. It has been noticed that the duplex stability was $D_{TmN}/R_{Tm} > D_{TmS}/R_{Tm} > D_{TmSe}/R_{Tm}$.

All duplexes (Figure 9, 10, and 11) we investigated gave cooperative, reversible melting transitions in different concentrations that allow the accurate determination of T_m by UV absorption method. Each duplex formation monitored by UV absorption methods to have a single melting transition with very similar curve shapes and melting temperatures. The result indicated two state melting behaviors for these duplexes. The order of stability for the duplexes under similar condition is $D_{TmN}/R_{Tm} > D_{TmS}/R_{Tm} > D_{TmSe}/R_{Tm}$. The stability of native DNA is significantly higher than those of modified DNA's, and that has the selenium been being the least. By calculating slope and intercept of the plot using Microsoft Excel the thermodynamic parameters, entropy and enthalpy, were determined by van't Hoff methods. These parameters have been used to calculate free energies for duplex formation. The thermodynamic parameters of duplex formation are given in the Table- 1.

Thermodynamic Parameters for Duplex Formation by Native and Modified DNA with RNA (vant Hoff's Method)

Abbreviations	Tm (°C)	-Δ*G* (Kcal/mol)	-Δ*H*° (Kcal/mol)	-Δ*S*° (Kcal/mol-deg)
D_{TmN} / R_{Tm}	54.5	14.6	79.5	0.203
D_{TmS} /R_{Tm}	44.7	12.2	75.3	0.2
D_{TmSe}/R_{Tm}	42.4	11.3	68.6	0.198

D_{TmN} : 5'-TGTCGTGTCG-3'
D_{TmS}: 5'-TGTCGT^{S}GTCG-3'
D_{TmSe} : 5'-TGTCGT^{Se}GTCG-3'
R_{Tm} : 5'-CGACACGACA-3'

$$1/T_m = (n\text{-}1)R \ln[C_T] /\Delta H^o + \Delta S^o/\Delta H^o$$

$\Delta G^o = \Delta H^o - T\Delta S^o$,
where T is the absolute temperature

Table 1: Thermodynamic Parameters for Duplex Formation by Native and Modified DNA with RNA (vant Hoff's Method). Melting temperatures (T_m), free energies (ΔG), enthalpies (ΔH°), and entropies (ΔS°) of native and modified duplexes are shown. Free energy (-ΔG) for native duplex is higher than the other two duplexes where as it is the lowest for selenium modified duplex.

The free energy difference of duplex formation between D_{TmN} / R_{Tm} (native) and D_{TmSe}/R_{Tm} (selenium modified) was 3.2 Kcal/mol. In comparing the D_{TmN} / R_{Tm} (native) with D_{TmS} /R_{Tm} (sulfur modified) the difference was 1.7 Kcal/mol. In terms of duplex stability the D_{TmN} / R_{Tm} (native) was the most stable in compare with the other two which was consisted with T_m data. Enthalpy data showed the similar trends. The enthalpy of D_{TmN} / R_{Tm} (native) duplex was 5.6 Kcal/mol higher than that of D_{TmSe}/R_{Tm} (selenium modified) duplex. Whereas there was little difference between D_{TmN} / R_{Tm} (native) and D_{TmS} / R_{Tm} (sulfur modified) duplex. Considering all thermodynamic parameters it could be concluded that the selenium modified DNA and RNA duplex (D_{TmSe}/R_{Tm}) has the lowest stability. This observation was consisted with the X-ray crystal structure study where it has been observed the base pair shifting (0.3 Å) due to selenium incorporation at the 6-position of G in place of oxygen atom.

3.4.3 RNase H (BH) enzyme binds to the 5'-AT^{Se}GTCG -3' (D_3)/ 5'-UCGACA-3' (R_N) with lower affinity

Gel shift assay was performed to detrmine the binding energy of the duplex D_3/R_N (5'-AT_{Se}GTCG -3'/ 5'-UCGACA-3') with RNase H (BH) enzyme. The duplexes D_2/R_N (5'-ATGTCG - P-3'/5'-UCGACA-3') and S_1/R_N (5'-AT^{S}GTCG-P-3'/5'-UCGACA-3') were used to compare the binding energies. In S_1, the oxygen atom at 6-position of the base G has been replaced with sulfur atom. The sulfur atom is in the same group as oxygen which is smaller than selenium but larger than oxygen. From these substitutions (selenium or sulfur) we have been trying to understand the effect of larger atom on melting temperature of the duplex and on binding affinity for RNase H (BH) and eventually the rate of substrate hydrolysis (RNA) using those modified DNA as templates. In all three types of duplex, D_2/R_N, $D3/R_N$, and S_1/R_N the the duplex concentration was 1 μM and enzyme concentration increased from 1 μM to 13.5 μM (Figure 12). Among the three duplexes the binding affinity for the selenium modified DNA/RNA duplex for RNase H (BH) was the lowest (Figure 13, c) and sulfur modified DNA/RNA being intermediate (Figure 13, b). It has observed that almost all the duplex occupied by the enzyme at the concentration 9.5 μM when D_3/R_N was used whereas the same amount of duplex was bound at enzyme concentration 7.5 μM for S_1/R_N (Figure 13, b). The affinity of the enzyme for native DNA/RNA duplex was the highest; almost all duplexes were bound to enzyme at concentration 2 μM (Figure 13a and 13d). The dissociation constant (K_d) of RNase H (BH) for all duplexes were determined by calculating the enzyme concentration where 50 % of the duplex was bound. This has been done by plotting the enzyme concentration at variable axis (X-axis) and fractional

occupancy on Y-axis (Figure 14). The calculated Km was 2.5 μM, 4.3 μM, and 6.4 μM for the duplex D_2/R_N, S_1/R_N, and D_3/R_N, respectively. From this dissociation constant it was clear the binding of duplex with RNase H (BH) stronger for native, lowest for selenium modified and intermediate for sulfur modified DNA with the order $D_2/R_N > S_1/R_N > D_3/R_N$. The free energy of duplex binding with RNase H (BH) for each duplex was calculated from the equilibrium constant by using the following equation.

$$\Delta G = - 2.303\, RT \log_{10} K_{eq}$$

Where R is gas constant, T is absolute temperature, and K_{eq} is the equilibrium constant ($1/K_d$). The calculated free energy for duplex D_2/R_N, S_1/R_N, and D_3/R_N binding to RNase H are + 0.32, + 0.93, and + 1.13 Kcal/mol at 25 C°. The order of the free energy of binding is $D_2/R_N > S_1/R_N > D_3/R_N$ which is consistent with gel analysis (Figure 13).

Analysis of RNase H (BH) binding to different modified and native DNA/RNA duplexes by gel-shift assay

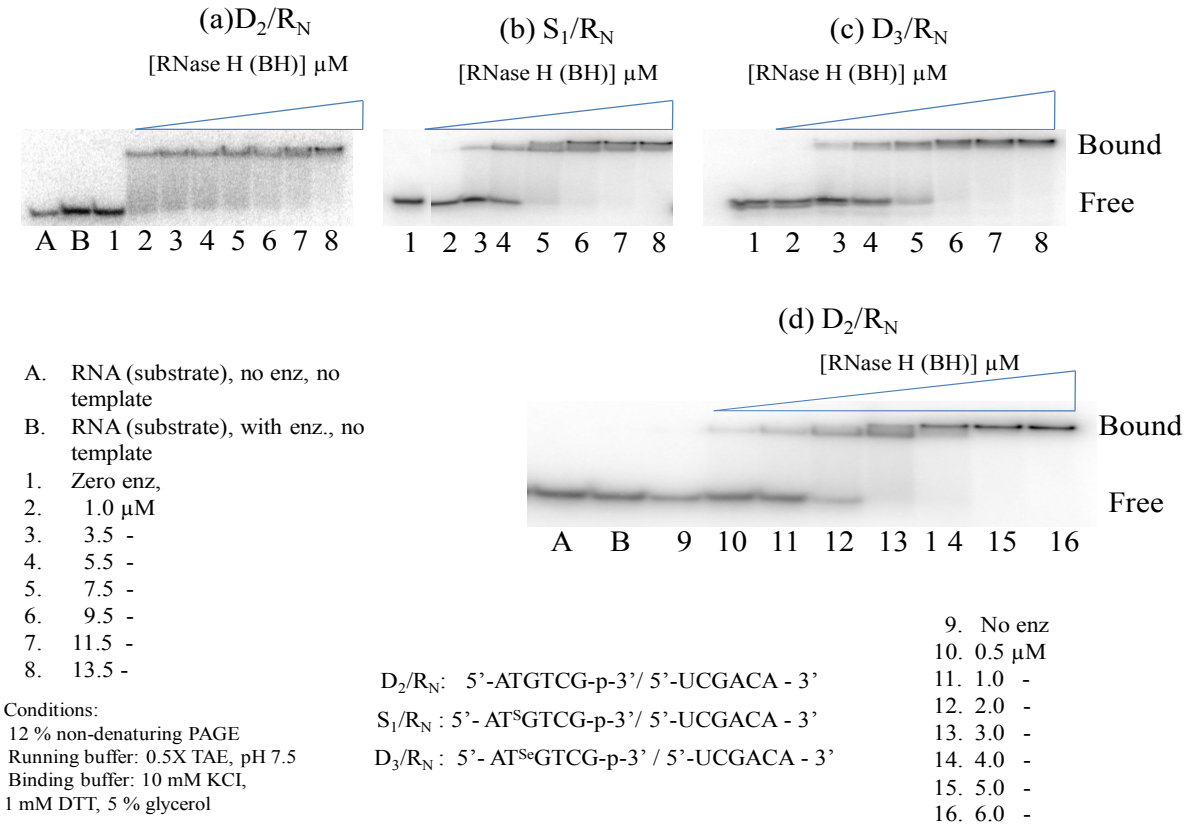

Figure 13: Analysis of RNase H (BH) binding to different modified and native DNA and RNA duplexes by gel-shift assay.

Figure 13: Analysis of RNase H (BH) binding to different modified and native DNA and RNA duplexes by gel-shift assay. (a) Binding of RNase H (BH) with the duplex D_2/R_N ((5'- ATGTCG - P-3'/5'-UCGACA-3') at 0 - 13.5 μM enzyme concentration. (b) Binding of RNase H (BH) with the duplex S_1/R_N (5'-AT^{S}GTCG-P-3'/5'-UCGACA-3') at 0-13.5 μM enzyme concentration (c) Binding of RNase H (BH) with the duplex D_3/R_N (5'-AT^{Se}GTCG -3'/ 5'-UCGACA-3') at 0-13.5 μM enzyme concentration (d) Binding of RNase H (BH) with the duplex D_2/R_N (5'- ATGTCG - P-3'/5'-UCGACA-3') at 0 - 6.0 μM enzyme concentration.

Measurement of dissociation constant by gel shift assay

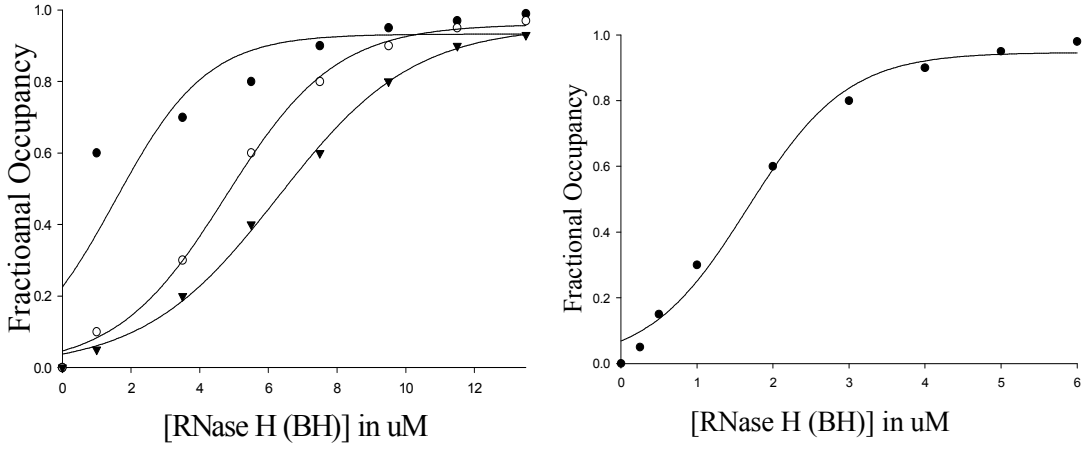

a b

● D_2/R_N: 5'-ATGTCG-p-3'/ 5'-UCGACA - 3'

o S_1/R_N : 5'- $AT^{S}GTCG$-p-3'/ 5'-UCGACA - 3'

▼ D_3/R_N : 5'- $AT^{Se}GTCG$-p-3' / 5'-UCGACA - 3'

K_d in µM

Native:	1.7
Sulfur:	4.83
Selenium:	6.4

..

Figure 14: Measurement of equilibrium constant (K_d) of RNase H (BH) binding to modified and native DNA /RNA duplexes by gel shift assay

Figure 14: Measurement of equilibrium constant (K_d) of RNase H (BH) binding to modified and native DNA /RNA duplexes by gel shift assay. The K_d was determined from the enzyme concentration at which 50 % of the duplex was bind to enzyme. (a) Fractional occupancy of the duplexes, D_2/R_N (5'-ATGTCG- P-3'/5'-UCGACA-3'), S_1/R_N (5'-AT^{S}GTCG-P-3'/5'-UCGACA-3') and D_3/R_N (5'-AT^{Se}GTCG-3'/ 5'-UCGACA-3') at 0-13 μM enzyme concentration. (b) Fractional occupancy of the duplex D_2/R_N (5'- ATGTCG - P-3'/5'-UCGACA-3') at 0 - 6 μM enzyme concentration. The K_d of the duplex D_2/R_N, S_1/R_N, and D_3/R_N are 1.7 μM, 4.83μM, and 6.4 μM, respectively.

Dissociation constant and free energies of native and modified DNA/RNA duplexes binding to RNase H (BH)

Parameters	$\Delta G_{\text{Binding}}$ (Kcal/mol)	K_d (µM)
D_2/R_N (5'- ATGTCG - P-3' /5'-UCGACA-3')	+ 0.32	1.7
S_1/R_N (5'-AT^{S}GTCG-P-3' /5'-UCGACA-3')	+ 0.93	4.83
D_3/R_N (5'-AT^{Se}GTCG -3' / 5'-UCGACA-3')	+ 1.13	6.4

Table 2: Dissociation constants and free energies of modified DNA/RNA duplexes binding to RNase H (BH). The dissociation and free energies (-ΔG) of $D_2/R_N > S_1/R_N > D_3/R_N$ binding to RNase H (BH) are 1.7, 4.83, and 6.4 µM and + 0.32, + 0.93, and +1.13 Kcal/mol, respectively.

The calculated free energy for duplex D_2/R_N, S_1/R_N, and D_3/R_N binding to RNase H are + 0.32, + 0.93, and + 1.13 Kcal/mol at 25 C°. The order of the free energy of binding is $D_2/R_N > S_1/R_N > D_3/R_N$. From the calculation of free energies it was clear that binding of RNase H (BH) to native duplex D_2/R_N (5'- ATGTCG - P-3'/5'-UCGACA-3') was the most favorable and for the duplex D_3/R_N R_N (5'-AT^{Se}GTCG -3'/ 5'-UCGACA-3') was the least favorable among the three duplexes under study which was consistent with the dissociation constants (K_d) and gel analysis (Figure 13).

3.4.4 Catalytic activities of truncated RNase H (BH) was higher on RNA substrate base paired with modified DNA templates

Catalytic activities of truncated RNase H (BH) on RNA substrate base paired with native and modified DNA templates. The 5'-^{32}P labeled RNA substrate were incubated with DNA templates D1, D2, D3, D4, S1, and S2, and wild type or truncated RNase H (RH) for 10 minutes at 37 C°. The reactions were analyzed on the 21 % PAGE after 1 hour of run and the gel was dried by gel dryer and image was taken by phosphoimager. From the gel analysis it has been shown that the template D1 and D3 have the better performance as a templates over others (a, lane 3 and lane 6, respectively). Among the modified templates, including that has the 3'-phosphate, the DNA template containing $_{Se}$G at the third position from 5'-end serving as a better template catalysis by the tr-RNase H (BH) enzymes.

Catalytic activities of truncated RNase H (BH) on RNA substrate base paired with native modified DNA templates

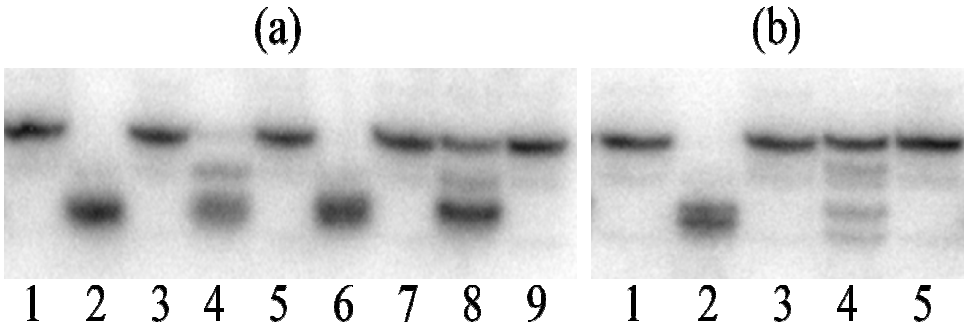

Figure 15: Catalytic activities of truncated RNase H (BH) on RNA substrate base paired with native modified DNA templates.

(a)Lane 1, D_1/R_N (5'-ATGTCG-3'/ 5'-UCGACA-3') NE; lane 2, D_1/R_N, WE; lane 3, D_2/R_N (5'-ATGTCG-P-3'/ 5'-UCGACA-3'), NE; lane 4, D_2/R_N WE; lane 5, D_3/R_N (5'-AT^{Se}GTCG -3'/5'-UCGACA-3') NE; lane 6, D_3/R_N WE; lane 7, D_4/R_N NE; lane 8, D_4/R_N (5'- AT^{Se}GTC^{Se}G -3'/5'-UCGACA-3') WE; lane 9, RNA substrate (no template) WE.

(b)Lane 1, S_1/R_N (5'- AT^{S}GTCG -3'/5'-UCGACA-3') NE; lane 2, S_1/ R_N WE;

lane 3, S_2/ R_N (5'- AT^{S}GTC^{S}G -3'/5'-UCGACA-3') NE; lane 4, S_2/ R_N WE; lane 5, RNA substrate NE, no template. NE: no enzyme, WE: with enzyme

We have made several observations for selenium incorporation into DNA base that paired with complementary RNA. X-ray diffraction results of the selenium modified DNA, RNA and RNase H (BH) showed that the ^{Se}G/C base pair shifted about 0.3 Å which might affect base stacking interaction. As a result of poor base stacking the duplex stability get lower what we observed from lower melting temperature studies and lower free energy (-Δ*G*) calculated by vant Hoff,s method. RNase H binds to the DNA/RNA duplex and stronger binding depends on the duplex stability. If the duplex is less stable then the enzyme binding will be less strong. This actually reflected in binding study where we observed that the RNase H has lower affinity for selenium modified DNA duplex than that of native and even to sulfur modified DNA duplex. Then we proceeded to understand the role of selenium on catalytic activity of RNase H (BH), if any. We used only one 6-mer RNA substrate (R_N, 5'-UCGACA-3') that has been co crystallized with RNase H (BH). There were five different DNA templates, D_2 (5'-ATGTCG-p-3'), D_3 (5'-AT^{Se}GTCG-p-3'), D_4 (5'-AT^{Se}GTC^{Se}G-p-3'), S_1 (5'-AT^{S}GTCG-p-3'), and S_2 (5'-AT^{S}GTC^{S}G-p-3') and used. In D_2 there was no modification but one phosphate group was placed at the 3'-end instead of hydroxyl (-OH) group. In selenium modified DNA the base G (^{Se}G) has been modified by replacing its oxygen at 6 positions by selenium. Template D_3 contained one ^{Se}G at the 3rd place from 5'-end of 6-mer DNA (Figure 1, 3') and template D_4 has two ^{Se}G at the 3rd and 6th from the same direction (Figure 1, 6'). We also considered another kind of modification, S_1 and S_2, where the sulfur was placed at the same position of the base G's to compare the effect of

different atoms from the same group in the periodic table. In order to observe catalytic the activity of RNase H (BH) for different modified templates we incubated different duplexes with tr-RNase H (BH) and the results analyzed by the polyacrylamide gel. The RNA substrate was labeled at 5'-end that visualized after exposing on X-ray film or phosphoimager. It has been observed that the catalytic activity of the tr-RNase H (BH) was the highest when the template D_1 (Figure 15, lane 2) and D_3 (Figure 15, lane 6) were used. Among the different modified DNA templates, including D_2 (Figure 15, lane 4) that has phosphate at the 3'-end, the DNA template with single selenium modified base found to be more active in catalysis by tr-RNase H (BH) enzyme.

3.4.5 Apparent reaction rate (K_{app}) and apparent catalytic rate (K_{cat}) was higher for truncated RNase H (BH) when base pair with selenium modified DNA template

The primary results we obtained from the experiment described in Figure 15 indicated that the activity of tr-RNase H (BH) was different for different DNA templates we used. It was observed that the DNA D_3 showed more efficient as template as comparing to other. In this DNA only one G base at the 3rd position from 5'-end (Figure 1, 3') has been modified. But interestingly, the D_4 DNA, where both the G bases at position 3rd and 6th from the 5'-end were modified (Figure 1, 3' and 6') did not demonstrated as an efficient template. On the other hand the S_1 DNA (Figure 15b, lane 2) has much better performance than D_4 DNA template and even to S_2 (Figure 15b, lane 4) but not as efficient as D_3. We proceeded further to determine the apparent rate constant (K_{app}), the turnover number (K_{cat}) of the enzyme tr-RNase H (BH) for substrate hydrolysis on different DNA templates. Equal amount of different DNA/RNA duplexes were mixed with equal amount of enzymes and aliquot was transferred at different time. The reactions were analyzed by paolyacrylamide gel and visualized by exposing on film or phosphorimazer. The results were shown in Figure 16. We used wild type (1-196 aa) and truncated RNase H (BH) enzymes on a single duplex in order to determine the efficiency of the enzyme. It has been found that the truncated version was more efficient in catalysis than that of wild type. We observed that when we used the template D_2 the truncated enzyme hydrolyzed the substrate about 70 % (Figure 16b, Figure 17) where the wild type hydrolyzed 25 % (Figure 16a, Figure 17) at the same time (in 10 minutes). Then we carried on the experiments with only truncated RNase H (BH) enzyme with different templates. It has been shown that the DNA D_3 was the most efficient template because

it hydrolyzed the substrate about 90% in 10 minutes (Figure 16c, Figure 17) which was the highest among the all templates used.

Kinetic analysis of WT (wild type) and tr (truncated) RNase H (BH) activities on different DNA templates

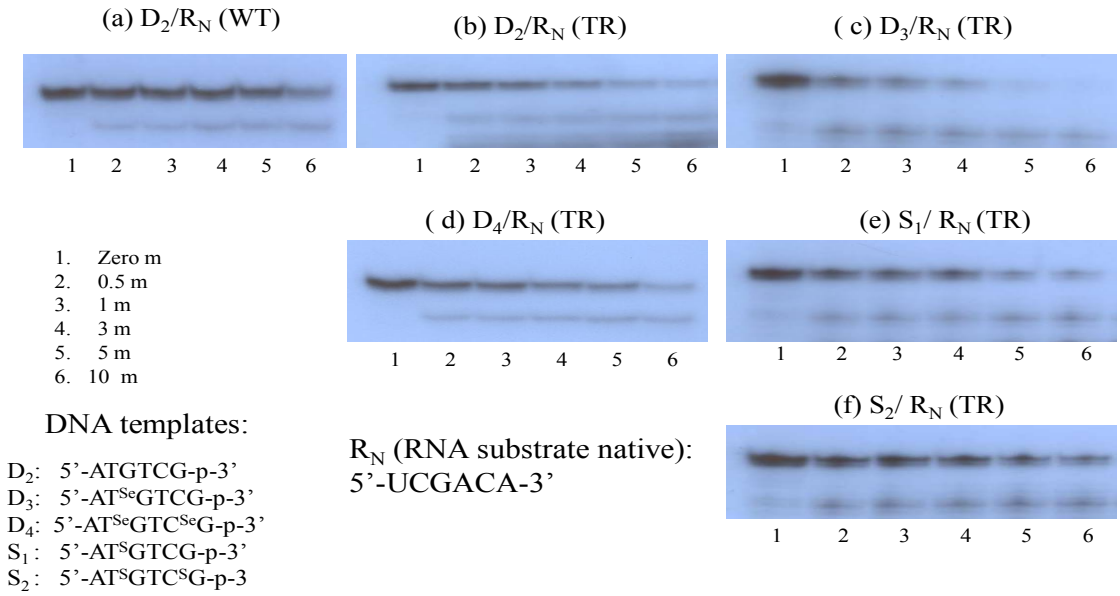

Figure 16: Kinetic analysis of RNase H (wild type and truncated) enzyme on RNA substrate base paired with native DNA_P and modified DNA templates. From these time-course analyses has been demonstrated that truncated enzyme was more efficient than wild type [gel (a) compared to the rest, wild type with DNA modified templates were not shown]. Among the DNA templates those were treated with truncated enzyme single selenium modified DNA template was more efficient in placing the sessile bond of the RNA substrate towards the active site of the enzyme [gel (c)]. It has shown that 90 % of the RNA substrate been hydrolyzed in 10 minutes [gel (c), lane 6] of reaction time.

RNase H (BH) catalysis on native and modified DNA templates

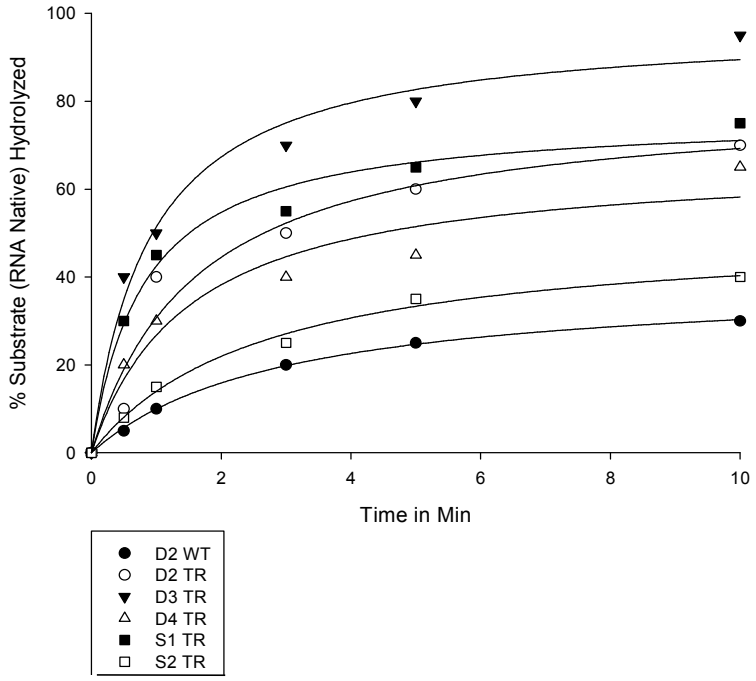

Figure 17: Graph showing RNase H catalytic activities of different DNA templates monitored at different reaction time. Wild type enzymes with native DNA template has lowest activity [♦], data with wild type enzyme on modified DNA templates were not shown] compared to truncated enzyme with all other DNA templates used in this study. Among the modified DNA templates with truncated enzyme single selenium modified DNA template has the highest catalytic activity which was about 95 %.

Apparent reaction rate constants, which can be defined as the increase in molar concentration of products in unit time, were determined from the slope of first minute reaction curve (Figure 17) and the slopes were calculated by using Microsoft excel. From the data in Table 3 it was obvious the K_{app} and K_{cat} of tr- RNase H (BH) were four folds higher than WT RNase (BH) while using D_2 template. The K_{app} of tr-RNase H (BH) was higher for the template D_3 and lowest for D_4. The K_{app} of tr-RNase H (BH) for the templates D_2, D_3, D_4, S_1 and S_2 were 9.96, 12.38, 7.45, 11.24, and 3.68 nM/min, respectively, which were 3.9, 44.9, 2.98, 4.49, and 1.47 nM/min, respectively, times higher than the D_2 WT RNase H (BH) enzyme. The order of K_{app} for tr-RNase H (BH) enzyme was $D_3 > D_2 > S_1 > S_2 > D_4$ (Table 3). We observed the same trends for K_{cat} as K_{app} of the tr-RNAse H (BH) enzyme. The calculated Kcat of tr-RNase H (BH) for the templates D_2, D_3, D_4, S_1 and S_2 were 9.96, 12.38, 7.45, 11.24, and 3.68 M/min/mole enzyme, respectively, which were 3.9, 44.9, 2.98, 4.49, and 1.47 nM/min, respectively, times higher than the D_2 WT RNase H (BH) enzyme (Table 3).

Apparent rate constant (K_{app}) and catalytic rate (K_{cat}) of tr-RNase H (BH) enzyme on different DNA templates

Apparent Rate Constant (*Kapp*) of tr-RNase H (BH) enzyme on Different DNA Templates: A Comparison Over D2 WT

D_2(wt) nM/min (K_{app})	D_2 (tr) nM/min(K_{app})	D_3 (tr) nM/min (K_{app})	D_4 (tr) nM/min (K_{app})	S_1 (tr) nM/min (K_{app})	S_2 (tr) nM/min (K_{app})
1 (12.5)	3.9 (49.8)	44.9 (61.9)	2.98 (37.25)	4.49 (56.22)	1.47 (18.39)

K_{cat} of tr-RNase H (BH) enzyme on Different DNA Templates: A Comparison Over D2 WT

D_2 (WT) M/min /mole enzyme	D_2 (Truncated) M/min /mole enzyme	D_3 (Truncated) M/min /mole enzyme	D_4 (Truncated) M/min /mole enzyme	S_1 (Truncated) M/min /mole enzyme	S_2 (Truncated) M/min /mole enzyme
1 (2.5)	3.98 (9.96)	4.9 (12.38)	2.98 (7.45)	4.49 (11.24)	1.47 (3.68)

Table 3: Apparent rate constant (K_{app}) and catalytic rate (K_{cat}) of tr-RNase H (BH) enzyme on different DNA templates

Table 3: Apparent rate constant (K_{app}) and catalytic rate (K_{cat}) of tr-RNase H (BH) enzyme on different DNA templates. Table showing apparent rate constants (K_{app}) and turnover numbers (K_{cat}) of the tr-RNase H (BH) enzyme with native and modified DNA templates. Apparent rate constants were determined from the slope of first minute reaction curve and the slopes were calculated by using Microsoft Excel. A comparison of apparent constants of wild type enzyme with native DNA template to truncated enzyme with native and modified DNA templates has also shown. The K_{app} of the truncated enzyme was higher than the wild type enzyme and among the different DNA templates single selenium modified templates has the highest rate. Overall the K_{app} and K_{cat} of the truncated enzyme were higher than the wild type enzyme. Among the different DNA templates, the template with single selenium modification has the highest K_{app} and K_{cat}.

Synthesis of the 6-(2-cyanoethyl)seleno guanosine phosphoramidite (3) and oligonucleotides containing the 6-Se-G (4)

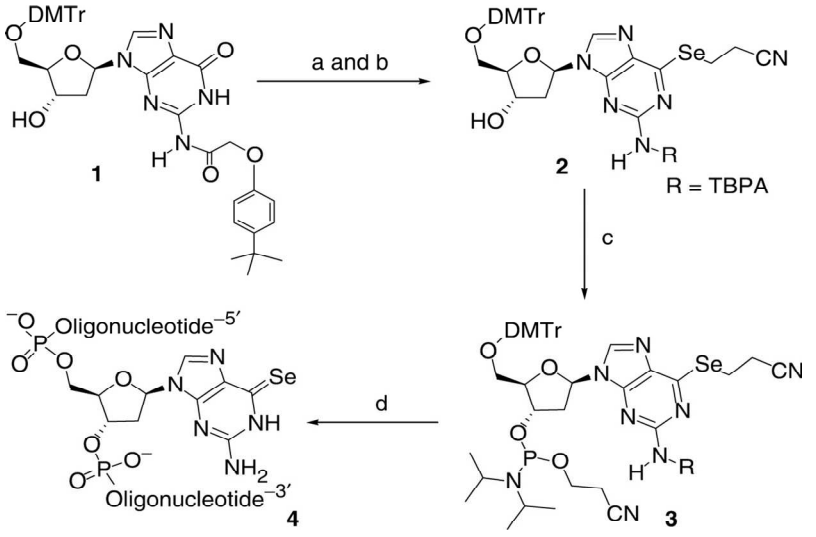

Salon J et al. Nucl. Acids Res. 2008;36:7009-7018

Nucleic Acids Research

Scheme 1: Synthesis of the 6-(2-cyanoethyl)seleno guanosine phosphoramidite (3) and oligonucleotides containing the 6-Se-G (4). Reagents and conditions: (a) TIBS, DMAP, TEA, CH2Cl2, room temperature; (b) diselenide, NaBH4/EtOH, −5°C, 80% yield in two steps; (c) phosphoramidite, BTT, CH2Cl2, 75% yield; (d) solid-phase synthesis. TIBS = 2,4,6-triisopropylbenzene-1-sulfonyl chloride, DMAP = 4-dimethylaminopyridine, CH2Cl2 = dichloromethane, TEA = triethylamine, EtOH = ethanol, NaBH4 = sodium borohydride, diselenide = (NCCH2CH2Se)2, phosphoramidite = 2-cyanoethyl tetraisopropyl phosphorodiamidite, BTT = 5-(benzylthio)-1H-tetrazole

Catalytic pathway of RNase H (BH) on native and modified DNA template base pair with RNA

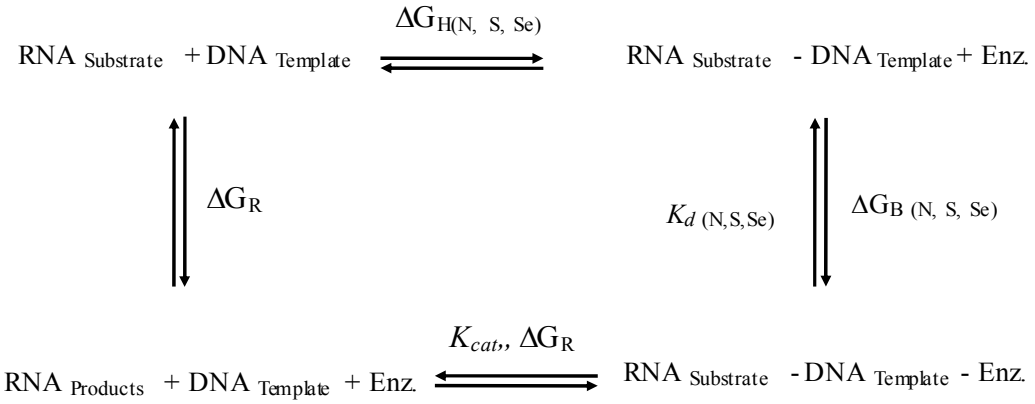

Parameters	ΔG_T Kcal/mol	ΔG_R Kcal/mol	ΔG_H Kcal/mol	ΔG_B Kcal/mol	K_d µM	K_{cat} M/min /mole enz.
DNA Template (Native,N)	- 16.06	- 0.38	- 14.6	+ 0.32	1.7	9.96
DNA Template (Sulfur, S)	- 16.07	- 1.3	- 12.2	+ 0.93	4.83	11.24
DNA Template (Selenium, Se)	- 18.37	- 8.2	- 11.3	+ 1.13	6.4	15.75

$$\Delta G^\circ = -2.303\, RT \log_{10} K_{eq}$$

Scheme 2: Catalytic pathway of RNase H (BH) on native and modified DNA template base pair with RNA.

Different kinetic parameters were shown in the table. It can be observed that the catalytic activity of RNase H (BH) was the highest with selenium modified DNA template. Free energies (ΔG) of the ^{Se}DNA template for binding (ΔG_B), hybrid formation (ΔG_H) is downhill in comparing to the native. But the free energy of ^{Se}DNA template is about 8 unit uphill than native. The overall free energy (ΔG_T) for the ^{Se}DNA template is uphill about two units compare to the native.

Kinetic parameters of the native, selenium, and sulfur modified DNA templates have been analysed and free energies for hybrid formation (ΔG_H), duplex binding (ΔG_B) to RNase H (BH), have determined. The results are illustrated in Scheme 2. It has been found that the free energies of hybrid formation (ΔG_H) and duplex binding (ΔG_B) to RNase H (BH) higher (downhill) for ^{Se}DNA template in comparing to the native and sulfur modified DNA templates. But the free energy of the ^{Se}DNA template for catalytic reaction (ΔG_T) is eight units uphill in contrast to native and seven units to sulfur modified DNA templates. On the other hand, the total free energy (ΔG_T) for the ^{Se}DNA is two units uphill (-18.37) than native (-16.06) which gives about 1000 folds higher performance by RNase H (BH) when using selenium modified DNA template.

3.5 Summary

RNase H (BH) enzyme became a model enzyme owing to its stability, higher expression in *E. coli* system, and for excellent X-ray crystallographic properties. This enzyme has been using to elucidate catalytic mechanism at molecular level by different research laboratories. The structure of RNase H (BH) and nucleic acid complex were solved by heavy atom soaking method. Selenium atom is now being using to determine crystal structure. Its anomalous scattering property helps to solve the major obstacle in X-ray crystallography, the phase problem. Selenium atom incorporation into protein is accomplished by growing bacteria in selenomethionine supplemented medium. In nucleic acid, selenium modified phosphoramide is used through solid phase synthesis for incorporation. Enzymatic incorporation of seleno modified nucleotides into DNA and RNA also has been demonstrated by Huang laboratory. This laboratory pioneered selenium incorporation into nucleic acid and structure determination by X-ray crystallography. Among many useful properties of selenium atom, its anomalous scattering property is found to solve phase problem largely. The crystal structure of selenium modified DNA revealed the DNA structure is flexible and it can accommodate larger atom while keeing its integrity and biologic function. The modification allows forming Watson-Crick H-bonds and can fit into enzyme active site with no or little distortion. We observed that the selenium introduction in the DNA can form base pair with the complementary RNA and can stably introduce into the RNAse H (BH) active site. In this selenium modified DNA and RNA duplex selenium has introduced into 6-position of the base guanine in DNA strand. Interestingly, the ^{Se}G forms seleno-hydrogen (Se- - - H-O) bond with the 4-oxygen of the base cytosine on the opposite RNA strand. The selenium introduction causes base pair shifting about 0.3 Å. From enzymatic activity study it has been noticed that this

subtle change in the duplex conformation enhances the RNase (BH) enzymatic activity about thousands fold. This enhancement primarily attributed to the closer positioning of the attacking water molecule to the scissile phosphate that acts as an electrophile. Here we are reporting the novel functionality of selenium which can accelerate the enzyme activity.

3.6 Conclusions

Selenium is an essential trace element. Its role has been implicated in many pathological conditions in human. Selenium has been recognized as the 21st amino acid which translated into protein by ribosome mediated protein synthesis mechinary. As being of its anomalous scattering properties, the phase problem, the major obstacle in X-ray crystallography, has been solved efficiently. In the crystal structure of RNase H (BH) and ^{Se}DNA/RNA duplex it has found that selenium incorporation into template DNA did not affect the base pairing between DNA and RNA, although the ^{Se}G:C base shifted 0.3 Å. This shifting pushed the scissile bond of the RNA substrate towards the active site. As a result the catalytic effiency of RNase H (BH) has been increased thousand folds. This property of selenium is novel which can be described as enhancing effect. This property suggests a novel approach which can be used to enhance catalytic property of many enzymes.

Chapter 4

4. References

1. Vousden, K. H., and Lu, X. (2002) Live or let die: the cell's response to p53, *Nat Rev Cancer 2*, 594-604.

2. Wang, W., and El-Deiry, W. S. (2008) Restoration of p53 to limit tumor growth, *Curr Opin Oncol 20*, 90-96.

3. Ang, H. C., Joerger, A. C., Mayer, S., and Fersht, A. R. (2006) Effects of common cancer mutations on stability and DNA binding of full-length p53 compared with isolated core domains, *J Biol Chem 281*, 21934-21941.

4. Joerger, A. C., Ang, H. C., and Fersht, A. R. (2006) Structural basis for understanding oncogenic p53 mutations and designing rescue drugs, *Proc Natl Acad Sci U S A 103*, 15056-15061.

5. Cai, D. H., Wang, D., Keefer, J., Yeamans, C., Hensley, K., and Friedman, A. D. (2008) C/EBP alpha:AP-1 leucine zipper heterodimers bind novel DNA elements, activate the PU.1 promoter and direct monocyte lineage commitment more potently than C/EBP alpha homodimers or AP-1, *Oncogene 27*, 2772-2779.

6. Erlanson, D. A., Chytil, M., and Verdine, G. L. (1996) The leucine zipper domain controls the orientation of AP-1 in the NFAT.AP-1.DNA complex, *Chem Biol 3*, 981-991.

7. Wu, L., and Belasco, J. G. (2005) Micro-RNA regulation of the mammalian lin-28 gene during neuronal differentiation of embryonal carcinoma cells, *Mol Cell Biol 25*, 9198-9208.

8. Monticelli, S., Ansel, K. M., Lee, D. U., and Rao, A. (2005) Regulation of gene expression in mast cells: micro-rNA expression and chromatin structural analysis of cytokine genes, *Novartis Found Symp 271*, 179-187; discussion 187-190, 198-179.

9. Slezak, S., Jin, P., Caruccio, L., Ren, J., Bennett, M., Zia, N., Adams, S., Wang, E., Ascensao, J., Schechter, G., and Stroncek, D. (2009) Gene and microRNA analysis of

neutrophils from patients with polycythemia vera and essential thrombocytosis: down-regulation of micro RNA-1 and -133a, *J Transl Med 7*, 39.

10. Braconi, C., Huang, N., and Patel, T. MicroRNA-dependent regulation of DNA methyltransferase-1 and tumor suppressor gene expression by interleukin-6 in human malignant cholangiocytes, *Hepatology 51*, 881-890.

11. Zhang, R., and Su, B. (2008) MicroRNA regulation and the variability of human cortical gene expression, *Nucleic Acids Res 36*, 4621-4628.

12. Borchert, G. M., Lanier, W., and Davidson, B. L. (2006) RNA polymerase III transcribes human microRNAs, *Nat Struct Mol Biol 13*, 1097-1101.

13. Lee, Y., Ahn, C., Han, J., Choi, H., Kim, J., Yim, J., Lee, J., Provost, P., Radmark, O., Kim, S., and Kim, V. N. (2003) The nuclear RNase III Drosha initiates microRNA processing, *Nature 425*, 415-419.

14. Lee, Y., Jeon, K., Lee, J. T., Kim, S., and Kim, V. N. (2002) MicroRNA maturation: stepwise processing and subcellular localization, *EMBO J 21*, 4663-4670.

15. Bartel, D. P. (2004) MicroRNAs: genomics, biogenesis, mechanism, and function, *Cell 116*, 281-297.

16. Suzuki, H. I., Yamagata, K., Sugimoto, K., Iwamoto, T., Kato, S., and Miyazono, K. (2009) Modulation of microRNA processing by p53, *Nature 460*, 529-533.

17. Korolev, N., Vorontsova, O. V., and Nordenskiold, L. (2007) Physicochemical analysis of electrostatic foundation for DNA-protein interactions in chromatin transformations, *Prog Biophys Mol Biol 95*, 23-49.

18. Dzheliadin, T. R., Sorokin, A. A., Ivanova, N. N., Sivozhelezov, V. S., Kamzolova, S. G., and Polozov, R. V. (2001) [Characteristics of electrostatic interaction of Escherichia coli RNA polymerase with promoters of T4 phage DNA], *Biofizika 46*, 1022-1026.

19. Bayer, P., Varani, L., and Varani, G. (1999) Refinement of the structure of protein-RNA complexes by residual dipolar coupling analysis, *J Biomol NMR 14*, 149-155.

20. Azurmendi, H. F., Martin-Pastor, M., and Bush, C. A. (2002) Conformational studies of Lewis X and Lewis A trisaccharides using NMR residual dipolar couplings, *Biopolymers 63*, 89-98.

21. Du, Z., Lee, J. K., Fenn, S., Tjhen, R., Stroud, R. M., and James, T. L. (2007) X-ray crystallographic and NMR studies of protein-protein and protein-nucleic acid interactions involving the KH domains from human poly(C)-binding protein-2, *RNA 13*, 1043-1051.

22. Varani, G., Chen, Y., and Leeper, T. C. (2004) NMR studies of protein-nucleic acid interactions, *Methods Mol Biol 278*, 289-312.

23. Tomita, K. (1989) [X-ray structural studies of nucleic acid molecular structure and nucleic acid-protein interaction mechanism], *Yakugaku Zasshi 109*, 439-459.

24. Anzellotti, A. I., Ma, E. S., and Farrell, N. (2005) Platination of nucleobases to enhance noncovalent recognition in protein-DNA/RNA complexes, *Inorg Chem 44*, 483-485.

25. Nishinaka, T., Shinohara, A., Ito, Y., Yokoyama, S., and Shibata, T. (1998) Base pair switching by interconversion of sugar puckers in DNA extended by proteins of RecA-family: a model for homology search in homologous genetic recombination, *Proc Natl Acad Sci U S A 95*, 11071-11076.

26. Sinex, F. M. (1970) The interaction of protein with single strands of DNA and RNA, *Adv Enzyme Regul 9*, 309-315.

27. Nagaoka, M., Kondo, Y., Uno, Y., and Sugiura, Y. (2002) Influence of amino acid numbers between two ligand cysteines of zinc finger proteins on affinity and specificity of DNA binding, *Biochem Biophys Res Commun 296*, 553-559.

28. Aravind, L., Anantharaman, V., Balaji, S., Babu, M. M., and Iyer, L. M. (2005) The many faces of the helix-turn-helix domain: transcription regulation and beyond, *FEMS Microbiol Rev 29*, 231-262.

29. Massari, M. E., and Murre, C. (2000) Helix-loop-helix proteins: regulators of transcription in eucaryotic organisms, *Mol Cell Biol 20*, 429-440.

30. Gajiwala, K. S., and Burley, S. K. (2000) Winged helix proteins, *Curr Opin Struct Biol 10*, 110-116.

31. Gajiwala, K. S., Chen, H., Cornille, F., Roques, B. P., Reith, W., Mach, B., and Burley, S. K. (2000) Structure of the winged-helix protein hRFX1 reveals a new mode of DNA binding, *Nature 403*, 916-921.

32. Kouzarides, T., and Ziff, E. (1988) The role of the leucine zipper in the fos-jun interaction, *Nature 336*, 646-651.

33. Lorkovic, Z. J., and Barta, A. (2002) Genome analysis: RNA recognition motif (RRM) and K homology (KH) domain RNA-binding proteins from the flowering plant Arabidopsis thaliana, *Nucleic Acids Res 30*, 623-635.

34. Merida, I., Williamson, P., Kuziel, W. A., Greene, W. C., and Gaulton, G. N. (1993) The serine-rich cytoplasmic domain of the interleukin-2 receptor beta chain is essential for interleukin-2-dependent tyrosine protein kinase and phosphatidylinositol-3-kinase activation, *J Biol Chem 268*, 6765-6770.

35. Tsiang, M., Lentz, S. R., and Sadler, J. E. (1992) Functional domains of membrane-bound human thrombomodulin. EGF-like domains four to six and the serine/threonine-rich domain are required for cofactor activity, *J Biol Chem 267*, 6164-6170.

36. Moro, O., Lameh, J., and Sadee, W. (1993) Serine- and threonine-rich domain regulates internalization of muscarinic cholinergic receptors, *J Biol Chem 268*, 6862-6865.

37. Tahbaz, N., Kolb, F. A., Zhang, H., Jaronczyk, K., Filipowicz, W., and Hobman, T. C. (2004) Characterization of the interactions between mammalian PAZ PIWI domain proteins and Dicer, *EMBO Rep 5*, 189-194.

38. Lingel, A., Simon, B., Izaurralde, E., and Sattler, M. (2004) Nucleic acid 3'-end recognition by the Argonaute2 PAZ domain, *Nat Struct Mol Biol 11*, 576-577.

39. Wharton, R. P., and Aggarwal, A. K. (2006) mRNA regulation by Puf domain proteins, *Sci STKE 2006*, pe37.

40. Jenkins, H. T., Baker-Wilding, R., and Edwards, T. A. (2009) Structure and RNA binding of the mouse Pumilio-2 Puf domain, *J Struct Biol 167*, 271-276.

41. Dye, B. T., and Patton, J. G. (2001) An RNA recognition motif (RRM) is required for the localization of PTB-associated splicing factor (PSF) to subnuclear speckles, *Exp Cell Res 263*, 131-144.

42. Jacks, A., Kelly, G., Curry, S., and Conte, M. R. (2002) Resonance assignment and secondary structure determination of a C-terminal fragment of the lupus autoantigen (La) protein containing a putative RNA recognition motif (RRM), *J Biomol NMR 22*, 387-388.

43. Inoue, A., Takahashi, K. P., Kimura, M., Watanabe, T., and Morisawa, S. (1996) Molecular cloning of a RNA binding protein, S1-1, *Nucleic Acids Res 24*, 2990-2997.

44. Hall, M. P., and Ho, C. K. (2006) Characterization of a Trypanosoma brucei RNA cap (guanine N-7) methyltransferase, *RNA 12*, 488-497.

45. Pillutla, R. C., Yue, Z., Maldonado, E., and Shatkin, A. J. (1998) Recombinant human mRNA cap methyltransferase binds capping enzyme/RNA polymerase IIo complexes, *J Biol Chem 273*, 21443-21446.

46. Misquitta, C. M., Iyer, V. R., Werstiuk, E. S., and Grover, A. K. (2001) The role of 3'-untranslated region (3'-UTR) mediated mRNA stability in cardiovascular pathophysiology, *Mol Cell Biochem 224*, 53-67.

47. Butler, P. J., and Lomonossoff, G. P. (1980) RNA-protein interactions in the assembly of tobacco mosaic virus, *Biophys J 32*, 295-312.

48. Jovin, T. M., Englund, P. T., and Kornberg, A. (1969) Enzymatic synthesis of deoxyribonucleic acid. XXVII. Chemical modifications of deoxyribonucleic acid polymerase, *J Biol Chem 244*, 3009-3018.

49. Goulian, M., Kornberg, A., and Sinsheimer, R. L. (1967) Enzymatic synthesis of DNA, XXIV. Synthesis of infectious phage phi-X174 DNA, *Proc Natl Acad Sci U S A 58*, 2321-2328.

50. Cerritelli, S. M., Frolova, E. G., Feng, C., Grinberg, A., Love, P. E., and Crouch, R. J. (2003) Failure to produce mitochondrial DNA results in embryonic lethality in Rnaseh1 null mice, *Mol Cell 11*, 807-815.

51. Turchi, J. J., Huang, L., Murante, R. S., Kim, Y., and Bambara, R. A. (1994) Enzymatic completion of mammalian lagging-strand DNA replication, *Proc Natl Acad Sci U S A 91*, 9803-9807.

52. Kao, H. I., and Bambara, R. A. (2003) The protein components and mechanism of eukaryotic Okazaki fragment maturation, *Crit Rev Biochem Mol Biol 38*, 433-452.

53. Bubeck, D., Reijns, M. A., Graham, S. C., Astell, K. R., Jones, E. Y., and Jackson, A. P. PCNA directs type 2 RNase H activity on DNA replication and repair substrates, *Nucleic Acids Res*.

54. Barzilay, G., Walker, L. J., Robson, C. N., and Hickson, I. D. (1995) Site-directed mutagenesis of the human DNA repair enzyme HAP1: identification of residues important for AP endonuclease and RNase H activity, *Nucleic Acids Res 23*, 1544-1550.

55. Eder, P. S., Walder, R. Y., and Walder, J. A. (1993) Substrate specificity of human RNase H1 and its role in excision repair of ribose residues misincorporated in DNA, *Biochimie 75*, 123-126.

56. Kunkel, T. A. (1988) Exonucleolytic proofreading, *Cell 53*, 837-840.

57. Moser, M. J., Holley, W. R., Chatterjee, A., and Mian, I. S. (1997) The proofreading domain of Escherichia coli DNA polymerase I and other DNA and/or RNA exonuclease domains, *Nucleic Acids Res 25*, 5110-5118.

58. Cooper, P. K., and Hanawalt, P. C. (1972) Role of DNA polymerase I and the rec system in excision-repair in Escherichia coli, *Proc Natl Acad Sci U S A 69*, 1156-1160.

59. Lehman, I. R., Bessman, M. J., Simms, E. S., and Kornberg, A. (1958) Enzymatic synthesis of deoxyribonucleic acid. I. Preparation of substrates and partial purification of an enzyme from Escherichia coli, *J Biol Chem 233*, 163-170.

60. Friedberg, E. C. (2006) The eureka enzyme: the discovery of DNA polymerase, *Nat Rev Mol Cell Biol 7*, 143-147.

61. Ollis, D. L., Kline, C., and Steitz, T. A. (1985) Domain of E. coli DNA polymerase I showing sequence homology to T7 DNA polymerase, *Nature 313*, 818-819.

62. Korolev, V. G. (2005) [Base excision repair: AP endonucleases and DNA polymerases], *Genetika 41*, 1301-1309.

63. Kuchta, R. D., Benkovic, P., and Benkovic, S. J. (1988) Kinetic mechanism whereby DNA polymerase I (Klenow) replicates DNA with high fidelity, *Biochemistry 27*, 6716-6725.

64. Beese, L. S., and Steitz, T. A. (1991) Structural basis for the 3'-5' exonuclease activity of Escherichia coli DNA polymerase I: a two metal ion mechanism, *EMBO J 10*, 25-33.

65. Derbyshire, V., Freemont, P. S., Sanderson, M. R., Beese, L., Friedman, J. M., Joyce, C. M., and Steitz, T. A. (1988) Genetic and crystallographic studies of the 3',5'-exonucleolytic site of DNA polymerase I, *Science 240*, 199-201.

66. Freemont, P. S., Friedman, J. M., Beese, L. S., Sanderson, M. R., and Steitz, T. A. (1988) Cocrystal structure of an editing complex of Klenow fragment with DNA, *Proc Natl Acad Sci U S A 85*, 8924-8928.

67. Beese, L. S., Derbyshire, V., and Steitz, T. A. (1993) Structure of DNA polymerase I Klenow fragment bound to duplex DNA, *Science 260*, 352-355.

68. Kunz, B. A., Kohalmi, S. E., Kunkel, T. A., Mathews, C. K., McIntosh, E. M., and Reidy, J. A. (1994) International Commission for Protection Against Environmental Mutagens and Carcinogens. Deoxyribonucleoside triphosphate levels: a critical factor in the maintenance of genetic stability, *Mutat Res 318*, 1-64.

69. Kunkel, T. A. (2004) DNA replication fidelity, *J Biol Chem 279*, 16895-16898.

70. Kunkel, T. A., and Mosbaugh, D. W. (1989) Exonucleolytic proofreading by a mammalian DNA polymerase, *Biochemistry 28*, 988-995.

71. Angus, S. P., Wheeler, L. J., Ranmal, S. A., Zhang, X., Markey, M. P., Mathews, C. K., and Knudsen, E. S. (2002) Retinoblastoma tumor suppressor targets dNTP metabolism to regulate DNA replication, *J Biol Chem 277*, 44376-44384.

72. Hanke, P. D., and Fuchs, J. A. (1983) Characterization of the mRNA coding for ribonucleoside diphosphate reductase in Escherichia coli, *J Bacteriol 156*, 1192-1197.

73. Carlson, J., Fuchs, J. A., and Messing, J. (1984) Primary structure of the Escherichia coli ribonucleoside diphosphate reductase operon, *Proc Natl Acad Sci U S A 81*, 4294-4297.

74. Elledge, S. J., and Davis, R. W. (1990) Two genes differentially regulated in the cell cycle and by DNA-damaging agents encode alternative regulatory subunits of ribonucleotide reductase, *Genes Dev 4*, 740-751.

75. Ke, P. Y., Kuo, Y. Y., Hu, C. M., and Chang, Z. F. (2005) Control of dTTP pool size by anaphase promoting complex/cyclosome is essential for the maintenance of genetic stability, *Genes Dev 19*, 1920-1933.

76. Chabes, A. L., Bjorklund, S., and Thelander, L. (2004) S Phase-specific transcription of the mouse ribonucleotide reductase R2 gene requires both a proximal repressive E2F-binding site and an upstream promoter activating region, *J Biol Chem 279*, 10796-10807.

77. Dong, Z., Liu, Y., and Zhang, J. T. (2005) Regulation of ribonucleotide reductase M2 expression by the upstream AUGs, *Nucleic Acids Res 33*, 2715-2725.

78. Oliver, F. J., Collins, M. K., and Lopez-Rivas, A. (1996) Regulation of the salvage pathway of deoxynucleotides synthesis in apoptosis induced by growth factor deprivation, *Biochem J 316 (Pt 2)*, 421-425.

79. Reichard, P., Eliasson, R., Ingemarson, R., and Thelander, L. (2000) Cross-talk between the allosteric effector-binding sites in mouse ribonucleotide reductase, *J Biol Chem 275*, 33021-33026.

80. Spyrou, G., and Reichard, P. (1989) Intracellular compartmentation of deoxycytidine nucleotide pools in S phase mouse 3T3 fibroblasts, *J Biol Chem 264*, 960-964.

81. Maki, H., and Sekiguchi, M. (1992) MutT protein specifically hydrolyses a potent mutagenic substrate for DNA synthesis, *Nature 355*, 273-275.

82. Bhatnagar, S. K., Bullions, L. C., and Bessman, M. J. (1991) Characterization of the mutT nucleoside triphosphatase of Escherichia coli, *J Biol Chem 266*, 9050-9054.

83. Fujikawa, K., Kamiya, H., Yakushiji, H., Fujii, Y., Nakabeppu, Y., and Kasai, H. (1999) The oxidized forms of dATP are substrates for the human MutT homologue, the hMTH1 protein, *J Biol Chem 274*, 18201-18205.

84. Beauchamp, B. B., and Richardson, C. C. (1988) A unique deoxyguanosine triphosphatase is responsible for the optA1 phenotype of Escherichia coli, *Proc Natl Acad Sci U S A 85*, 2563-2567.

85. Seto, D., Bhatnagar, S. K., and Bessman, M. J. (1988) The purification and properties of deoxyguanosine triphosphate triphosphohydrolase from Escherichia coli, *J Biol Chem 263*, 1494-1499.

86. Kornberg, S. R., Lehman, I. R., Bessman, M. J., Simms, E. S., and Kornberg, A. (1958) Enzymatic cleavage of deoxyguanosine triphosphate to deoxyguanosine and tripolyphosphate, *J Biol Chem 233*, 159-162.

87. Wurgler, S. M., and Richardson, C. C. (1990) Structure and regulation of the gene for dGTP triphosphohydrolase from Escherichia coli, *Proc Natl Acad Sci U S A 87*, 2740-2744.

88. Myers, J. C., and Shamoo, Y. (2004) Human UP1 as a model for understanding purine recognition in the family of proteins containing the RNA recognition motif (RRM), *J Mol Biol 342*, 743-756.

89. Myers, J. A., Beauchamp, B. B., and Richardson, C. C. (1987) Gene 1.2 protein of bacteriophage T7. Effect on deoxyribonucleotide pools, *J Biol Chem 262*, 5288-5292.

90. Huber, H. E., Beauchamp, B. B., and Richardson, C. C. (1988) Escherichia coli dGTP triphosphohydrolase is inhibited by gene 1.2 protein of bacteriophage T7, *J Biol Chem 263*, 13549-13556.

91. Knofel, T., and Strater, N. (1999) X-ray structure of the Escherichia coli periplasmic 5'-nucleotidase containing a dimetal catalytic site, *Nat Struct Biol 6*, 448-453.

92. Rinaldo-Matthis, A., Rampazzo, C., Reichard, P., Bianchi, V., and Nordlund, P. (2002) Crystal structure of a human mitochondrial deoxyribonucleotidase, *Nat Struct Biol 9*, 779-787.

93. Bianchi, V., and Spychala, J. (2003) Mammalian 5'-nucleotidases, *J Biol Chem 278*, 46195-46198.

94. Song, S., Pursell, Z. F., Copeland, W. C., Longley, M. J., Kunkel, T. A., and Mathews, C. K. (2005) DNA precursor asymmetries in mammalian tissue mitochondria and possible contribution to mutagenesis through reduced replication fidelity, *Proc Natl Acad Sci U S A 102*, 4990-4995.

95. Spratt, T. E. (2001) Identification of hydrogen bonds between Escherichia coli DNA polymerase I (Klenow fragment) and the minor groove of DNA by amino acid substitution of the polymerase and atomic substitution of the DNA, *Biochemistry 40*, 2647-2652.

96. McCain, M. D., Meyer, A. S., Schultz, S. S., Glekas, A., and Spratt, T. E. (2005) Fidelity of mispair formation and mispair extension is dependent on the interaction between the minor groove of the primer terminus and Arg668 of DNA polymerase I of Escherichia coli, *Biochemistry 44*, 5647-5659.

97. McClure, W. R., and Jovin, T. M. (1975) The steady state kinetic parameters and non-processivity of Escherichia coli deoxyribonucleic acid polymerase I, *J Biol Chem 250*, 4073-4080.

98. Carrasco, N., Buzin, Y., Tyson, E., Halpert, E., and Huang, Z. (2004) Selenium derivatization and crystallization of DNA and RNA oligonucleotides for X-ray crystallography using multiple anomalous dispersion, *Nucleic Acids Res 32*, 1638-1646.

99. Alsaidi, M., Lum, E., and Huang, Z. (2004) Direct detection of a specific cellular mRNA on functionalized microplate, *Chembiochem 5*, 1136-1139.

100. Lin, T. C., Wang, C. X., Joyce, C. M., and Konigsberg, W. H. (2001) 3'-5' Exonucleolytic activity of DNA polymerases: structural features that allow kinetic discrimination between ribo- and deoxyribonucleotide residues, *Biochemistry 40*, 8749-8755.

101. Tuske, S., Singh, K., Kaushik, N., and Modak, M. J. (2000) The J-helix of Escherichia coli DNA polymerase I (Klenow fragment) regulates polymerase and 3'- 5'-exonuclease functions, *J Biol Chem 275*, 23759-23768.

102. Dzantiev, L., and Romano, L. J. (1999) Interaction of Escherichia coli DNA polymerase I (Klenow fragment) with primer-templates containing N-acetyl-2-aminofluorene or N-2-aminofluorene adducts in the active site, *J Biol Chem 274*, 3279-3284.

103. Johnson, K. A. (1993) Conformational coupling in DNA polymerase fidelity, *Annu Rev Biochem 62*, 685-713.

104. Arion, D., Kaushik, N., McCormick, S., Borkow, G., and Parniak, M. A. (1998) Phenotypic mechanism of HIV-1 resistance to 3'-azido-3'-deoxythymidine (AZT): increased polymerization processivity and enhanced sensitivity to pyrophosphate of the mutant viral reverse transcriptase, *Biochemistry 37*, 15908-15917.

105. Kohlstaedt, L. A., Wang, J., Friedman, J. M., Rice, P. A., and Steitz, T. A. (1992) Crystal structure at 3.5 A resolution of HIV-1 reverse transcriptase complexed with an inhibitor, *Science 256*, 1783-1790.

106. Kuchta, R. D., Mizrahi, V., Benkovic, P. A., Johnson, K. A., and Benkovic, S. J. (1987) Kinetic mechanism of DNA polymerase I (Klenow), *Biochemistry 26*, 8410-8417.

107. Dahlberg, M. E., and Benkovic, S. J. (1991) Kinetic mechanism of DNA polymerase I (Klenow fragment): identification of a second conformational change and evaluation of the internal equilibrium constant, *Biochemistry 30*, 4835-4843.

108. Holland, P. M., Abramson, R. D., Watson, R., and Gelfand, D. H. (1991) Detection of specific polymerase chain reaction product by utilizing the 5'----3' exonuclease activity of Thermus aquaticus DNA polymerase, *Proc Natl Acad Sci U S A 88*, 7276-7280.

109. Patel, P. H., Suzuki, M., Adman, E., Shinkai, A., and Loeb, L. A. (2001) Prokaryotic DNA polymerase I: evolution, structure, and "base flipping" mechanism for nucleotide selection, *J Mol Biol 308*, 823-837.

110. Eom, S. H., Wang, J., and Steitz, T. A. (1996) Structure of Taq polymerase with DNA at the polymerase active site, *Nature 382*, 278-281.

111. Joyce, C. M., and Steitz, T. A. (1994) Function and structure relationships in DNA polymerases, *Annu Rev Biochem 63*, 777-822.

112. Wrobel, J. A., Conrad, M. J., Bloedon, E., Swanstrom, R., and Hutchison, C. A., 3rd. (2000) Analysis of HIV type 1 reverse transcriptase: comparing sequences of viral isolates with mutational data, *AIDS Res Hum Retroviruses 16*, 2049-2054.

113. Yang, W. (2005) Portraits of a Y-family DNA polymerase, *FEBS Lett 579*, 868-872.

114. Boudsocq, F., Ling, H., Yang, W., and Woodgate, R. (2002) Structure-based interpretation of missense mutations in Y-family DNA polymerases and their implications for polymerase function and lesion bypass, *DNA Repair (Amst) 1*, 343-358.

115. Ling, H., Boudsocq, F., Woodgate, R., and Yang, W. (2001) Crystal structure of a Y-family DNA polymerase in action: a mechanism for error-prone and lesion-bypass replication, *Cell 107*, 91-102.

116. Plosky, B. S., and Woodgate, R. (2004) Switching from high-fidelity replicases to low-fidelity lesion-bypass polymerases, *Curr Opin Genet Dev 14*, 113-119.

117. Friedberg, E. C., Lehmann, A. R., and Fuchs, R. P. (2005) Trading places: how do DNA polymerases switch during translesion DNA synthesis?, *Mol Cell 18*, 499-505.

118. Xu, H., Faber, C., Uchiki, T., Racca, J., and Dealwis, C. (2006) Structures of eukaryotic ribonucleotide reductase I define gemcitabine diphosphate binding and subunit assembly, *Proc Natl Acad Sci U S A 103*, 4028-4033.

119. Larsson, K. M., Jordan, A., Eliasson, R., Reichard, P., Logan, D. T., and Nordlund, P. (2004) Structural mechanism of allosteric substrate specificity regulation in a ribonucleotide reductase, *Nat Struct Mol Biol 11*, 1142-1149.

120. Kurosawa, Y., and Okazaki, T. (1979) Structure of the RNA portion of the RNA-linked DNA pieces in bacteriophage T4-infected Escherichia coli cells, *J Mol Biol 135*, 841-861.

121. Mohapatra, S. M., Dev, B. N., Mishra, K. C., Gibson, W. M., and Das, T. P. (1988) Investigation of location, electronic structures, and associated properties of chalcogen atoms adsorbed on silicon surfaces: Sulfur and selenium, *Phys Rev B Condens Matter 38*, 13335-13342.

122. Strub, M. P., Hoh, F., Sanchez, J. F., Strub, J. M., Bock, A., Aumelas, A., and Dumas, C. (2003) Selenomethionine and selenocysteine double labeling strategy for crystallographic phasing, *Structure 11*, 1359-1367.

123. Encinar, J. R., Schaumloffel, D., Ogra, Y., and Lobinski, R. (2004) Determination of selenomethionine and selenocysteine in human serum using speciated isotope dilution-capillary HPLC-inductively coupled plasma collision cell mass spectrometry, *Anal Chem 76*, 6635-6642.

124. Lipiec, E., Siara, G., Bierla, K., Ouerdane, L., and Szpunar, J. Determination of selenomethionine, selenocysteine, and inorganic selenium in eggs by HPLC-inductively coupled plasma mass spectrometry, *Anal Bioanal Chem 397*, 731-741.

125. Hammel, C., Kyriakopoulos, A., Rosick, U., and Behne, D. (1997) Identification of selenocysteine and selenomethionine in protein hydrolysates by high-performance liquid chromatography of their o-phthaldialdehyde derivatives, *Analyst 122*, 1359-1363.

126. Bock, A., Forchhammer, K., Heider, J., Leinfelder, W., Sawers, G., Veprek, B., and Zinoni, F. (1991) Selenocysteine: the 21st amino acid, *Mol Microbiol 5*, 515-520.

127. Longtin, R. (2004) A forgotten debate: is selenocysteine the 21st amino acid?, *J Natl Cancer Inst 96*, 504-505.

128. Castellano, S., Andres, A. M., Bosch, E., Bayes, M., Guigo, R., and Clark, A. G. (2009) Low exchangeability of selenocysteine, the 21st amino acid, in vertebrate proteins, *Mol Biol Evol 26*, 2031-2040.

129. Mizutani, T., and Yamada, K. (1994) [Biosynthesis of selenocysteine (the 21st amino acid)], *Seikagaku 66*, 525-530.

130. Bock, A., Forchhammer, K., Heider, J., and Baron, C. (1991) Selenoprotein synthesis: an expansion of the genetic code, *Trends Biochem Sci 16*, 463-467.

131. Bock, A., and Stadtman, T. C. (1988) Selenocysteine, a highly specific component of certain enzymes, is incorporated by a UGA-directed co-translational mechanism, *Biofactors 1*, 245-250.

132. Hatfield, D. L., and Gladyshev, V. N. (2002) How selenium has altered our understanding of the genetic code, *Mol Cell Biol 22*, 3565-3576.

133. Burk, R. F. (2002) Selenium, an antioxidant nutrient, *Nutr Clin Care 5*, 75-79.

134. Boisseau-Garsaud, A. M., Garsaud, P., Lejoly-Boisseau, H., Robert, M., Quist, D., and Arveiler, B. (2002) Increase in total blood antioxidant status and selenium levels in black patients with active vitiligo, *Int J Dermatol 41*, 640-642.

135. Fryer, M. J. (2002) Rationale for clinical trials of selenium as an antioxidant for the treatment of the cardiomyopathy of Friedreich's ataxia, *Med Hypotheses 58*, 127-132.

136. Giray, B., and Hincal, F. (2002) Oxidative DNA base damage, antioxidant enzyme activities and selenium status in highly iodine-deficient goitrous children, *Free Radic Res 36*, 55-62.

137. Hawkes, W. C., and Alkan, Z. Regulation of redox signaling by selenoproteins, *Biol Trace Elem Res 134*, 235-251.

138. Schroeder, H. A., Frost, D. V., and Balassa, J. J. (1970) Essential trace metals in man: selenium, *J Chronic Dis 23*, 227-243.

139. Lee, C. Y., and Wan, J. M. (2002) Immunoregulatory and antioxidant performance of alpha-tocopherol and selenium on human lymphocytes, *Biol Trace Elem Res 86*, 123-136.

140. Rotruck, J. T., Pope, A. L., Ganther, H. E., Swanson, A. B., Hafeman, D. G., and Hoekstra, W. G. (1973) Selenium: biochemical role as a component of glutathione peroxidase, *Science 179*, 588-590.

141. Stadtman, T. C. (1983) New biologic functions--selenium-dependent nucleic acids and proteins, *Fundam Appl Toxicol 3*, 420-423.

142. (1973) Selenium: an essential element for glutathione peroxidase activity, *Nutr Rev 31*, 289-291.

143. Zinoni, F., Birkmann, A., Leinfelder, W., and Bock, A. (1987) Cotranslational insertion of selenocysteine into formate dehydrogenase from Escherichia coli directed by a UGA codon, *Proc Natl Acad Sci U S A 84*, 3156-3160.

144. Fu, L. H., Wang, X. F., Eyal, Y., She, Y. M., Donald, L. J., Standing, K. G., and Ben-Hayyim, G. (2002) A selenoprotein in the plant kingdom. Mass spectrometry confirms that an opal codon (UGA) encodes selenocysteine in Chlamydomonas reinhardtii gluththione peroxidase, *J Biol Chem 277*, 25983-25991.

145. Wen, W., Weiss, S. L., and Sunde, R. A. (1998) UGA codon position affects the efficiency of selenocysteine incorporation into glutathione peroxidase-1, *J Biol Chem 273*, 28533-28541.

146. Berry, M. J., Harney, J. W., Ohama, T., and Hatfield, D. L. (1994) Selenocysteine insertion or termination: factors affecting UGA codon fate and complementary anticodon:codon mutations, *Nucleic Acids Res 22*, 3753-3759.

147. Shen, Q., Chu, F. F., and Newburger, P. E. (1993) Sequences in the 3'-untranslated region of the human cellular glutathione peroxidase gene are necessary and sufficient for selenocysteine incorporation at the UGA codon, *J Biol Chem 268*, 11463-11469.

148. Berry, M. J., Banu, L., Chen, Y. Y., Mandel, S. J., Kieffer, J. D., Harney, J. W., and Larsen, P. R. (1991) Recognition of UGA as a selenocysteine codon in type I deiodinase requires sequences in the 3' untranslated region, *Nature 353*, 273-276.

149. Adachi, K., Katsuyama, M., Song, S., and Oka, T. (2000) Genomic organization, chromosomal mapping and promoter analysis of the mouse selenocysteine tRNA gene transcription-activating factor (mStaf) gene, *Biochem J 346 Pt 1*, 45-51.

150. Mizutani, T., and Goto, C. (2000) Eukaryotic selenocysteine tRNA has the 9/4 secondary structure, *FEBS Lett 466*, 359-362.

151. Liu, S. Y., and Stadtman, T. C. (1997) Selenophosphate synthetase: enzyme labeling studies with [gamma-32P]ATP, [beta-32P]ATP, [8-14C]ATP, and [75Se]selenide, *Arch Biochem Biophys 341*, 353-359.

152. Veres, Z., Kim, I. Y., Scholz, T. D., and Stadtman, T. C. (1994) Selenophosphate synthetase. Enzyme properties and catalytic reaction, *J Biol Chem 269*, 10597-10603.

153. Kim, I. Y., and Stadtman, T. C. (1995) Selenophosphate synthetase: detection in extracts of rat tissues by immunoblot assay and partial purification of the enzyme from the archaean Methanococcus vannielii, *Proc Natl Acad Sci U S A 92*, 7710-7713.

154. Meuillet, E., Stratton, S., Prasad Cherukuri, D., Goulet, A. C., Kagey, J., Porterfield, B., and Nelson, M. A. (2004) Chemoprevention of prostate cancer with selenium: an update on current clinical trials and preclinical findings, *J Cell Biochem 91*, 443-458.

155. Cao, S., Durrani, F. A., and Rustum, Y. M. (2004) Selective modulation of the therapeutic efficacy of anticancer drugs by selenium containing compounds against human tumor xenografts, *Clin Cancer Res 10*, 2561-2569.

156. Fakih, M. G., Pendyala, L., Brady, W., Smith, P. F., Ross, M. E., Creaven, P. J., Badmaev, V., Prey, J. D., and Rustum, Y. M. (2008) A Phase I and pharmacokinetic study of selenomethionine in combination with a fixed dose of irinotecan in solid tumors, *Cancer Chemother Pharmacol 62*, 499-508.

157. Fakih, M. G., Pendyala, L., Smith, P. F., Creaven, P. J., Reid, M. E., Badmaev, V., Azrak, R. G., Prey, J. D., Lawrence, D., and Rustum, Y. M. (2006) A phase I and pharmacokinetic study of fixed-dose selenomethionine and irinotecan in solid tumors, *Clin Cancer Res 12*, 1237-1244.

158. Diamond, A. M., Kataoka, Y., Murray, J., Duan, C., Folks, T. M., and Sandstrom, P. A. (1997) A T-cell model for the biological role of selenium-dependent glutathione peroxidase, *Biomed Environ Sci 10*, 246-252.

159. Fischer, J. L., Mihelc, E. M., Pollok, K. E., and Smith, M. L. (2007) Chemotherapeutic selectivity conferred by selenium: a role for p53-dependent DNA repair, *Mol Cancer Ther 6*, 355-361.

160. Makropoulos, V., Bruning, T., and Schulze-Osthoff, K. (1996) Selenium-mediated inhibition of transcription factor NF-kappa B and HIV-1 LTR promoter activity, *Arch Toxicol 70*, 277-283.

161. Hori, K., Hatfield, D., Maldarelli, F., Lee, B. J., and Clouse, K. A. (1997) Selenium supplementation suppresses tumor necrosis factor alpha-induced human immunodeficiency virus type 1 replication in vitro, *AIDS Res Hum Retroviruses 13*, 1325-1332.

162. Yang, X., Tian, Y., Ha, P., and Gu, L. (1997) [Determination of the selenomethionine content in grain and human blood], *Wei Sheng Yan Jiu 26*, 113-116.

163. Boles, J. O., Cisneros, R. J., Weir, M. S., Odom, J. D., Villafranca, J. E., and Dunlap, R. B. (1991) Purification and characterization of selenomethionyl thymidylate synthase from Escherichia coli: comparison with the wild-type enzyme, *Biochemistry 30*, 11073-11080.

164. Demirci, A., Pometto, A. L., 3rd, and Cox, D. J. (1999) Enhanced organically bound selenium yeast production by fed-batch fermentation, *J Agric Food Chem 47*, 2496-2500.

165. Schrauzer, G. N. (2000) Selenomethionine: a review of its nutritional significance, metabolism and toxicity, *J Nutr 130*, 1653-1656.

166. Braun, W., Epp, O., Wuthrich, K., and Huber, R. (1989) Solution of the phase problem in the X-ray diffraction method for proteins with the nuclear magnetic resonance solution structure as initial model. Patterson search and refinement for the alpha-amylase inhibitor tendamistat, *J Mol Biol 206*, 669-676.

167. Jiang, F., and Rao, Z. (2001) A new implementation of the molecular replacement method using a six-dimensional Patterson vector search, *J Synchrotron Radiat 8*, 1051-1053.

168. Epp, O., Ladenstein, R., and Wendel, A. (1983) The refined structure of the selenoenzyme glutathione peroxidase at 0.2-nm resolution, *Eur J Biochem 133*, 51-69.

169. Hendrickson, W. A. (1985) Stereochemically restrained refinement of macromolecular structures, *Methods Enzymol 115*, 252-270.

170. Hendrickson, W. A. (1991) Determination of macromolecular structures from anomalous diffraction of synchrotron radiation, *Science 254*, 51-58.

171. Hendrickson, W. A., Horton, J. R., and LeMaster, D. M. (1990) Selenomethionyl proteins produced for analysis by multiwavelength anomalous diffraction (MAD): a vehicle for direct determination of three-dimensional structure, *EMBO J 9*, 1665-1672.

172. Hendrickson, W. A., Smith, J. L., and Sheriff, S. (1985) Direct phase determination based on anomalous scattering, *Methods Enzymol 115*, 41-55.

173. Wang, B. C. (1985) Resolution of phase ambiguity in macromolecular crystallography, *Methods Enzymol 115*, 90-112.

174. Lehmann, M. S., Muller, H. H., and Stuhrmann, H. B. (1993) Protein single-crystal diffraction with 5 A synchrotron X-rays at the sulfur K-absorption edge, *Acta Crystallogr D Biol Crystallogr 49*, 308-310.

175. Ferre-D'Amare, A. R., Zhou, K., and Doudna, J. A. (1998) Crystal structure of a hepatitis delta virus ribozyme, *Nature 395*, 567-574.

176. Xiao, H., Murakami, H., Suga, H., and Ferre-D'Amare, A. R. (2008) Structural basis of specific tRNA aminoacylation by a small in vitro selected ribozyme, *Nature 454*, 358-361.

177. Sheng, J., and Huang, Z. (2008) Selenium derivatization of nucleic acids for phase and structure determination in nucleic acid X-ray crystallography, *Int J Mol Sci 9*, 258-271.

178. Sheng, J., and Huang, Z. Selenium derivatization of nucleic acids for X-ray crystal-structure and function studies, *Chem Biodivers 7*, 753-785.

179. Salon, J., Jiang, J., Sheng, J., Gerlits, O. O., and Huang, Z. (2008) Derivatization of DNAs with selenium at 6-position of guanine for function and crystal structure studies, *Nucleic Acids Res 36*, 7009-7018.

180. Brandt, G., Carrasco, N., and Huang, Z. (2006) Efficient substrate cleavage catalyzed by hammerhead ribozymes derivatized with selenium for X-ray crystallography, *Biochemistry 45*, 8972-8977.

181. Caton-Williams, J., and Huang, Z. (2008) Biochemistry of selenium-derivatized naturally occurring and unnatural nucleic acids, *Chem Biodivers 5*, 396-407.

182. Stein, H., and Hausen, P. (1969) Enzyme from calf thymus degrading the RNA moiety of DNA-RNA Hybrids: effect on DNA-dependent RNA polymerase, *Science 166*, 393-395.

183. Ohtani, N., Haruki, M., Morikawa, M., and Kanaya, S. (1999) Molecular diversities of RNases H, *J Biosci Bioeng 88*, 12-19.

184. Karwan, R., and Wintersberger, U. (1988) In addition to RNase H(70) two other proteins of Saccharomyces cerevisiae exhibit ribonuclease H activity, *J Biol Chem 263*, 14970-14977.

185. Frank, P., Braunshofer-Reiter, C., Wintersberger, U., Grimm, R., and Busen, W. (1998) Cloning of the cDNA encoding the large subunit of human RNase HI, a homologue of the prokaryotic RNase HII, *Proc Natl Acad Sci U S A 95*, 12872-12877.

186. Cazenave, C., Frank, P., Toulme, J. J., and Busen, W. (1994) Characterization and subcellular localization of ribonuclease H activities from Xenopus laevis oocytes, *J Biol Chem 269*, 25185-25192.

187. Kanaya, S., and Crouch, R. J. (1983) DNA sequence of the gene coding for Escherichia coli ribonuclease H, *J Biol Chem 258*, 1276-1281.

188. Katayanagi, K., Miyagawa, M., Matsushima, M., Ishikawa, M., Kanaya, S., Ikehara, M., Matsuzaki, T., and Morikawa, K. (1990) Three-dimensional structure of ribonuclease H from E. coli, *Nature 347*, 306-309.

189. Katayanagi, K., Okumura, M., and Morikawa, K. (1993) Crystal structure of Escherichia coli RNase HI in complex with Mg2+ at 2.8 A resolution: proof for a single Mg(2+)-binding site, *Proteins 17*, 337-346.

190. Ohtani, N., Haruki, M., Morikawa, M., Crouch, R. J., Itaya, M., and Kanaya, S. (1999) Identification of the genes encoding Mn2+-dependent RNase HII and Mg2+-dependent RNase HIII from Bacillus subtilis: classification of RNases H into three families, *Biochemistry 38*, 605-618.

191. Itaya, M. (1990) Isolation and characterization of a second RNase H (RNase HII) of Escherichia coli K-12 encoded by the rnhB gene, *Proc Natl Acad Sci U S A 87*, 8587-8591.

192. Nowotny, M., and Yang, W. (2006) Stepwise analyses of metal ions in RNase H catalysis from substrate destabilization to product release, *EMBO J 25*, 1924-1933.

193. Nowotny, M., Gaidamakov, S. A., Crouch, R. J., and Yang, W. (2005) Crystal structures of RNase H bound to an RNA/DNA hybrid: substrate specificity and metal-dependent catalysis, *Cell 121*, 1005-1016.

194. De Vivo, M., Dal Peraro, M., and Klein, M. L. (2008) Phosphodiester cleavage in ribonuclease H occurs via an associative two-metal-aided catalytic mechanism, *J Am Chem Soc 130*, 10955-10962.

195. Steitz, T. A., and Steitz, J. A. (1993) A general two-metal-ion mechanism for catalytic RNA, *Proc Natl Acad Sci U S A 90*, 6498-6502.